Off-Design Performance Prediction of the CFM56-3 Aircraft Engine

Daniel Alexandre Rodrigues Martins

Thesis to obtain the Master of Science Degree in

Aerospace Engineering

Supervisor(s): Prof. André Calado Marta
Eng. António Miguel Abreu Ribeiro Henriques

Examination Committee

Chairperson: Prof. Filipe Szolnoky Ramos Pinto Cunha
Supervisor: Prof. André Calado Marta
Member of the Committee: Prof. João Eduardo de Barros Teixeira Borges

November 2015

To my family and friends.

Acknowledgments

Firstly I would like to thank Engineer António Ferreira, for the opportunity of developing this work in TAP Portugal.

To both my supervisors, Engineer António Miguel Abreu Ribeiro Henriques, of TAP, and Professor André Calado Marta, of IST, for all the support, confidence, solutions and encouragements. I am extremely thankful and indebted to them for sharing expertise, and sincere and valuable guidance which resulted in all the improvements that led to the final version of this thesis.

To every person that I have worked with in TAP M&E during my internship. Their knowledge in their areas of expertise contributed to the development of this work.

To my colleagues Mário Ferreira, Julien Pabiot and Luis de Botton.

I am also grateful to my IST colleagues who supported me throughout these last five years of my academic life.

To my parents, I would like to thank their unconditional support, encouragements all across my life.

Finally, to the rest of my family and friends, for being present, in all the good, but specially, in all the bad moments.

Resumo

Desde o aparecimento das aeronaves no inicio do século passado, estas têm transformado o mundo. A sua capacidade de viajar a velocidades muito superiores àquelas que os comboios ou navios conseguem atingir ajudou o mundo facilitando trocas económicas e ajudando as pessoas a conhecer outras culturas.

O desempenho global de um turbina de gás pode ser estimado sabendo os principais parâmetros de desenho do motor, no entanto, isto é bastante difícil devido à quantidade limitada de informação que os productores de motores deixam escapar para o público em geral. Apesar de os productores de turbinas normalmente fornecerem informações sobre a interface desta, a informação que é necessária para estimar o ciclo termodinâmico de uma certa turbina a gás não está disponível. Um modelo capaz de estimar estes dados desconhecidos tem então de ser criado.

Nesta tese, um modelo de desempenho do motor CFM56-3 foi desenvolvido utilizando o software de modelação GasTurb. O motor escolhido foi o CFM56-3 pelos factos de ser um dos mais utilizados por todo o mundo e de a TAP Manutenção & Engenharia estar certificada para o receber na sua Oficina. O modelo é criado em primeiro lugar para as suas condições nominais, onde a sua geometria é definida. O desempenho fora das condições nominais é depois modelada utilizando dados provenientes do banco de ensaios da TAP M&E. O modelo é útil para prever os dados que não são revelados pelos contructores dos motores.

A melhor aplicação deste trabalho é analisar a condição de motores CFM56-3. Com alguns dados provenientes do banco de ensaios de um motor em particular, o modelo permite perceber os problemas desse mesmo motor.

Esta dissertação coloca maior ênfase no desenvolvimento e validação do modelo do motor, bem como na sua utilidade para a Oficina de Motores da TAP Manutenção e Engenharia. O modelo do motor possibilitará à TAP Manutenção e Engenharia analisar o desempenho de uma turbina a gás bem como comparar o desempenho de qualquer motor CFM56-3 com o desempenho do modelo com vista a estimar degradações nos seus componentes.

O maior benefício para a TAP M&E por usar o modelo de desempenho é a possibilidade de efectuar reparos selectivos, permitindo poupar horas de trabalho e reduzindo os custos de reparação.

Palavras-chave: Turbina de gás, modelo de desempenho, GasTurb, efeitos de degradações, custos de reparação, folgas na ponta das pás.

Abstract

Ever since the appearance of aircrafts at the beginning of the past century, they have been transforming the world. Their capability of travelling at speeds much greater than that of trains or ships helped the world by facilitating economic trades and helped people to learn about other cultures.

The overall performance of a gas turbine can be estimated by knowing the main design parameters, however, this is quite challenging due to the limited data that the engine manufacturer releases to the general public. Although a turbine manufacturer usually provides data about the turbine interface, the data required to estimate the thermodynamic cycle of a particular gas turbine remains hidden. A model of that engine capable of estimating that data must then be created.

In this thesis, a performance model of the CFM56-3 engine has been developed using the modelling software GasTurb. The chosen engine was the CFM56-3 due to the facts that it is one of the world's most used aircraft engines and that TAP M&E Engine Shop is certified to maintain it. The model is first created for its design point, where its geometry is defined. The off-design performance of the engine is then modelled using data from TAP M&E test bed. The model is useful to predict the data that the engine manufacturers do not reveal.

The best application of this work is the analysis of the condition of CFM56-3 engines. With some test bed data from a particular engine, the model might diagnose the problems of that same engine.

The thesis places major emphasis on the development and validation of the engine model, as well as its use in TAP M&E Engine Shop. The developed model allows TAP M&E to analyse the performance of the gas turbine as well as to compare the performance of any CFM56-3 engine to the performance of the model in order to estimate components degradation.

The main benefit to TAP M&E by using the performance model is the possibility of performing selective repairs, allowing to save work hours and reducing repair costs.

Keywords: Gas turbine, Thermodynamics, Performance model, GasTurb, Degradation effects, Repair costs, Tip clearance.

x

Contents

List of Tables

List of Figures

Nomenclature

Greek symbols

α Flow angle in cascade terminology.

β Flow angle in rotor stage terminology.

δ Pressure ratio; Blade tip clearance.

η Efficiency.

γ Heat capacity ratio.

ν Specific volume.

$\overline{\omega}$ Static pressure losses.

ϕ Diameter.

ρ Density.

Θ Temperature ratio.

θ Angle between flow direction and normal of an element of area.

Roman symbols

A Surface area.

c Velocity; Blade chord lenght.

C_D Total drag coefficient.

C_L Lift coefficient.

c_p Specific heat capacity (isobaric process).

c_v Specific heat capacity (isochoric process).

C_{DA} Annulus drag coefficient.

C_{Di} Induced drag coefficient.

C_{DP} Profile drag coefficient.

C_{DS} Secondary drag coefficient.

D Drag force vector.

F Force vector.

f Fuel-to-air ratio.

H Head.

h Blade height; Specific enthalpy.

$K1$ K1 Corrections performed in TAP test bed.

$K2$ K2 Corrections performed in TAP test bed.

$K3$ K3 Corrections performed in TAP test bed.

L Lift force vector.

$\dot{m}$ Mass rate.

M Mach number.

m Mass.

N Spool rotational speed.

n Normal vector.

p Pressure.

P_R Pressure ratio.

Q_r Fuel heating value.

R Degree of reaction; Standard day corrected value; Gas constant.

r Recovery factor.

S Blade spacing; Entropy.

s Specific entropy.

t Time.

T Temperature; Thrust.

V Volume.

$\dot{W}$ Power.

W Mass flow.

x x Cartesian coordinate.

y y Cartesian coordinate.

z z Cartesian coordinate; elevation.

Subscripts

0   Total property.

1   Inlet.

2   Outlet.

$22Rstd$ Station 22 property corrected for Standard day conditions.

$ambSTD$ Ambient value corrected for Standard day conditions.

a   Ambient conditions; axial component.

$corr$ Corrected value.

$corrected/model$ Corrected model data.

$corrected/test$ Corrected test data.

C   Cold flow.

c   Compressor.

cs   Control surface.

$Disk$ Rotor disk.

$efficiency$ Adiabatic efficiency.

H   Hot flow.

ind Indicated value.

in/i Inlet conditions.

is   Isentropic.

m Mean value.

$model$ Model data.

n Normal component; Nozzle

OVR Overall property.

out/e Outlet conditions.

$rotor$ Rotor stage.

$read$ Read value.

$desired$ Scalled component map.

Stg Stage property.

$test$ Test data.

$true$ True value.

t Turbine.

$unscaled$ Unscalled component map.

x, y, z Cartesian components.

Glossary

APU	Auxiliary Power Unit is a device on a vehicle that provides energy for functions other than propulsion. They are commonly found on large aircraft, naval ships, as well as some large land vehicles.
BPR	By-Pass Ratio is defined as the ratio between the by-pass and core mass flows.
CFD	Computational Fluid Dynamics is a branch of fluid mechanics that uses numerical methods and algorithms to solve problems that involve fluid flows.
CFMI	CFM International is a joint venture between GE Aviation, a division of General Electric of the United States and Snecma, a division of Safran of France. The joint venture was formed to build and support the CFM56 series of turbofan engine.
CMM	Coordinate Measuring Machine is a device for measuring the physical geometrical characteristics of an object. This machine may be manually controlled by an operator or it may be computer controlled.
CROR	Counter Rotating Open Rotor is a type of engine often refered as ultra high by-pass ratio engine.
CRP	Cycle Reference Point, or simply Design point, is the operating point for which the geometry of the engine is defined.
CS	Control Surface is the surface enclosing the control volume.

CTR	Correlation Test Report is a document developed by CFMI to define the facility modifiers for the CFM56-3 in TAP M&E test bed.
CV	Control Volume is a mathematical abstraction employed in the process of creating mathematical models of physical processes.
EFC	Engine Flight Cycle is composed by: one startup, one warm up, one takeoff, one landing, one cool down and one shutdown.
EFH	Engine Flight Hour is defined as the elapsed time from takeoff to landing.
EGT	Exhaust Gas Temperature is a primary measure of gas turbine engine health. EGT is minimal when the engine is new, or has been overhauled.
ESM	Engine Shop Manual is a formal document which details the way in which all maintenance tasks carried out on an aircraft shall be accomplished.
FM	Facility Modifiers are factors that relate the performance of an engine tested in different test cells.
GSP	Gas turbine Simulation Program is a component based modeling environment, is the National Aerospace Laboratory primary tool for gas turbine engine performance analysis.
HD	Hot Day atmosphere is defined as the Standard Day atmosphere but with an ambient temperature of 30°C.
HPC	High Pressure Compressor is an aero-engine component.
HPTCC	High Pressure Turbine Clearance Control is a system that optimizes the efficiency of this component by regulating the tip clearance between the blades and the case encircling them.
HPT	High Pressure Turbine is an aero-engine component.

IGB / AGB / TGB   Inlet, Accessory and Transfer Gear Boxes, respectively, are used to extract energy between the engine and the other aircraft components.

IGV   Inlet Guide Vane is an airfoil located in front of the first stage of an axial compressor. The compressor's first stator stage are composed of IGVs which, usually, are able to rotate in order to control the flow of air.

IPC   Intermediate Pressure Compressor, also referred as Booster, is an aero-engine component.

ISA   International Standard Atmosphere is an atmospheric model of how the pressure, temperature, density, and viscosity of the Earth's atmosphere change over a wide range of altitudes or elevations.

LLP   Life Limited Parts are parts that, as a condition of their type certificate, may not exceed a specified time, or number of operating cycles, in service.

LPC   Low Pressure Compressor, also referred as Fan, is an aero-engine component.

LPT   Low Pressure Turbine is an aero-engine component.

M/C   Maximum Continuous is an operating point in an engine flight envelope. Two types of M/C exist, functional (to test engine condition) and performance (to test engine performance).

MBTA   Model Based Test Analysis is a GasTurb tool used for comparison between experimental and model data.

MRO   Maintenance Repair and Overhaul are facilities that perform actions to retain and restore an item performance to its original state.

MSL   Mean Sea Level is an average level for the surface of one or more of Earth's oceans from which heights such as elevations may be measured.

NASA	National Aeronautics and Space Administration is the United States government agency responsible for the civilian space program as well as aeronautics and aerospace research.
OAT	Outside Air Temperature refers to the temperature of the air around an aircraft, but unaffected by the passage of the aircraft through it.
OEM	Original Equipment Manufacturer is a term used when one company makes a part or subsystem that is used in another company's end product.
OGV	Outlet Guide Vane is an airfoil located in the fan (cold stream) exit area, used to direct the flow exiting the fan.
PR	Pressure Ratio is the ratio between inlet and outlet pressures in a component.
RPM	Revolutions Per Minute is a measure of the velocity of rotation, specifically the number of rotations around a fixed axis in one minute.
SD	Standard Day model of the atmosphere is defined at sea level, with certain present conditions such as temperature and pressure.
SI	International System of Units is the modern form of the metric system and is the most widely used system of measurement. It comprises a coherent system of units of measurement built on seven base units.
T/O	Take-Off is an operating point in an engine flight envelope.
T/W	Thrust-to-Weight ratio is a dimensionless ratio of thrust to weight of a rocket, jet engine, propeller engine, or a vehicle propelled by such an engine that indicates the performance of the engine or vehicle.
TAP M&E	TAP Maintenance & Engineering is a leading global maintenance, repair, and overhaul (MRO) solution provider for Airbus, Boeing, Embraer, and legacy fleets.

TAP	TAP Portugal is the flag carrier airline of Portugal head-quartered at Lisbon Airport.
TRF	Turbine Rear Frame, located in the back of the engine, is used for structural suport and to fix the engine to the aircraft wing.
TSFC / SFC	Thrust Specific Fuel Consumption is an engineering term that is used to describe the fuel efficiency of an engine design with respect to thrust output.
VBV	Variable Bleed Valve are valves whose position is related to the high pressure compressor (HPC) operation.
VSV	Variable Stator Vanes are variable geometry stators which are able to rotate. In the CFM56-3 engine the VSV system is composed by the first three stator stages of the HPC.

Chapter 1

Introduction

The phenomenon of deterioration in gas turbine engines can make their operation uneconomical to airline companies as well as unsafe and untrustworthy for their clients. That fact leads to the requirement of a proper knowledge of the true state of the gas turbine. Without it, one cannot assess its performance capability and meet the operational and the maintenance contractual requirements.

The knowledge of the behaviour of a gas turbine leads to early detection of the cause of deteriorations or failures of its components, which allows appropriate maintenance activity to be undertaken to restore the engine performance and/or ensure safe operation.

These operations are the responsibility of Maintenance, Repair and Overhaul (MRO) companies such as TAP Maintenance & Engineering [1], MTU Aero-engines [2] or Lufthansa Technik [3]. MRO facilities are of primary importance to make sure that aero engines remain safe and functional for their operating role [4].

There are several reasons that make an engine take an intervention in an MRO facility such as:

- repair of any damage caused during normal operation;

- planned shop visits to replace some of their life-limited parts;

- engine performance restoration.

Tap M&E is part of the TAP Group [5] and is a leading global maintenance, repair, and overhaul solution provider for Airbus, Boeing, Embraer, and legacy fleets. Having extended experience from servicing its own TAP fleet for 70 years, it can offer the advantages of a complete set of integrated MRO services ranging from airframe, engines and components, to engineering and material support.

TAP M&E has a department focused on engines, where this thesis was developed, that offers a wide range of solutions for its clients such as on-wing repairs or engine performance restoration by substitution of an engine component.

This MRO facility is certified to work with the following engines:

- CFM56-3, -5A, -5B- -5C, -7B, produced by CFM International;

- PW4168A, PW4156A, produced by Pratt & Whitney;

- CF6-80C2, CFM80-E2, produced by General Electric.

According to TAP quality report and a thesis from Julio Ridaura named Correlation Analysis between HPC blade chord and compressor efficiency for the CFM56-3 [6, 7], between 2009 and 2013, an average of 78 engines per year went to TAP M&E facilities for shop visits, with CFM56-3 leading with the highest number of visits. Figure 1.1 presents the CFM56-3 engine in the engine stand, where it is mounted during shop visits and during on-wing repairs, mounted on the wing of a Boeing 737 [8].

(a) CFM56-3 on engine stand.
(b) CFM56-3 during on-wing repairs.

Figure 1.1: CFM56-3 engine [8].

The thesis cited above, as well as this one, shows the commitment of TAP M&E in improving the quality of its services, by trying to implement new diagnosis techniques which will allow to save time and money to customers by reducing the time spent searching for the issue with the engine [7].

According to Meherwan P. Boyce [9], maintenance is defined as the "upkeep of property" and it is crucial to extend the engines lifetime. In his book entitled Gas Turbine Engineering Handbook, Boyce refers that maintenance has to be an active part in a gas turbine lifetime and should go together with operation, due to the fact that a good operation requires less maintenance and a good maintenance facilitates a good operation.

Worldwide, MRO facilities seek to maintain engines performance at its peak throughout their lifetime, each one with their specific approach to the challenge.

A widely known case is Lufthansa Technik, which is a branch of the German airline company Lufthansa. This MRO is known for several projects, one of them being of the same field of expertise as this thesis, named Engine Performance Analysis [10]. This project had the scope of revealing the internal interactions of the engine components with other components of the engine, improving overhauls efficiencies by making them faster and more accurate. It was a three-level project, where a thermodynamic model of an engine was developed.

The levels of the engine model were:

- creation of a model of the overall engine, in which general engine parameters such as thrust, fuel consumption and Exhaust Gas Temperature, EGT, were calculated;

- modular level models, for which simplified flow simulations were used;

- construction of detailed computational fluid dynamics (CFD) flow models for individual groups of components.

To improve the accuracy of the analyses during test runs, improved instrumentation was also developed for the test rig. The insights gained as a result of the work carried out made it possible to work selectively on the major components of the engine during an overhaul or to develop improved repairs. The project aimed to study the reliability of engine components after the end of their operating life and to get the maximum use out of the available life limited parts (LLP).

Gas turbines have always been studied using thermodynamic models to study and improve their performance. Computer programs simulating such models have proved to be a useful tool for developing models of specific engines, helping Original Equipment Manufacturers (OEM) developing their new engines and MRO facilities to save money by making interventions on engines in a more precise manner. For this thesis, a software named GasTurb 11 will be used.

GasTurb 11 is a gas turbine simulator [11] on which the user has the possibility of modelling a gas turbine from its design point, which is the operating point that defines the engine geometry, or studying its performance across a range of off-design points. A more detailed description of the software will be presented later in this thesis.

Engine simulation computer programs normally incorporate steady state maps for the component modules, and these are modified in the present program to simulate the deteriorated gas turbine engines. These programs can model any type of gas turbine whose standard component maps are integrated within the software so that an inexperienced user can use them to make some simpler simulations. The necessary changes in the characteristics are incorporated for the compressor (or compressors) and the turbine (or turbines) modules only, since they are considered to be the ones that deteriorate the most. Simulation of a deteriorated engine is achieved by re-matching these components with modified characteristic maps. The author of GasTurb, Dr. Joachim Kurzke, is known for introducing a new set of coordinates, called $\beta - lines$, which simplify the positioning of operating points in component maps, even though they do not have any physical meaning.

1.1 Motivation

TAP M&E is interested in understanding the degradations affecting the engines throughout their life time and what effects those degradations bring. To study the effect of tip clearance in the engine performance, the maximum amount of data from that engine is needed. The acquirement of test data from an engine is not easy. Testing an engine multiple times to study performance variations due to a single change in the engine is very costly and does not come in line with the objectives of TAP M&E. Such tests are called back-to-back tests.

Thus, to accomplish the above presented objective, it is required a trustworthy thermodynamic model that can represent the CFM56-3 engine all across its operating range.

To develop an engine model that simulates its response with precision, one would need to have the maps for that engine components, however, when delivering the gas turbines to the customers, the

OEMs do not share that kind of data. They keep that data hidden and deliver only the data of the gas turbine that is used for control purposes; the OEMs do not share data about any thermodynamic properties of the engine components, e.g. turbine and compressor efficiencies. The turbine manufacturers usually supply five main parameters in their catalogues that are sufficient for installation requirements, they are: pressure ratio, gas turbine electrical output, overall efficiency, gas turbine exhaust temperature and exhaust mass flow rate.

For the engine in study, the test data is taken from a document produced by CFM [12].

1.2 Objectives

The goal of this thesis is firstly to model the CFM56-3 engine in the software GasTurb, a commercial engine performance modelling software. The model will be used for estimating the engine performance by comparing it to engine performance data from the engine described in reference [12]. Secondly, apply the tuned model to test cases from engines that had shop visits in TAP M&E facilities, studying their degradation and the effects on the overall efficiency of the engine. Lastly, the model will be used to study the replacement of HPC blades in the CFM56-3 engine.

1.3 Thesis Outline

A presentation of TAP M&E facilities and the services provided to its costumers will be given in Chapter 2. In that same chapter, TAP engine test bed will be briefly presented as well as the set-up for the CFM56-3 engine and the measurements taken during the test runs.

Chapter 3 will give the reader insights about the theory of aircraft engines and their thermodynamic cycles.

The modelling of the CFM56-3 engine will be developed in Chapter 4, which will be divided in three sections, the first one presenting the simulation software GasTurb, the second reveals the method used to model the engine and the last part of the chapter will be used for verification and validation of the model. In Chapters 5 and 6, respectively, the model will be applied to solve real problems in the GasTurb environment and to map the performance degradation of the engine due to increases in High Pressure Compressor tip clearances.

The seventh and last chapter is where the results are going to be commented and where conclusions are made.

Chapter 2

Maintenance, Repair and Overhaul Facilities

In order to maintain the engines safe and operable, airliners must submit them to shop visits during their life cycle. The engines are sent to MRO facilities, that are capable to perform these routine actions. The European Federation of National Maintenance Societies [13] define MRO operations as "All actions which have the objective of retaining or restoring an item in or to a state in which it can perform its required function. The actions include the combination of all technical and corresponding administrative, managerial, and supervision actions." MRO operations can be categorised by whether the product remains the property of the customer, i.e. a service is being offered, or whether the product is bought by the reprocessing organisation and sold to any customer wishing to make the purchase. They can be as well be of three types:

- Preventive maintenance, where equipment is maintained before break down occurs;

- Operational maintenance, where equipment is maintained while being used;

- Corrective maintenance, where equipment is repaired after break down. This maintenance is often most expensive because worn equipment can damage other parts, cause multiple damages to the item and even interrupt regular operations.

TAP M&E, and more specifically its engine shop, performs mostly preventive and corrective maintenance to the engines, e.g. scheduled shop visits due to life-limited parts or fan blade substitution due to bird strike, respectively.

2.1   TAP M&E

TAP M&E is an MRO facility based in Lisbon, Portugal. Although it is responsible for maintaining TAP Air Portugal fleet, TAP M&E also has external customers from all around the world. As an MRO, it provides solutions in many different areas of an airplane, such as:

- $Care^2 Airframe$, from light to heavy maintenance, TAP M&E covers pre-flight, transit and daily checks, troubleshooting, engine trend monitoring, and pool agreements. Divided in two divisions, Base Maintenance and Line Maintenance, the first performed in its facilities in Lisbon and Brazil (Rio de Janeiro and Porto Alegre), originally built to service TAP airlines fleets, capacity has grown over the years and it is now able to offer that same level of expertise and quality of service to all its customers. Line Maintenance is performed in all major Portuguese International Airports as well as other foreign stations, created for simpler maintenance actions, avoiding sending components to one of TAP's bases;

- $Care^2 Engines$, divided in two bases, turbofan base is located in Lisbon and turboprop base in Porto Alegre, Brazil. Offer services in repair and overhaul areas, certified to act on the following engines: CFM56-3, -5A, -5B, -5C, -7B and CF6-80C2/A/B and PW4000 in Lisbon's base, PW118/A/B, PW120/A, PW121 PW124B, PW125B, PW127 and PT6 in Brazil's base. Apart from engines, TAP M&E is capable of repair/overhaul actions on the Auxiliary Power Units (APU's), used in Boeing 737 and Airbus A320 family;

- $Care^2 Components$, division responsible for repair/overhaul in part-level, it's able to act on components from aircraft's avionic, pneumatic, hydraulic, mechanical, fuel and oil systems. Apart from aircraft's systems, it is also responsible for the landing gear maintenance;

- $Care^2 Engineering$, offering services as training, logistics, fleet management or certification of aircraft modifications performed in TAP's facilities.

Focusing on engines, 2014's quality report [14] features the distribution of engines coming to TAP M&E facilities, the distribution for the year 2014 are presented in Figure 2.1 in three graphs according to:

1. Percentage of total shop visits performed by each model of engine, without considering the engine operator;

2. Number of shop visits for each engine, considering if the operator is either TAP or other airliner;

3. Number of shop visits for TAP and other costumers.

From Figure 2.1 it is possible to see that only half of the engines coming to TAP M&E engine shop are from TAP fleet, the other half is from external customers. Also, the CFM56-3 engine is the third engine with more visits, losing only to the CFM56-5B and CFM56-5C engines.

2.2 TAP Test Bed

The design and conception of an aircraft engine is a long process that can take up to 7 years from the first concepts to service entry [15]. Being such a complex machine, it is not expectable to get the optimal[1] design at the first try, its development must include test runs for data acquisition as well
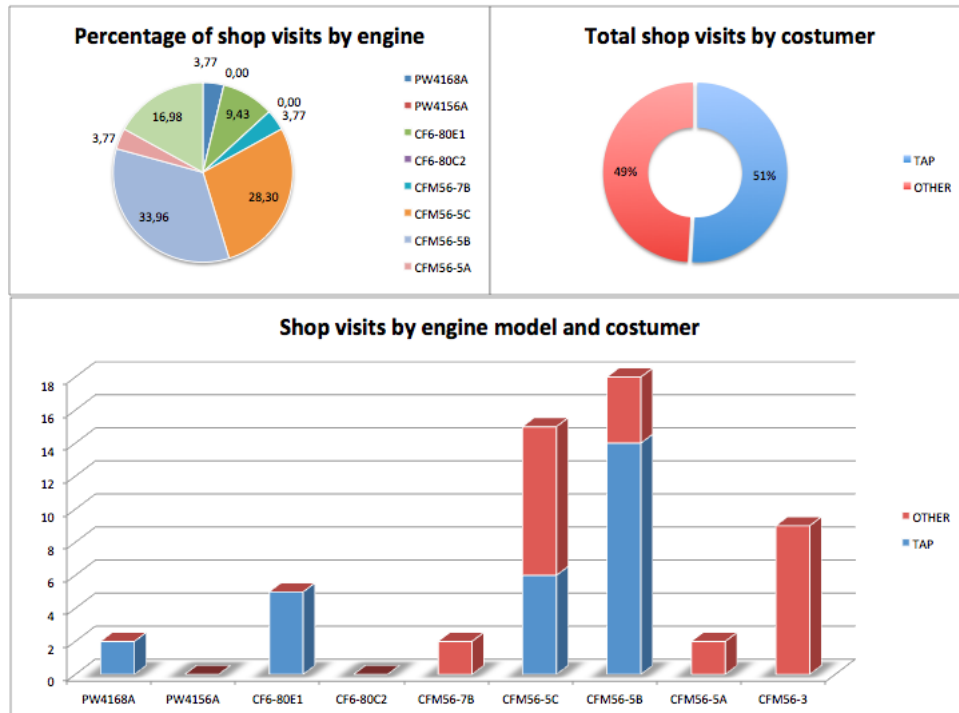
Figure 2.1: TAP M&E shop visits [14].

as tests to individual components and their interactions with each other. The easier way to conduct such tests is in a test bed. A test bed is still needed after an engine entry in service, in MRO facilities, where an acceptance test is conducted to reveal its condition and performance level after a maintenance intervention; a test bed can be seen as a diagnosis tool which define the workscope in an engine maintenance, repair and overhaul operation.

2.2.1 Test Bed Set-up

Not all test beds are equal, they can be of two types according to their elevation from mean sea level (MSL) [16]:

- Sea level facilities, designed to replicate sea level conditions, are appropriate to test regimes as idle, take off or approach, the resultant performance figures are then corrected for International Standard Atmosphere (ISA) sea level conditions;

- Altitude test bed, used to replicate in-flight conditions, are required because the engine's operation is affected by ambient conditions. Such tests cover characteristics as anti-icing, combustion and reheat efficiencies, mechanical reliability or fuel and oil consumptions. There are two ways to evaluate engine condition at high altitude: the engine can either be tested in an altitude test cell, where the engine is enclosed by the cell and the atmospheric conditions are mechanically simulated or it can be installed in a testing aircraft. High altitude tests are meant to test the effects of variations of humidity, temperature and pressure in the engine.

Test beds can also be divided into two groups: exterior or interior test beds. An exterior test bed

facility is composed by a support and a protection in the engine inlet. The support is mounted on a dynamometer which measures the net thrust produced by the engine, to make sure that all the measurements are valid, both the engine and support must be clear of obstructions so that the flow enters the engine undistorted. Apart from that, the engine must be maintained at a proper elevation of the ground so as to eliminate interferences and to minimize dust ingestion from the ground. An interior test bed cancels the above mentioned problems since the test cell is enclosed in a building. Both types of test cells are presented in Figure 2.2.

Figure 2.2: Exterior (left) and interior (right) test cells [17].

TAP M&E's test cell is an 'L' type cell and its schematic is presented is Figure 2.3. It has a cross section of approximately 8.65m X 9.75m. The facility uses down-draft inlet with turning vanes as it can be seen it the left side of Figure 2.3. The incoming flow passes through noise reduction splitters and a bird screen before entering the working section of the test cell. Once the flow pass the working section, the exhaust gases pass rearward though a conventional cylindrical augmenter with a wedge diffuser section and then upwards through a folded vertical exhaust stack [12].
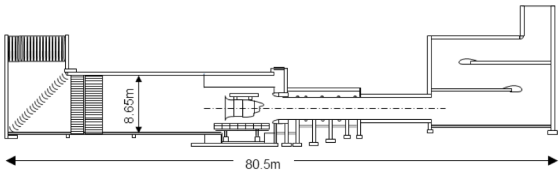
Figure 2.3: TAP test cell [12].

2.2.2 Data Acquired and Limitation of TAP Test Bed

The purpose of a test cell is to acquire data from the tested engines. In order to make a good performance analysis, it is required to understand deeply which measurements are made in the test cell, called raw data, the corrections applied to the raw data to standardize them, as well as the limitations of the sensors and the test cell itself. A description of this point will be made based on the work of [7], [17] and [18].

Limitations of the TAP test bed

It is of most importance to understand the limitations of the test bed to understand which measurements can and cannot be taken in TAP's test cell.

Kurzke states [19] that the factor which makes the modelling of a turbofan engine so hard is the lack of knowledge of the engine secondary flow, i.e. the air entering the engine core.

The limitations are mostly connected to the lack of instrumentation on the engine. This problem affects MRO facilities since they do not reach the levels of instrumentation that an OEM reach. The lack of instrumentation is due to the difficulty of producing sensors that make good measurements in places with large temperature gradients and where they are exposed to high velocity flow, creating form or pressure drag. Pressure drag arises because of the shape of the object. The general size and shape of the body are the most important factors in form drag, e.g. bodies with a larger presented cross-section will have a higher drag than thinner bodies and, at the same time, the drag created by the shape of the object depends on the velocity of the flow. It is then important to design sensors capable of resisting the harsh conditions experienced in a gas turbine [20].

TAP M&E, as well as other MROs, should be interested in developing sensors since it would provide useful test data, even considering the great investment of time and money required to do so. An aggravating factor is the possibility of damaging an engine if a sensor created by TAP M&E unclasps and goes downstream putting at risk the engine integrity. This is a risk that TAP M&E cannot afford.

As stated before, the difficulty of calculating or measuring some parameters, e.g. the primary or core mass flow, introduces limitations such as:

- Difficulties obtaining the combustion chamber exit temperature, T4. Strong temperature gradients and high pressures make the installation of a proper, safe and resistant sensor in this station very difficult. This measurement would be fundamental to study the expansion of the flow through both the High pressure turbine (HPT) and the Low pressure turbine (LPT);

- Study the separate relationship between the LPT and HPT with the overall engine performance is not possible since the first sensor downstream from the combustion chamber is located in the second stage vane of the LPT. It is used to measure EGT, whose importance in performance studies will be explained later in this thesis. The solution would be to produce sensors in order to measure temperature and pressure between the two turbines. This solution has been tried by Henriques [18], but the sensor developed was not robust enough to endure the harsh conditions experienced in that area of the engine;

- Obtain the bleed flow between the Booster (IPC) and the High pressure compressor (HPC) accurately is not possible; to calculate this parameter, deeper knowledge about the air system would be required;

- The difficulty in placing sensors in the secondary flow duct, due to high pressure drag produced by the high speed flow passing, the sensors can separate from engine and go downstream; leads to lack of knowledge about the parameters of this area;

- The most important limitation, described in reference [18], is the difficulty in placing sensors in station 25, between the Booster's exit and the HPC's entry; this station is essential to isolate the Booster from the HPC in order to study their separate relationships with the engine performance. These sensors are located in some of the engines tested in TAP's test cell, but they were installed only on some of the tested engines. An alternative to this problem is given in reference [21], where a methodology to calculate T25 is given.

The calculations that require the primary flow can be done assuming a value for the by-pass ratio (BPR). This parameter relates the primary and the secondary flows. According to reference [22], this value is 5 for the engine in study, the CFM56-3, which means that for every kilogram of air that flows through the core per second, five kilogram of air will flow through the secondary flow duct, for the same time interval. Of course this value is assumed, the reference does not specify the conditions where such measurement was made. TAP is currently developing a project to obtain the correct amount of primary airflow, which will make the modelling of the by-pass ratio much easier.

Engine's parameters measured in TAP Test bed

A test cell has the primary objective of measuring and recording data about the engine operation, usually, any engine coming to TAP M&E facilities is tested in the following sequence of five operating points:

1. 4000 N1K, low rotation regime in which the high pressure spool speed is kept at 4000rpm, is used to check engine condition;

2. M/C func, where the engine regime is kept bellow maximum continuous regime, M/C, to check the condition (functionality) of the engine, e.g. check if there are any leakages of any fluid;

3. M/C #1 Perf, the engine rotational speed is increased to M/C to study its performance, this is the first of two M/C runs;

4. T/O Perf, engine rotational speed is maximized to study its performance during Take-off, T/O;

5. M/C #2 Perf, the engine rotational speed is decreased to M/C to study its performance, this is the second of two M/C runs.

A $.log$ file is then generated with all the measured data. Note that all the values are raw data, meaning that they are observed values, they are not yet corrected.
The work done by Henriques [18] to compile a secondary $.log$ file from the original one is now useful, maintaining only the data relevant to this thesis. An example of a reduced .log file is shown in Figure 2.4.

In Figure 2.4 it can be seen the five operating points where the engine parameters are measured. A value of 99999 means that the sensor was not able to record data. The positions of the engine thermo-dynamic stations are given in reference [18] and will be presented in Section 4.1.2 while a summary of all the data measured in TAP test bed, as well as its accuracy and units is given by Ridaura [7].

10

```
DATE;
TEST NO;      2013/054B
ENG TYPE;     3C
ESN;
TIME;

PARAMETER                      4000 N1K   M/C Func  M/C #1 Perf   T/O Perf  M/C #2 Perf
FNa                               12095      20733       20923      22417       20735
N1a Observed                       4073       4908        4907       5044        4893
N2a Observed                      13380      14303       14332      14454       14265
W2AR                           518.8743   674.6724    677.6510   701.8103    674.6931
WFa                                5003       8724        8739       9492        8645
Barometer                       14.5970    14.5966     14.5915    14.5930     14.5912
T2 Temp Avg                        25.53      25.90       24.33      24.01       24.03
T17 – FAN Discharge Temp        99999.00   99999.00    99999.00   99999.00    99999.00
T2.5 HP Compressor Inlet temp   99999.00   99999.00    99999.00   99999.00    99999.00
CDT T3                            437.9      523.7       522.2      536.3       520.9
EGT                               692.1      848.9       835.4      862.5       828.6
T54 – LPT Exhaust Gas Temp       554.26     647.88      639.60     663.51      638.43
PT2 F [N1R]                       14.566     14.550      14.545     14.544      14.545
PS2                               12.766     11.078      11.031     10.639      11.075
PT17 – FAN Discharge Pressure     19.848     23.271      23.378     24.053      23.301
PT25                              15.068     15.559      15.569     15.672      15.550
CDP or PS3                        218.1      324.3       326.7      345.3       324.8
PT495                              40.0       59.0        59.4       62.8        59.0
PT54_1                            14.873     15.029      14.789     14.784      14.761
PS42                                  0          1           1          1           1
PS42                              15.07      15.56       15.56      15.69       15.56
T54 LPT Exhaust Gas Static Tem  99999.00   99999.00    99999.00   99999.00    99999.00
T42 – HPT Static Temperature    99999.00   99999.00    99999.00   99999.00    99999.00
```

Figure 2.4: Example of $.log$ file [18].

The location of some of the more important thermodynamic stations can be observed in Figure 2.5 for the CFM56-3 engine. The prefixes TS and TT refer to static and total temperatures, respectively, while the prefixes PS and PT refer to static and total pressures, respectively.
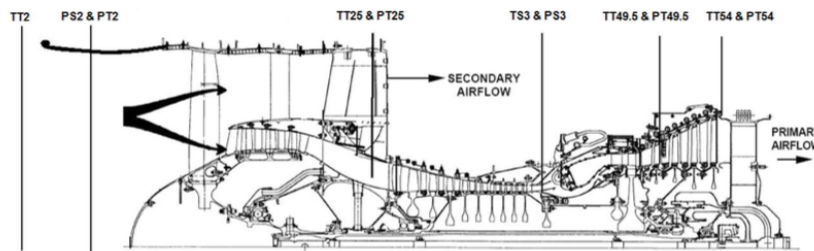
Figure 2.5: Position of thermodynamic stations in CFM56-3 [18].

Figure 2.6 represents all the variables measured in TAP M&E test bed, their units and the positions of the engine where they are taken. Some of the measurements presented in Figure 2.6 are corrected data, the rest being still raw data. The following section will emphasize these corrections made to the parameters measured.

Thermodynamic corrections of the engine's parameters

In Figure 2.6 some parameters have the subscript R, K1, K2 or K3, that means that those parameters have been corrected for:

- R - corrected for Standard Day conditions, i.e. corrected for standard humidity, condensation and temperature;

- K1 - corrected for SD conditions, facility modifiers (FM) and HPT clearance control. The facility modifiers are corrections used to take into account the influence of the test bed geometry on the engine performance;

- K2 - corrected for K1 corrections and installation effects, to simulate the engine mounted on the aircraft;

- K3 - corrected for K2 corrections and for rated vs actual N1 speed factor.

A description of the corrections K1, K2 and K3 is given in reference [7]. Note that all the measurements apart from N1, N2, net thrust (FN), EGT and Specific fuel consumption (SFC) are all raw data, whose corrections will be introduced in Chapter 4.

Variable	Unit	Position	Accuracy	Comment
T_2	[ºC]	Total inlet fan temperature.	0.25 ºC	
P_{T2}	[psia[3]]	Inlet fan pressure.	± 0.15% Full scale	Test cell facility is equipped with barometers, which measure the atmospheric pressure. However, atmospheric pressure is a little bigger than the inlet fan pressure. P_{T2} is obtained from an equation contained in the *Correlation Test Report* (Explained in *Chapter 3, Section 3.1*), and it is a function of the low pressure spool speed and the barometric pressure.
N_{1K}[4]	[rpm]	Spool speed of the low pressure components (Fan, LPC and LPT).		
N_{2K3}	[rpm]	Spool speed of the high pressure components (HPC and HPT).		
FN_{K3}	[lb]	Net thrust.		
EGT_{K3}	[ºC]	Exhaust Gas Temperature ($T_{49.5}$).	0.25 ºC	Despite of the fact that this temperature is known as Exhaust Gas Temperature, the sensor is located in the second stage of the LPT. There are not sensors upstream of the aerodynamic station 49.5 due to harsh conditions. In Figure 2.6, the EGT sensor is represented.
P_{S3}	[psia]	Inlet combustion chamber static pressure.	± 0.15% Full scale	
$P_{T49.5}$	[psia]	Total pressure in the second stage of LPT.	± 0.15% Full scale	
P_{T25}	[psia]	Total HPC inlet pressure.	± 0.15% Full scale	Data of this station is difficult to obtain. The sensor is rarely set due to its high tendency to go downstream.
T_{25}	[ºC]	Total HPC inlet temperature.	0.25 ºC	
T_{54}	[ºC]	Total LPT exit temperature.	0.25 ºC	
P_{T54}	[psia]	Total LPT exit pressure.	± 0.15% Full scale	
H.R.	[%]	Relative humidity.		This parameter is important to apply standard day corrections to the measured data.
SFC_{K3}	[pph[5]]	Specific Fuel Consumption.		
W2AR	[pps[6]]	Mass flow rate at station 2 corrected for the standard day.		.

Figure 2.6: Data measured in TAP test bed [7].

Chapter 3

Principles of Aircraft Engines

Gas turbines are widely used power plants, known for their multiple applications [9]. The most notable factor of this type of power generators is their thrust-to-weight ratio,Gas turbines reduced weight and size lead them to an increasing service over the last years in the power industry, mainly the aeronautical one, and other utilities throughout the world. Today there are gas turbines, that run on natural gas, diesel fuel, naphtha, methane, crude, low-BTU gases, vaporized fuel oils, and biomass gases [9].

The increase in compressor and turbine pressure ratios, use of new materials and new coatings all lead to a growth in gas turbine performance, specifically in terms of thermal efficiency; doubling of efficiency has occurred for simple cycles and the introduction of combined cycles caused the efficiency to triple when compared with older engines [23], as illustrated in Figure 3.1.

(a) Evolution of pressure ratio   (b) Evolution of efficiency.
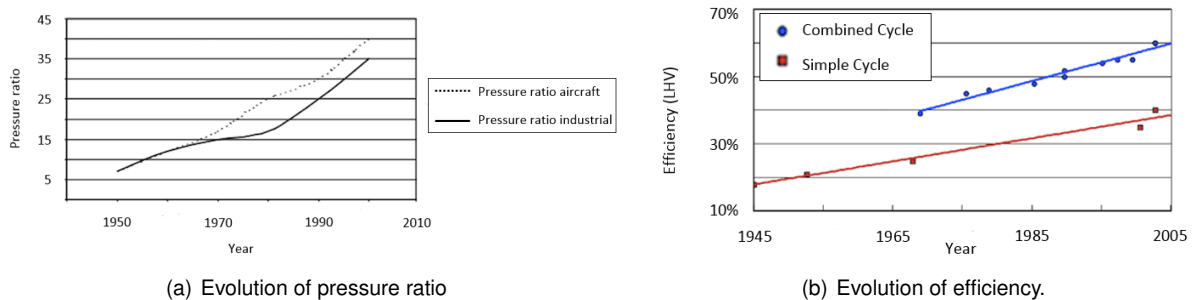
Figure 3.1: Evolution of pressure ratio and thermal efficiency over the years [23].

The efficiency increase was only possible by raising pressure ratios and firing temperatures in the engine. This was achieved with the combined use of more heat resistant materials and new turbine cooling methods, otherwise the increase in burner exit temperature would deteriorate the turbine blades and reduce the engine's lifetime [23].

3.1 Types of Aircraft Engines

Gas turbine engines exist in many configurations, depending on their role. Different configurations are needed since there is a wide range of operating roles of aircrafts [24], e.g. an engine of a maritime

surveillance aircraft could not be the same as the engine from a military combat jet; a surveillance aircraft demands an engine with lower specific fuel consumption than a combat jet, which requires an engine with a faster response and higher speeds.

According to [25] the basic configurations of aircraft engines are Turboprop, Turbofan, Turbojet, Ramjet and Propfan.

Since the CFM56-3 is a Turbofan engine, only this type will be described next.

3.1.1 Turbofan

The turbofan engine is derived from the turbojet engine, with the intention of reducing the mean exit air velocity [26]. The main difference is that a turbofan engine has two gas paths instead of a single one as in the turbojet engines. The only difference in the primary flow in a turbofan is that in these engines this flow is slightly accelerated by the fan, which does not exist in turbojet engines. The additional flow present in turbofan engines, named secondary flow, is accelerated in the fan and does not enter the engine core. Instead, it flows through the by-pass duct. Thus, the main core remains unchanged, i.e. it is composed by an inlet, compressor, burner, turbine, and nozzle, however, the turbofan has an additional turbine to turn the large Fan located at the front of the engine [25].

The size of the fan will be of primary importance to define one of the most important characteristics of a turbofan engine, the by-pass ratio (BPR) which is defined as the ratio between the air mass flow rate that passes through the by-pass duct and the air mass flow that passes through the engine's core; nowadays, BPR's of 10 are achievable by means of bigger fans and additional gears [27]. The effect of BPR in the engine aspect can be observed in Figure 3.2.
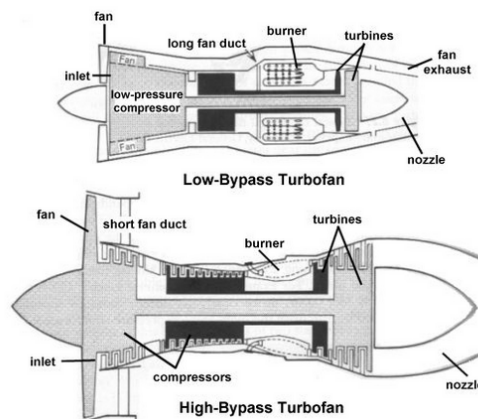
Figure 3.2: Low by-pass and high by-pass engines [25].

Turbofan engines come in three configurations depending on the number of spools [28]:

- One-spool turbofan: although it is an uncommon engine, it does exist in some aircrafts like the Mirage 2000B. It has the Fan, an high pressure compressor and a single turbine all connected in one single shaft;

- Two-spool turbofan: the most common one. It has the Fan and the low pressure turbine (LPT) connected by the low pressure spool and the HPC connected to the high pressure turbine connected

14

by the high-pressure spool; it is usual to have an extra compressor, named booster or intermediate pressure compressor (IPC), linked to the low-pressure spool;

- Three-spool turbofan, this configuration is identical to the two-spool one but it has an intermediate pressure stage, composed by Booster and intermediate pressure turbine (IPT).

Since the engine has two gas paths, it will have two contributions to total thrust. Some of the air from the fan enters the engine core where fuel is burned to provide some thrust, but up to 90 percent of it goes around or "bypasses" the core of the engine. As much as 80 percent of the total thrust of the engine comes from the by-pass air [25]. This amount of thrust that is created by a single-stage compressor, the Fan, is possible due to the very large amount of air that is moved by it.

Notably, the increase in fuel consumption caused by adding the Fan is small, making the turbofan very economical it terms of specific fuel consumption (SFC) and ideal for cruising at higher speeds than a propeller driven aircraft, since the fan having more blades and possessing a duct allows it to operate faster and, at the same time, more efficiently.

For all those reasons, turbofan are the engine of choice for powering large passenger aircrafts since they can operate at high subsonic speeds, around Mach 0.8 and still use fuel in a efficient manner [15]. Remarkably, even jet fighters are now using low by-pass turbofan engines, allowing them to save fuel while cruising and to maintain efficiency at lower speeds.

3.2 Physics of Aircraft Propulsion Systems

Turbomachines are classified as devices in which energy is transferred either to, or from, a continuously flowing fluid by the dynamic action of one or more moving blade rows. The word *turbo* or *turbinis* is of Latin origin and implies that which spins or whirls around.

Essentially, a rotating set of blades changes the stagnation enthalpy of the moving fluid and, depending of the turbomachine, it can either extract or add energy to the fluid. A change in enthalpy is directly linked with the pressure changes observed in the fluid [29].

This section will present the principles of the physics of propulsion systems, both mechanical and thermodynamics. This knowledge is essential to the development of any jet propulsion system [30]. Mechanics and thermodynamics are of first importance in the study of propulsion systems. The creation of thrust by the engine is a consequence of imparting momentum to the working fluid. Most methods of creating thrust involve thermal effects in one way or the other [30].

3.2.1 Thrust Equation

Having air flows up to 50 times larger than fuel flows, gas turbine engines can be considered air breathing machines. They are able to produce thrust in various ways, turbofan or turbojets get their thrust from the acceleration of the air leaving the engine while turboprop engines use the fluid to rotate a turbine which is connected to a propeller, as mentioned in Section 3.1. With thrust being proportional to the air flow

through the engine, engine developers always aim to maximize this value so that an engine produce maximum thrust maintaining its size and weight, getting higher values for thrust over weight ratios, T/W.

Thrust equations can be easily derived from *momentum* and mass laws without the need for consideration of the engine's internal mechanisms [30], by considering the generalized thrust-producing device represented in Figure 3.3. The results that will be next presented are valid for any air breathing device with a single exhaust.
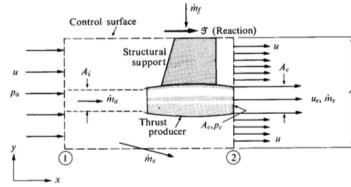
Figure 3.3: Generalized thrust-producing device [30].

The reaction to the thrust created by the engines is transmitted to the aircraft by their structural supports as presented in Figure 3.3, in this sense, thrust will be considered as the summation of all forces applied both on the interior and exterior of the engine and on the nacelle [30].

Thrust is derived from Equation (**??**), assuming steady conditions and considering the axial direction,

$$\Sigma F_x = \int_{cs} \rho c_x \left(c.n \right) dA \,.$$ (3.1)

Considering the reversibility of the external flow and excluding the exhaust area of the engine, the pressure and the velocity on the control surface may be assumed constant. With that assumption, a force is created in that area caused by the pressure differential between the ambient and exhaust pressures, respectively p_a and p_e; this pressure force is given by $(p_a - p_e)A_e$. Taking into account that the mass flow rate of the air entering the engine is $\dot{m}_a = \rho c A_i$ and that the mass flux exiting is $\dot{m}_e = \rho_e c_e A_e$, one can calculate the fuel flow using a mass flux balance to the engine as

$$\dot{m}_f = \rho_e c_e A_e - \rho c A_i \,.$$ (3.2)

From Equation (3.1), the *x-momentum* created by the engine is given by

$$\int_{cs} \rho c_x \left(c.n \right) dA = \dot{m}_e c_e - \dot{m}_a c \,,$$ (3.3)

which introducing the fuel to air ratio, $f = \frac{\dot{m}_f}{\dot{m}_a}$, becomes

$$T = \dot{m}_a[(1 + f)c_e - c] + (p_a - p_e)A_e \,.$$ (3.4)

Bear in mind that Equation (3.4) is only valid for reversible external flow, otherwise the losses from interaction of the flow with the engine nacelle and support should be accounted. At last, for engines with two separate air flows, such as turbofan, the procedure must be used for each flow separately, and

Equation (3.4) becomes

$$T = \dot{m}_{aH}[(1+f)c_{eH} - c] + \dot{m}_{aC}(c_{eC} - c)\,, \tag{3.5}$$

where the subscripts H and C refer to the hot (primary) and cold (secondary) flows, respectively.

3.3 Engine Performance

Engine performance is always an area of concern for engine developers since better performances lead to lower maintenance and lower fuel consumption which, in turn, lead to lower operating costs. To study the performance of an engine, one has to study individual components inside the gas turbine since they play a major role in power output and the overall efficiency. Compressor, turbine, combustion chamber, inlet and nozzle can be considered as individual components inside the engine. By reducing the individual internal component losses, the overall performance of the gas turbine can be increased [31].

3.3.1 Stagnation or Total Properties

Considering a gas moving with velocity *c*, temperature *T* and specific enthalpy *h*, if it is brought to rest adiabatically and without energy transfer to or from the gas, the new specific enthalpy h_0 is the stagnation or total specific enthalpy and its value is found applying the steady state energy equation for the two states as [20]

$$h_0 = h + \frac{c^2}{2}\,. \tag{3.6}$$

Considering that the temperature of the gas is $T = \frac{h}{C_p}$, the stagnation temperature T_0 is then

$$T_0 = T + \frac{c^2}{2c_p}\,. \tag{3.7}$$

Where c_p is the specific heat capacity for constant pressure. For a compressible flow, considering an isentropic process, results

$$T_0 = T\left(1 + \frac{\gamma - 1}{2}M^2\right)\,. \tag{3.8}$$

Similarly, the stagnation pressure p_0 for both incompressible and compressible flows is given respectively by:

$$p_0 = p + \frac{\rho v^2}{2}\,, \tag{3.9}$$

$$p_0 = p\left(1 + \frac{\gamma - 1}{2}M^2\right)^{\frac{\gamma}{\gamma - 1}}\,, \tag{3.10}$$

where p is the static pressure, γ is the polytropic ratio defined as $\gamma = c_p/c_v$ and M is the local Mach number defined as $M = (\gamma R T)^{0.5}$.

3.3.2 Isentropic Efficiency

Engineers frequently use efficiencies to characterize mechanical components such as turbines, compressors, nozzles, inlets or combustion chambers. Isentropic efficiency make the comparison between real and idealized performances of a given process having the same initial conditions and the same exit pressure [32].

Figure 3.4 represents the differences between an isentropic and an actual expansion in a generic turbine.
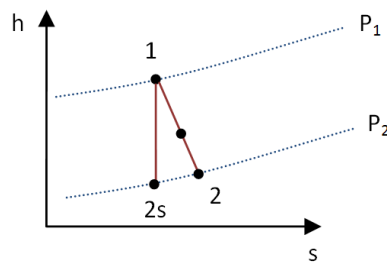
Figure 3.4: Ideal and real expansion in a turbine.

The process 1 to 2s in Figure 3.4 represents isentropic expansion, while process 1 to 2 represents an actual expansion. From the enthalpy difference of the two situations, one can see that in the expansion process the amount of work that can be recovered during the expansion is less than the available amount of work, the amount of enthalpy that is lost is $h_{2s} - h_2$. For a compression process the opposite happens, i.e. the amount of energy needed to move a fluid particle from one pressure to another pressure is higher than that of the ideal case. Table 3.1 summarizes the efficiencies for the different components of an engine.

Component	Efficiency
Compressor	$\eta_{is,c} = \frac{h_{2s} - h_1}{h_2 - h_1}$
Turbine	$\eta_{is,t} = \frac{h_1 - h_2}{h_1 - h_{2s}}$
Nozzle	$\eta_{is,n} = \frac{V_2^2/2}{\left(V_2^2/2\right)_s}$

Table 3.1: Isentropic efficiencies for different engine components.

The introduction of the relation between stagnation temperatures in Equation (3.8) and pressures in $\frac{p_0}{p} = \left(\frac{T_0}{T}\right)^{\frac{\gamma}{\gamma-1}}$, leads to a new set of equations for the component efficiencies, as summarized in Table 3.2.

18

Component	Efficiency
Compressor	$\eta_{is,c} = \frac{T_{01}}{T_{02}-T_{01}}\left[\left(\frac{p_{02}}{p_{01}}\right)^{\frac{\gamma-1}{\gamma}} - 1\right]$
Turbine	$\eta_{is,t} = \frac{T_{03}-T_{04}}{T_{03}\left[1-\left(\frac{p_{04}}{p_{03}}\right)^{\frac{\gamma-1}{\gamma}}\right]}$

Table 3.2: Isentropic efficiencies for turbine and compressor.

3.4 Deterioration of Aircraft Engine Components

It is a given fact that gas turbines, during normal operation, suffer deterioration like any other mechanical device. Gas turbine are particularly subjected to deterioration as they operate over a wide range of temperatures, pressures, speeds, loads and environments. All these deviations from design point cause a deterioration of the gas turbine performance, which can be defined as the cumulative effect of the performance degradations of various modules that constitute the engine, which are themselves composed of components such as blades, casings and spools.

According to reference [33], deteriorations that occur in gas turbines are divided into two time frames according to the number of cycles between entry in service and failure:

- Short term deterioration: those which occur in the first few hundred flights;

- Long term deterioration: those which occur more gradually as service usage accumulates.

The four major causes of engine degradation as well as some of its consequences are:

1. Flight loads which are responsible for rubbing contact on any of the seals between the static and rotating parts of the engine. These deteriorations appear in the early cycles of the engine's life time. The effects of flight loads cause degradation of the engine performance. They can be:

   (a) Centrifugal growth of rotating members, creating contact between rotating parts and casings;

   (b) Distortion of the engine's main casing;

   (c) Axial movement of rotating parts, this movement occurs due to induced vibrations.

2. Thermal distortion caused by changes in the original temperature pattern of the turbine inlet, this thermal effect can cause:

   (a) Changes in areas and consequently in clearances;

   (b) Increase in leakages;

   (c) Increase of temperature gradient between static and rotating parts.

3. Erosion of aerofoils in compressor or turbine blades and outer seals, which cause:

   (a) Increased roughness and pitting on blade's surface;

19

(b) Increase in bluntness of blades' leading edge;

(c) Loss of blade material, losing both camber and length;

(d) Increase in clearances.

4. Deposits, several particles enter the engine along with the air and can be deposited on compressor blades or even go farther and reach the turbine, these particles can also deposit in the cooling air ports, reducing the cooling air flow.

For this thesis, it will be emphasized the deteriorations that affect the compressors efficiency, since they are the ones whose effect will be studied using the modelling software GasTurb.

Aircraft engines have to produce thrust through the acceleration of the flow of air across the engine as explained in Section 3.2, the air used is not clear of solid particles which will affect the engine long term performance. The solid particles, either ingested (as illustrated in Figure 3.5) or by-product of combustion, along with the air flow, form a two-phase flow condition [33].
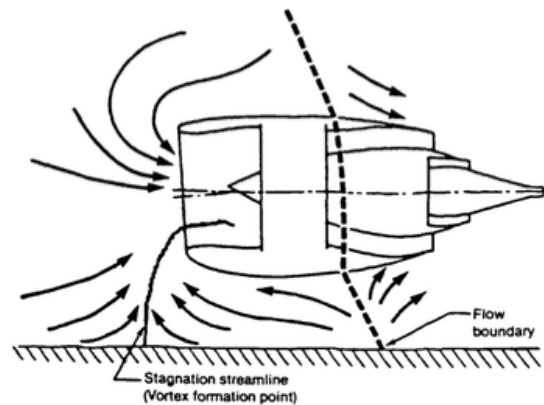
Figure 3.5: Dust ingestion in a turbine due to ground vortex formation [33].

The acting forces on air and particles are not the same since they have different inertias. As a consequence, the particles of dust or combustion products experience accelerations, decelerations and turning angles lower to the ones that the air experience, preventing those particles from following the path of the air through the blade passages, leading them to impact in the surface of the blades and the inner and the outer annulus.

The impact of particles on the blade surface increases pitting and roughness, altering the pressure distribution on it, therefore reducing its performance. Physically this can be explained by the increase of the friction coefficient, which leads to an increase in boundary layer thickness, changing the flow characteristics and surface area [20]. Blade chord restoration and refurbishment of blade surface are required after some operation time and can be conducted in MRO facilities such as TAP M&E [34].

The overall effect of compressor blades damage, from aerodynamic viewpoint, is an increase in the total pressure loss across the blade row. The prediction of this erosion, as well as the change in the compressor performance, represents a difficult problem [33]. Compressor performance deterioration by particulate environment can be represented in terms of efficiency variation as shown in Figure 3.6.
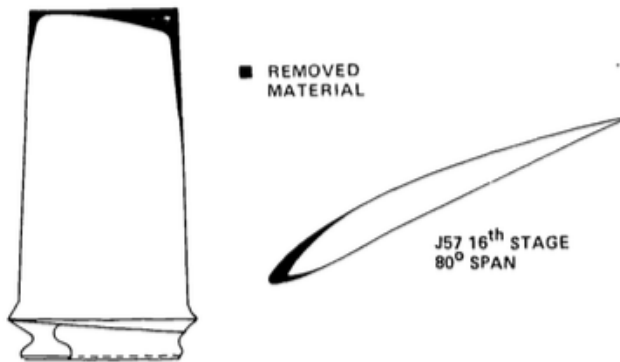
(a) Erosion on a compressor blade
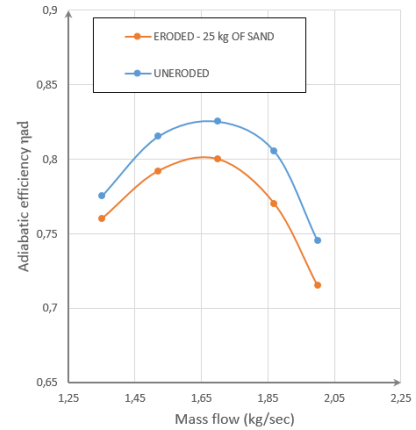
(b) Performance deterioration of a compressor.

Figure 3.6: Erosion of compressor blades and performance deterioration (adapted from [33]).

Finally, the last effect of the impact of particles on compressor blades is the increase in clearance between the compressor blade rows and casings. Tip clearance increase of HPC blades is a consequence of three mechanisms:

1. The trench dug in the rub strip during engine transient manoeuvres, this happens at low cyclic ages; the trench is caused by rubbing while there is no erosion of the blade;

2. Erosion of rub strip, this happens at moderate cycle age; both the blade and the flow path wall, ahead and aft of the blade tip erode over time;

3. Loss of blade length, at high cyclic ages, the blade is shortened as well as the flow-path wall, the latter to the extent that the trench is no longer visible.

The level of erosion depends on the stage of the compressor, the first stages are usually the ones which erode the most because they are the most exposed of all. Differences in erosion can be related to the use of different material for fabrication of different stages of the compressor. Figure 3.7 represents the different levels of erosion present during the engine's life time.
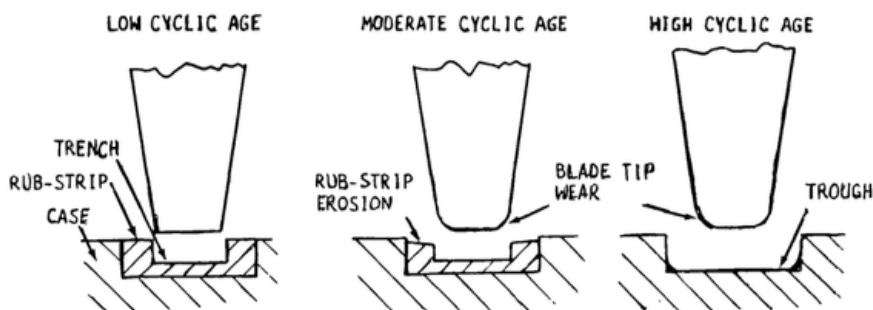
Figure 3.7: Evolution of erosion on HPC blades and rub-strips [33].

Chapter 4

Modelling of the CFM56-3 Engine

The present chapter will introduce the reader to the modelling of the CFM56-3 in GasTurb. The chapter is divided into four sections. The first section will introduce the modelled engine, the CFM56-3. The section number two will present the modelling software GasTurb and discuss alternatives to this software. The third section will present the modelling method used as well as a comparison with other modelling approaches used in past projects and, at last, in the fourth section results will be presented and discussed.

4.1   The CFM56-3 Engine

The CFM56-3 engine was developed in the second half of 70's and was certified in 1984 to be incorporated in Boeing 737. It is a high by-pass ratio engine (5:1), has two spools and axial flow.

The CFM56-3 exists in four different versions [22] as summarized in Table 4.1.

Version	Thrust	Application
CFM56-3-B1	20000 lb	B737-300/-500
CFM56-3-B2	22000 lb	B737-300/-500
CFM56-3-C1	23500 lb	B737-400
CFM56-3-B1 Derated	18500 lb	B737-500

Table 4.1: Versions of the CFM56-3.

About 4,500 CFM56-3s operate globally with 195 different airlines. The -3 fleet has accumulated more than 150 million Engine Flight Hours (EFH) and 108 million Engine Flight Cycles (EFC) and has an average EFC time of 1.4EFH (average of 1 hour and 24 minutes per flight)[35].

Although TAP M&E is capable of maintaining and overhauling the entire -3 family, TAP does not operates the CFM56-3 engine any more.

The versions of the engine with lower thrust ratings are obtained by de-rating successively the $-$C1 version, decreasing the thrust of the engine.

A brief description of the engine will be presented next. For further study, references [17, 22] present a more complete description of the engine.

4.1.1 General Constitution

The CFM56-3 is constituted by three main parts:

- Low pressure system;

- High pressure system;

- Accessory drive section.

A detailed cut-out of the engine can be seen in Figure 4.1. The Low Pressure (LP) system is constituted by the following components:

- Single-stage Fan, to which the Booster rotor is coupled;

- Three-stage Booster, with 4 stator stages. On a whole, the Fan and the Booster make the Low Pressure Compressor (LPC), when these parts are not coupled it is common to call the Fan and Booster as the Low and Intermediate (IPC) Pressure Compressors, respectively;

- Outlet Guide Vanes (OGV), used for guiding the Fan discharge air;

- 12 Variable Bleed Valves (VBV), used to control the flow of air to the engine core, they are located circumferentially in the Fan Frame between the Booster exit and the entrance of the High Pressure Compressor (HPC);

- Low Pressure Turbine (LPT), with 4 rotors and 3 stators, it is coupled to the Fan and Booster and it is used to power those components.

The High Pressure (HP) system is constituted by the following components:

- Nine-stage HPC rotor;

- Single-stage Inlet Guide Vanes (IGV), to guide the incoming air to the HPC;

- Three stages of Variable Stator Vanes, following the IGV, together they make the variable stator system of the HPC;

- Five stages of fixed geometry stators in the HPC's following stages;

- Outlet Guide Vanes (OGV), often referred as the stator of the 9th stage of the HPC, used to make the air enter the combustion chamber axially;

- Annular combustion chamber, with 20 fuel injectors;

- High Pressure Turbine (HPT) nozzles, for guiding the incoming air flow;

- HPT rotor, coupled with the HPC rotor, is used to power it;

- Nozzles of the LPT's first stage.

The Accessory drive section is used in two different moments. First, at engine start, it is used to move (start) the HPC. Once the engine starts, it is used to extract energy from the HPC for the multiple Accessories in the engine and airplane. It is composed by the following components:

- Inlet Gear Box (IGB);

- Transfer Gear Box (TGB);

- Horizontal Drive Shaft (HDS);

- Accessory Gear Box (AGB).
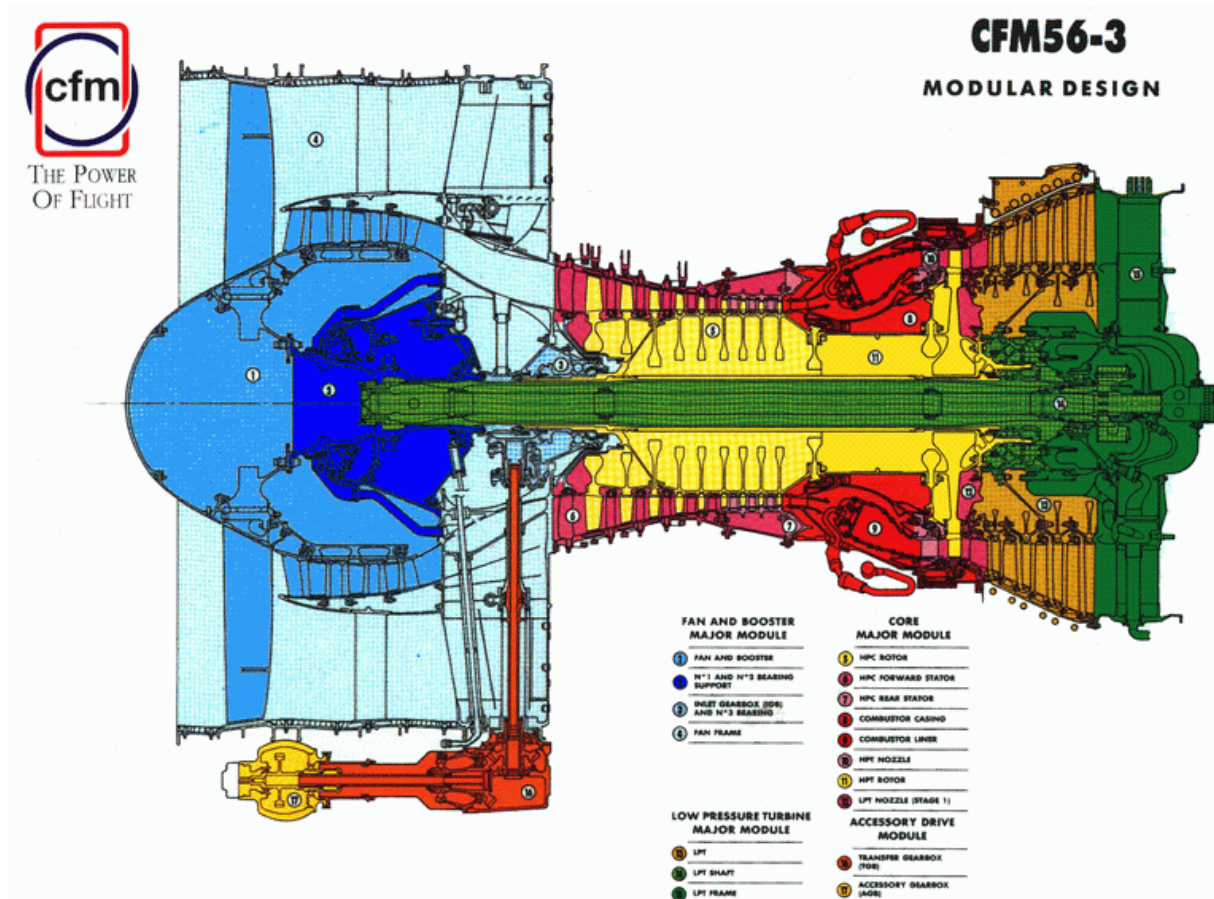
Figure 4.1: CFM56-3 schematic [22].

The CFM56-3 is a very simple and compact engine, comparing with its antecedent, the CF6. Its small length (2.833m) gives it robustness, making possible to reduce to two the number of frames supporting the engine, which are responsible for supporting the bearings which allow the various rotary parts of the engine to rotate.

The two frames are the Fan frame, located between the Booster and the HPC, and the Turbine Rear Frame (TRF), located at the rear of the engine [17].

4.1.2 Thermodynamic Stations

The flow in a turbofan engine follows two different paths which are independent from each other: primary and secondary flows.

The primary flow (also called core flow) enters the engine through the inlet and passes through the Fan, near its root, this passage leads to a small increase in its pressure. The primary air then enters the core passing through the Booster and HPC, where its pressure is raised greatly (around 24 times ambient pressure for this engine), it is then mixed with fuel and burnt in the combustion chamber, passes through the HPT and LPT, where it expands and it is discharged in the core nozzle.

The secondary flow (referred often as by-pass flow) enters the engine through its inlet as well, passes through the Fan in the periphery of its blades, suffering a pressure increase, it is then guided by the OGVs and is discharged. This flow is responsible for around 80 percent of the total thrust created in the engine [15].

The performance of an engine is studied making measurements in specific places in the engine, the measured parameters are mainly temperatures and pressures and the places where they are measured are referred as thermodynamic stations. A map showing the location of the stations and its nomenclature is given in references [17, 22], reproduced here in Figure 4.2.
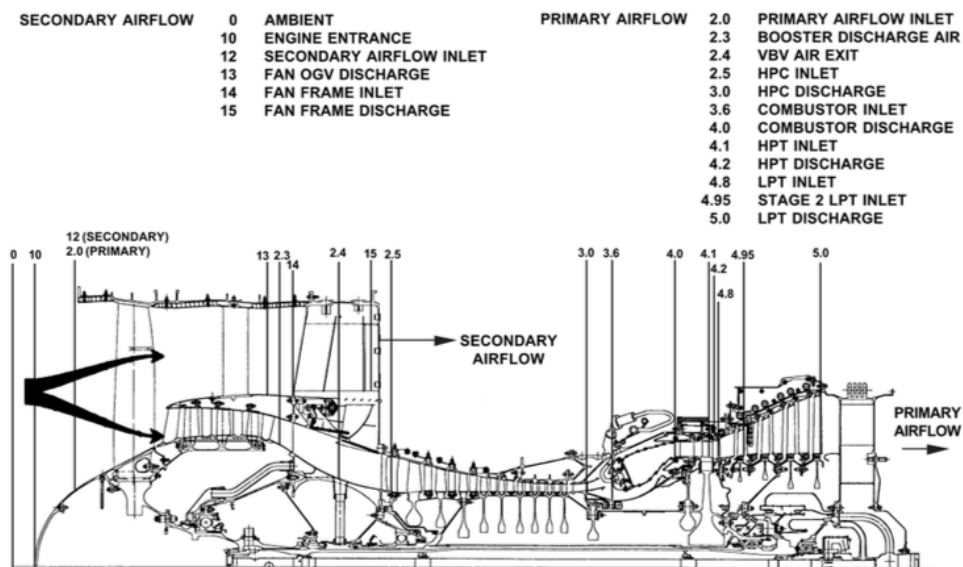
Figure 4.2: CFM56-3 thermodynamic stations [17].

The test bed in TAP M&E facilities follows the nomenclature presented in Figure 4.2, with a single difference in the temperature in the station 4.95, where T495 is exchanged for Exhaust Gas Temperature (EGT).

4.1.3 EGT Role in Performance Estimation

EGT is one of the most important parameters in engine performance studies, it is also the most important temperature in the hot section of the engine [7].

There are three main temperatures in the hot section of the engine: T4, T45 and EGT. T4 is the burner exit temperature, its value is affected by the amount of cooling air employed by the HPC, being this value unknown, it is also very difficult for TAP M&E to place a sensor in there due to the harsh conditions experienced (high temperature). T45 is measured in the LPT inlet, it is affected by the secondary air system and there is also the possibility of being affected by sensor biases [36]. On the other hand, EGT is independent of the secondary air flows since in that point all the internal secondary air flows have rejoined the main stream of air [7]. Thus, EGT becomes the best option for performance studies. The performance of an engine is estimated by means of an indicator, the EGT Margin. The EGT Margin is a complex parameter, it depends not only on the performance of the engine but also on the ambient conditions. The calculation of this engine parameter, for Standard and Hot days, is described in reference [7]. EGT Margin is defined as the difference between the EGT from the Performance Acceptance Checks in reference [21] and the EGT measured in the test bed, note that this value is corrected with K3 corrections(see Section 2.2). For Hot Day (HD) conditions, meaning an Outside Air Temperature (OAT) of 30 ^oC, the Engine Shop Manual [21] presents the EGT HD value, the EGT Margin HD is obtained subtracting to the given value the measured EGT HD.

EGT margins of the new CFM56-3 series engines are corrected and expressed for Hot Day conditions. These are:

- 115-120 ^oC for the $-$3B1 rated at 18,500lbs thrust;

- 90-100 ^oC for an engine rated at 20,000lbs thrust;

- 60-70 ^oC for the $-$3B2 or $-$3C1 rated at 22,000lbs thrust;

- 40-50 ^oC for the $-$3C1 rated at 23,500lbs thrust.

These EGT margins are only for new engines, and restored EGT margins following an engine first shop visit drop to about 70% of the new margin and the rate of EGT margin recovery and subsequent erosion also depends on the shop visit workscope [35]. Table 4.2 presents the values of the EGT Margin for the $-$3 Series for different OAT.

The EGT Margin deteriorates during the engine normal operation and it reduces faster for engines operated at higher thrust ratings. According to reference [35], a mature CFM56-3C1 rated at 23,500lbs operating in theatres where the average OAT is about 20 ^oC has an initial EGT margin erosion rate of 12 degrees in the first 1000EFC. It then loses about 6 degrees in the second 1000EFC, and 4 degrees per 1000EFC thereafter. Meaning that after 3000EFC this engine will have its EGT Margin reduced from 30 to about 8 ^oC, for a standard OAT of 30 ^oC. Some actions, such as de-rating the take-off thrust reduce the deterioration rate of the EGT Margin by reducing the EGT peak temperature, however, in hot and dusty environments this operation is not possible to perform.

VARIATION OF AVAILABLE EGT MARGIN WITH OAT FOR MATURE CFM56-3 SERIES ENGINES						
CFM56-3 rated at 23,500lbs Standard EGT margin = 30 degrees						
OAT deg C	0	10	20	30	35	40
Available EGT margin	126	94	62	30	14	0
CFM56-3 rated at 22,000lbs Standard EGT margin = 40 degrees						
OAT deg C	0	10	20	30	35	40
Available EGT margin	136	104	72	40	24	8
CFM56-3 rated at 20,000lbs Standard EGT margin = 80 degrees						
OAT deg C	0	10	20	30	35	40
Available EGT margin	176	144	112	80	64	48
CFM56-3 rated at 18,500lbs Standard EGT margin = 90 degrees						
OAT deg C	0	10	20	30	35	40
Available EGT margin	186	154	122	90	74	58

Table 4.2: EGT margin for different outside ambient temperature [35].

4.1.4 Correlation Test Report

The most important information for modelling an engine is to have reliable test data, without this information is not possible to model the engine since the modelling process consists in adapting a standard engine model to simulate the tested engine data.

The source of the data used in this thesis is a document composed by CFMI in 1991 named Correlation Test Report (CTR) [12]. The purpose of this document was to perform the correlation of the TAP M&E test cell, defining the facility modifiers (FM) for the CFM56-3 engine. To perform the correlation, CFMI used a stable engine, an engine whose parameters were known and had small variations. The engine is first tested in the CFMI facilities and the results were then compared with the ones from TAP test cell. The facility modifiers were defined as correlation factors between the two test runs.

The FM are defined for Net Thrust, EGT, Fuel Flow rate, High pressure spool speed (N2) and engine air flow (W2). They are described by polynomials that are only valid for a certain thrust range. Thus, apart from EGT, the parameters enumerated before must be corrected using these factors. EGT correction will be presented in Section 4.2.

The report [12] is also useful for calculating the Total Inlet pressure in bellmouth, PT2, which must be calculated by a function of N1R of the form:

$$PT2 = (a0 + a1 * N1R) * P0.$$

(4.1)

The engine used for the correlation is highly instrumented when compared with an engine coming to

28

TAP M&E facilities. The raw test data presented in the report was gathered across 41 operating points as presented in reference [7]. The temperatures and pressures presented in [12] are observed values, meaning that they are not corrected. In order to be able to compare data from different engines that may have been tested under different ambient conditions, temperatures and pressures must be corrected to Standard Day conditions using

$$\Theta = \frac{T2_{read}}{T_{ambSTD}} \,, \tag{4.2}$$

$$T_{corr} = \frac{T2_{read}}{\Theta} \,, \tag{4.3}$$

$$\delta = \frac{P2_{read}}{P_{ambSTD}} \,, \tag{4.4}$$

$$P_{corr} = \frac{P2_{read}}{\delta} \,, \tag{4.5}$$

where the temperatures and pressures with the subscript $read$ are the values measured in the test bed and the temperature and pressure with the subscripts $ambStd$ are 273.15K and 101.325kPa, respectively. These values are the standard values from the International Standard Atmosphere (ISA).

Remarks about Correlation Test Report   Before moving on to modelling the design point, some remarks on the data from the report must be presented, they will be based on reference [37].

The data in the report are from two different runs, the engine starts at Take-off, reduces its rotational speed from about 4900rpm to 3000rpm (Idle), 21 scans are printed for the first run. It goes back to Take-off and goes back to Idle, printing the other 20 scans.

In the first run the ambient temperature decreased from 20.8 to 18.5 ^{o}C while in the second run this temperature was constant and equal to 21.7 ^{o}C. During both runs, relative humidity was kept at 40 percent, the water-air-mass ratio is then 0.006. At these conditions, it is not expected that condensation shocks will occur, lower temperatures and higher relative humidities would be required for that. The occurrence of these shocks is important since they change flow properties such as temperature, pressure, velocity or entropy.

The mass flow entering the engine is found by calculation in reference [21]. It is a function of P2, T2, inlet flow coefficient and area. Since all the values used are consistent (show little scatter), the corrected mass flow for Standard day may be used without further corrections.

The reader may have noticed that the facility modifiers are a function of the engine thrust and that there is a facility modifier for the thrust itself. That is due to the fact that CFMI tested the engine in an open air test bed. In such conditions, measured thrust changes from one measured in an enclosed test cell like the one in TAP M&E facilities. This facility modifier is important since in an open air test cell the air approaches the engine in a stream tube, which creates an extra momentum causing a deviation between measured and true thrust [37]. This deviation must then be corrected in order to be possible to compare the thrust output of an engine tested in an open air test cell with other tested in an enclosed

test cell.

EGT is of most importance in performance studies as stated in subsection 4.1.3. Thus, its correction must be done with extra care. The official procedure for EGT correction is given in the Engine Shop Manual [21]. In that reference, EGT is corrected with $\Theta^{0,91}$, with factors concerning humidity and condensation, clearance correction and finally with the EGT facility modifier. However, there is no correction procedure for T5 (measured in the LPT outlet) in the Engine Shop Manual and, as it will be presented, these two temperatures are related. It is then impossible to reconcile EGT and T5 in a thermodynamic model if different correction procedures are used for the two parameters. Therefore both will be corrected with the Standard day correction, Θ.

Further analysis on temperatures measured in the correlation test report lead to a last modification on the data that will be later used for modelling the engine design point.

T3 is measured at the outer wall of the combustion chamber, as represented in figure 4.3. The proximity to the hot combustion chamber may be biasing the signal, increasing T3 by heat transfer. The Correlation Test Report presents an alternative, the sensor which measures the temperature of the HPT clearance control air, T4127.
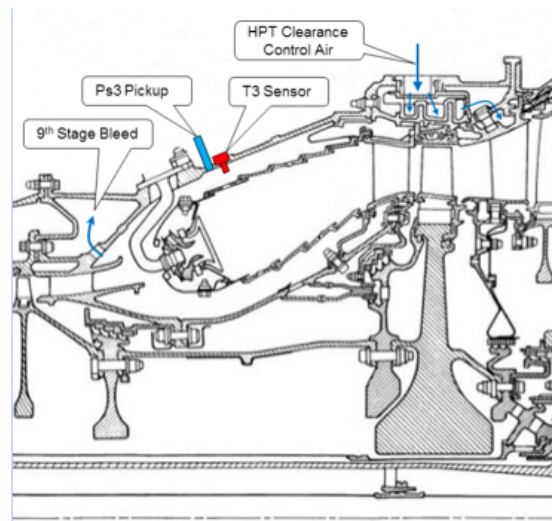
Figure 4.3: Location of T3 and Ps3 sensors [37].

However, this alternative can only be used while the clearance control air is being extracted from the HPC's 9th stage (for High Pressure spool speeds above 13760rpm [22]). According to reference [37], a valid way to surpass this limitation is to study the difference between T3 and T4127 while the 9th stage air is being extracted from the HPC. Figure 4.4 show the difference of these temperatures for the operational range of the engine.

The method used by Kurzke [37] was simply to extend the linear regression to the entire operational range of the engine, the results of this action will be presented in Section 4.4.

The last remark about the data from the Correlation Test Report is related with the fact that only the static pressure from the HPC's exit is measured and Total pressure will be required for GasTurb calculations. The relation between static and total pressure is given by Equation (3.9). From reference [37], the Mach number at HPC's exit is assumed to be M=0.2, which leads to $\frac{ps3}{p3} = 0.97$.
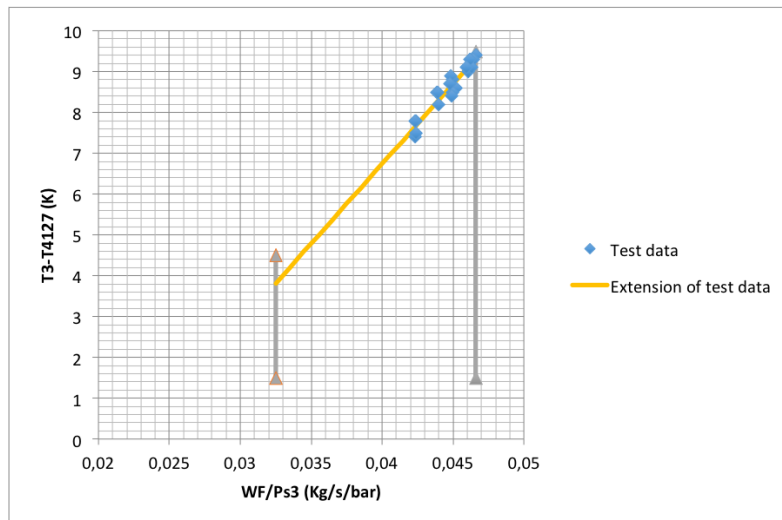
Figure 4.4: Difference between measured T3 and T4127.

4.2 GasTurb Modelling Software

GasTurb is a gas turbine performance calculation software, developed in the early 90's by Dr. Joachim Kurzke that continues to be updated to this day [11]. The gas turbine performance software is useful for working in gas turbine industry, airframe manufacturers and airlines, engine maintenance companies and operators of air, land and sea based gas turbines. It is helpful for consultants as well as research organizations and its graphical outputs make it suited to teach in universities. With it, users can evaluate easily the thermodynamic cycle of the most common gas turbine architectures, both for engine design and off- design conditions, this operating conditions will be explained in Section 4.3.

The software possesses three work scopes where different degrees of simulation detail are offered. They are, ordered by increasing complexity [11]:

1. **Basics**, if the objective is only to study fundamental questions such as gas turbine cycle analysis as described in many engineering textbooks. The input data are limited to the most important properties like pressure ratio, burner inlet temperature and the component efficiencies. All sophisticated details of the other two scopes are set to default values and hidden;

2. **Performance**, this scope adds the detail required for professional gas turbine performance simulations. The user get more data input options including the simulation of the internal air system and turbine cooling. Furthermore, there are more calculation options like cycle optimization and Monte Carlo studies;

3. **More**, the more complex working scope, while for the **Performance** scope only a few dimensions of the engine were required as the nozzle area of a turbojet engine, in **More** the flow area at all the thermodynamic stations will be calculated during cycle design and from that the static quantities are determined during both cycle design and off-design simulations. Additionally the dimensions of the flow annulus are derived, compressors and turbine disks designed and a cross section of the engine is shown.

For this thesis, since no information about internal dimensioning is available in the manual of the engine, the working scope that will be used is Performance.

The software allows to perform many tasks such as the optimization of a thermodynamic cycle, where the user is asked for the properties that will be varied to get the best solution for another engine variable, e.g., the user can use variables as the Outer Fan Pressure Ratio, HP Compressor Pressure Ratio as the second variable and as the third variable Burner Exit Temperature to minimize Specific Fuel Consumption. At the same time, the user is allowed to set restrictions to the optimization in other properties as the HP Turbine pressure ratio, for which values superior than 5 are not realistic. GasTurb requires from the user knowledge of thermodynamics. This and more examples for other tasks are presented in reference [11].

There are other softwares available in the market that are able to study the performance of a gas turbine, Gas Turbine Simulation Program, or GSP [38], is a good alternative to GasTurb. The work done by Sung [39] is useful for comparison purposes, the author successfully compared the results of this two softwares with the traditional method used in turbomachinery classes. A one-spool jet engine was used for the purpose.

Matlab-simulink [40] is another software used for developing models of gas turbines. *A Modular Code for Real Time Dynamic Simulation of Gas Turbines in Simulink*, by S. M. Camporeale, B. Fortunato and M. Mastrovito describe this procedure (see reference [41]). This simulation describes transient behaviour of any configuration of gas turbine. The work developed in reference [41] had satisfying results. Thus, it is then possible to state that Matlab-simulink is capable of monitoring in real time the performance of gas turbines. Both GasTurb and GSP allow transient analysis as well and their graphical interface makes them more user-friendly than this approach.

The modelling of a gas turbine starts with choice of its configuration from GasTurb's initial window, shown in Figure 4.5, and with the choice of the working scope, which will be Performance, as stated in beginning of this section. To model the CFM56-3 engine, the configuration to choose is the *Geared Unmixed Flow Turbofan*, since it is the one that has a Booster. Care must be taken with the gear ratio in this engine configuration, this value must be equal to one since the fan rotates at the same speed as the LP Turbine.

4.3   Method for Modelling an Aero Engine in GasTurb

The performance simulation of any gas turbine can be generally divided into two parts: design point analysis and off design modelling. Both are performed as part of engine design or performance studies of existing engines [11, 42].

When the purpose of a project is to develop a new engine, the engine manufacturer carries out a study to select the most suitable thermodynamic cycle in order to achieve the mission objectives, these cycles are representative of typical use of the engine and are referred as the engine design point. The result of such study is an optimized design point for that specific mission which will fix the choice of the components of the engine, such as nozzle areas, number of stages in a compressor or turbine or even
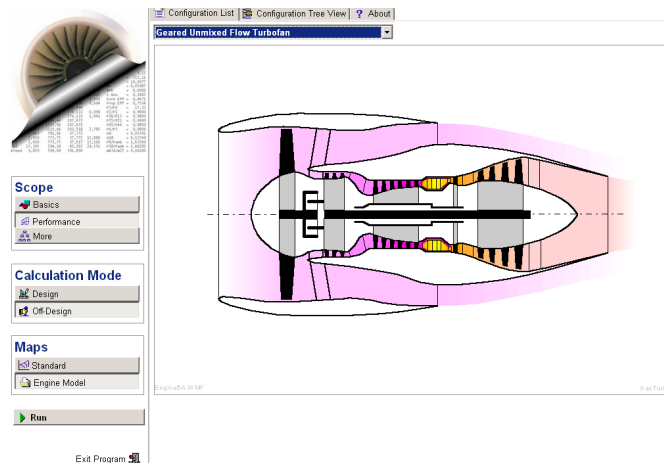
Figure 4.5: Selection of the engine configuration [11].

the number of blades per stage. Further analysis of this process is given in reference [26].

At this point, the performance of the engine is only known at its design point, the off-design performance of the engine will be found by varying the settings on the engine, such as ambient conditions or thrust levels. This step involves both the manufacturer and the user to analyse the engine over its expected operating envelope.

For this thesis, the objective is not to develop a new engine but to study the performance of an existing one, for which a limited amount of information is available. The available testing data will be used to match the performance of a standard two spool turbofan engine presented by the software to the performance of the engines whose tests data is available [43]. For this thesis the correlation test report [12] is the main source of test data. This data is used to create a whole engine system model: engine thermodynamic model with control commands.

Thus, design point analysis transits into selecting a suitable operating point at which the maximum engine data is available. The model is then tailored to match the data of that specific point. This point is referred to as cycle reference point (CRP) in the software and is the starting point of the modelling [19].

Next, the engine model is supplied with generic component maps, which are scaled to fit the cycle reference point. These maps will define operating points of the components at all off-design conditions throughout the engine operating envelope.

Various works on performance prediction reveal multiple utilities for thermodynamic models of engines. Shakariants [42] developed thermodynamic models of engines using Kurzke method [44, 19] and performed various study cases for different engines with the objective of predicting their exhaust gas emissions.

The modelling of the CFM56-3 engine will be based on reference [19], in which Kurzke reveal how to model an engine with a limited amount of information and how to verify the validity of the obtained model.

4.3.1 Design Point

As stated before, the design or cycle reference point (CRP) is the anchor for all performance studies. It is of most importance to be confident about the data used because this data will be used to adapt the nominal conditions of the standard engine model to simulate the data from a single operating point that was chosen to become the design point of the model. Thus, from the 41 operating points presented in the correlation test report (CTR), one will be chosen to become the design point of the model.

At medium thrust settings, the CFM56-3 has variable geometry, Variable Bleed Valves (VBV) and Variable Stator Vanes (VSV) have positioning schedules, these schedules are presented by Ridaura in reference [7]. Operating points with variable geometry should be avoided since their positioning of the VSV and VBV introduce modifications in the engine parameters and the exact positioning is not indicated in the CTR. Another aspect to consider is the existence of condensation shocks at the engine inlet, more likely to happen at higher thrust settings, for a given relative humidity [37]. Thus, the selection of the operating point will be between the higher thrust setting points. Since no large discrepancies occur between those higher load points, the occurrence of condensation shocks may be neglected. However, in the first calibration run, one of the T5 probes indicated rather low values and, for that reason, the operating point selected will be the one with the highest thrust in the second calibration run.

Next thing to do is to adjust the cycle model to the known data while using engineering judgement to estimate all the unknown model details. In the cycle design mode, input parameters are typically the compressor pressure ratios, burner exit temperature, total mass flow, by-pass ratio and the component efficiencies. At first, some of the required data can be obtained either directly or with some calculations from the CTR, while for the unknown data only estimations are needed at this point, these values will be obtained by iterating them. Together with assumptions about the secondary air system and parasitic losses, the turbine flow capacities, pressure ratios and nozzle areas may be derived. No component maps are needed for these cycle design mode calculations [19]. The software allows the user to iterate unknown parameters, requiring a known one for each iteration performed. The list of iterations used is presented in Table 4.3.

Variable			Target		
Nomenclature	Units	Range	Nomenclature	Units	Value
Isent. IPC Efficiency	-	[0.85 ; 0.95]	Booster Exit Temperature T25	K	369.92
Isent. HPC Efficiency	-	[0.85 ; 0.95]	HPC Exit Temperature T3	K	770.80
Burner Exit Temperature T4	K	[1550.00 ; 1700.00]	Fuel Flow WF	$Kg.s^{-1}$	1.095
Isent. LPT Efficiency	-	[0.85 ; 0.95]	LPT Exit Pressure P5	KPa	148.13
Design By-pass Ratio	-	[4.80 ; 5.50]	LPT Exit Temperature T5	K	862.60
By-pass Duct Pressure Ratio	-	[0.90 ; 1.00]	By-pass Nozzle Throat Area	m^2	0.7424
Design Core Nozzle Angle	o	[0.00 ; 10.00]	Core Nozzle Throat Area	m^2	0.2933

Table 4.3: Design point iterations.

The iterations require some caution since the user has to judge whether they are physically coherent or not, e.g. it does not make sense to iterate component efficiencies for values greater than unity, it would violate the 2nd Law of thermodynamics [32]. Additionally, the user must not restrict the variables

range too much or convergence problems may arise. Once the calculation of the cycle reference point is made, printing the output of the thermodynamic cycle is possible.

```
              W         T         P       WRstd
Station     kg/s        K        kPa      kg/s          FN        =      99,72 kN
  amb                 288,15   101,325                  TSFC      =   10,9815 g/(kN*s)
    2       313,798   288,15   101,325    313,798       WF        =    1,0951 kg/s
   13       260,957   338,15   167,693    170,812       s NOX     =    0,7837
   21        52,841   288,16   101,335     52,836
   22        52,841   288,16   101,335     52,836       Core Eff  =    0,4233
   24        52,841   369,92   221,113     27,436       Prop Eff  =    0,0000
   25        52,841   369,92   221,113     27,436       BPR       =    4,9386
    3        52,841   770,80  2447,503      3,578       P2/P1     =    1,0000
   31        45,391   770,80  2447,503                  P3/P2     =      24,15
    4        46,486  1577,62  2325,127      4,740       P5/P2     =    1,4619
   41        50,185  1522,97  2325,127      5,028
   43        50,185  1162,83   569,646                  P16/P6    =    1,12360
   44        53,355  1141,00   569,646                  P16/P2    =    1,62621
   45        53,355  1141,00   569,646     18,885       P6/P5     =    0,99000
   49        53,355   862,60   148,131                  A8        =    0,29330 m²
    5        53,355   862,60   148,131     63,145       A18       =    0,74236 m²
    8        53,936   861,65   146,650     64,441       XM8       =    0,75979
   18       260,957   338,15   164,776    173,836       XM18      =    0,86335
Bleed        0,000   770,80  2447,503                  WBld/W2   =    0,00000
-------------------------------------------            CD8       =    0,97863
Efficiency          isentr  polytr   RNI     P/P       CD18      =    0,98728
  Outer LPC         0,8901  0,8976  1,000   1,655      PWX       =       0,0 kW
  Inner LPC         0,9001  0,8934  1,000   1,000      V18/V8,id=    0,71064
  IP Compressor     0,8776  0,8902  1,000   2,182      WBLD/W22  =    0,00000
  HP Compressor     0,8677  0,9026  1,621  11,069      Wreci/W25=    0,00000
  Burner            0,9995                  0,950      Loading   =    100,00 %
  HP Turbine        0,8500  0,8273  3,281   4,082      e444 th   =    0,82491
  LP Turbine        0,8713  0,8510  1,119   3,846      WBLD/W25  =    0,00000
-------------------------------------------
HP Spool mech Eff 0,9900  Nom Spd  14324 rpm           WHNGV/W25=    0,07000
LP Spool mech Eff 1,0000  Nom Spd   4835 rpm           WHcl/W25  =    0,06000
-------------------------------------------
P22/P21=1,0000 P25/P24=1,0000 P45/P44=1,0000           P6/P5     =    0,9900
-------------------------------------------            P16/P13   =    0,9826

hum [%]    war0      FHV      Fuel
   0,0   0,00000   42,769   Generic
```

Figure 4.6: Cycle reference point.

Figure 4.6 shows the results of the simulation on GasTurb of the first scan of the second test run, scan number 22 of the Correlation Test Report.

It is also possible to print the iterations results for the design point, as exemplified in Figure 4.7.

```
Iteration converged after 1 loops.

Iteration Variables:
1:   Isentr.IPC Efficiency  (0,85...0,95)        = 0,877601
2:   Isentr.HPC Efficiency  (0,85...0,95)        = 0,867732
3:   Burner Exit Temperature K (1550...1700)     = 1577,62
4:   Isentr.LPT Efficiency  (0,85...0,95)        = 0,871299
5:   Design Bypass Ratio  (4,8...5,5)            = 4,93858
6:   Bypass Duct Pressure Ratio  (0...2)         = 0,982605
7:   Design Core Nozzle Angle [°]  (0...10)      = 6,05991

Iteration Targets:
1:   Booster Exit Temp T24                       = 369,92
2:   HPC Exit Temperature T3                     = 770,8
3:   Fuel Flow                                   = 1,0951
4:   LPT Exit Pressure P5                        = 148,131
5:   LPT Exit Temperature T5                     = 862,6
6:   Bypass Nozzle Area                          = 0,74236
7:   Core Nozzle Area                            = 0,2933
```

Figure 4.7: Iterations results.

From Figure 4.7 some important information can be extracted. This figure shows the results of the iterations and reveal if any of the variables is near the lower or upper limits of the range defined for them. This is important to correct any convergence problems that may arise in the process of defining

35

the design point, e.g. if a variable reaches a limit, the calculations will not converge and the user may have to increase the interval in which the variable is iterated.

Comparing Figures 4.6 and 4.7, one can see that the iteration targets were respected. Note that the Booster Exit Temperature or T24 in GasTurb is T25 in CFM nomenclature.

The calculated By-pass Ratio is 4.94:1, which is near the value given by CFM for this engine, 5:1. The By-pass Ratio cannot be an iteration target since the conditions at which the engine has the referred ratio are not revealed by the manufacturer.

Although EGT is one of the most important parameters for performance studies in an engine, this parameter was not used as an iteration target for the design point calculations due to the fact that it is not among the GasTurb parameters, it must be calculated as a composed value. Instead, the EGT will be used as a check of the design point validity.

EGT is measured with 9 probes in the vane of the 2nd LPT Stage [22]. Thus, EGT may be obtained knowing the inlet and outlet temperatures of the LPT (T45 and T5) and, with that, estimating the temperature drop due to work extraction on the first stage of the LPT. Such study was conducted by Kurzke in reference [37]. According to Kurzke, EGT may be calculated as:

$$EGT = 0.976 * [T45 - 0.217 * (T45 - T5)] . \tag{4.6}$$

This equation was composed by Kurzke and fits the data from the correlation test report. EGT is calculated as the difference between the inlet temperature and the temperature drop in the first stage of the LPT, multiplied by a factor 0.976. The use of the factors 0.976 and 0.217 will be explained next.

Although the LPT of the CFM56-3 has four stages, the temperature drop in the different stages will not be the same (the factor 0.217 would become 0.25, meaning that the in each stage the temperature would drop 25% of the total value), instead, Kurzke opted to take into account the different diameters of the rotor blade of the four stages. With the assumption of constant aerodynamic loading in the four stages, $\frac{\Delta H}{u^2} = const$, Kurzke reached a drop of 21.7% of the total temperature drop in the LPT, $\Delta T_{1ststage} = 0.217 * (T45 - T5)$.

The EGT is not measured in the main stream of the LPT air, it is measured by a thermocouple located in the interior of the vane. The air enters the support of the thermocouple through four holes disposed at different heights as presented in Figure 4.8.

The air has to enter the holes and flow through the thermocouple tip, this reduces the dynamic head of the gas, which leads to a recovery factor of the T495 lower than one [37]. A recovery factor relates true and indicated total temperatures:

$$r = \frac{T_{ind} - T_s}{T_{true} - T_s} , \tag{4.7}$$

where T_s is the static temperature.

According to this reference, the difference between T495 and the temperature after the first stage, $T451 = T45 - \Delta T_{1ststage}$, may be calculated using Equation (3.8) for a flow Mach number of around 0.3, which result in the presented factor of 0.976.

The design point is now successfully defined, the geometry of the virtual engine is defined and it is
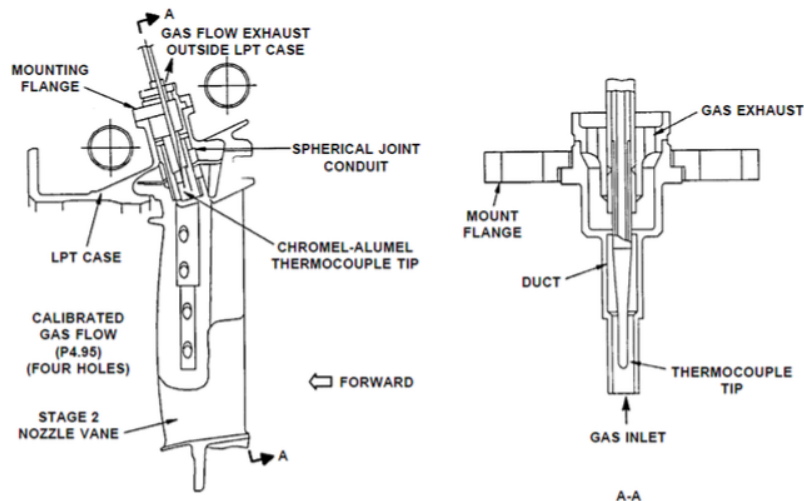
Figure 4.8: Schematic of the TT495 sensor [18].

now possible to start modelling the engine for off-design conditions.

4.3.2 Off-design Modelling

The Off-design performance analysis starts by selecting the proper components maps from the software library. In GasTurb, only the maps of the turbomachinery are supplied for the analysis, meaning that all the nozzles and ducts have fixed losses and the combustion chamber has fixed efficiency and pressure ratio throughout the entire operating range. Those losses were defined in the design point in Subsection 4.3.1.

As stated in Section 1.1, the OEM's do not reveal to the general public the original component maps. The solution is to use the generic maps provided by GasTurb and to adapt them to the Correlation Test Report data, following the procedure described in references [44, 19, 42].

The adaptation of the generic component maps to match the real ones is done by scaling the corrected mass flows, corrected rotational speeds, pressure ratios and efficiencies in the generic maps, the scaling procedures are described by Kurzke [19].

The suitability of the selected maps and location of the reference point in the map will essentially determine the degree of deviation between the simulated off-design performance and original engine data [42].

The matching procedure should start by the compressor maps and end with turbine maps since the latter ones have less influence in the overall performance of the model, as Kurzke states in reference [37].

Component Maps For the analysis of the performance, turbomachine parameters such as mass flow rate, rotational speed, pressure ratio and temperature ratio are needed. Thus, it is desirable to know the relationships between these parameters to understand what effects has the variation of one parameter on the others [45].

These parameters of the components are often calculated by complex codes using velocity diagrams, fluid mechanics, empirical correlations, and even computational fluid dynamics. The physics of turbomachinery flow simplify when corrected airflow is used rather than absolute flow and corrected speed is used instead of absolute speed in rpm. The measurement of the relationships between corrected flow, corrected speed, pressure ratio, and temperature ratio (or efficiency) for a turbomachine results in a component map.
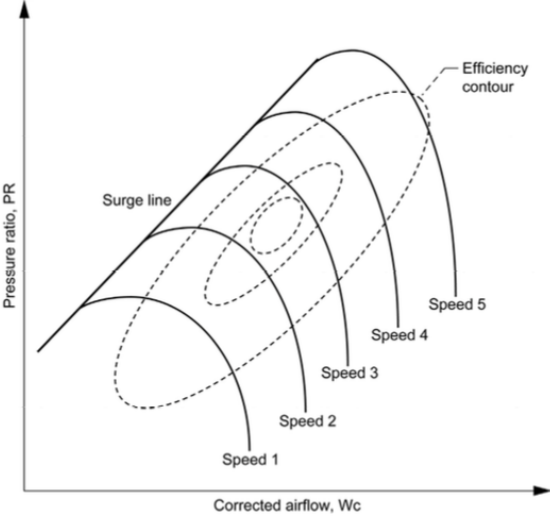
Figure 4.9: Generic compressor map [45].

Figure 4.9 presents a generic map with the nomenclature used to describe it. A compressor map is a plot of pressure ratio in the compressor versus corrected airflow that enters the turbomachine. In the map is shown the surge line of the component, the line that connects the upper left of each speed characteristic, it gives the maximum pressure ratio allowed without the compressor surging, for a given corrected flow. Each speed characteristic (or line) also has a lower limit: the line becomes vertical as the machine chokes and no further mass flow can be passed. The speed lines are normally given in relative corrected speed (relative to design point speed). Constant values of adiabatic efficiency of the compressor are given by the efficiency contours. The peak efficiency of the compressor happens in the center of the smallest efficiency island.

Figure 4.10 shows the scaling of a compressor map with some of the data values identified before and after the scaling. The application of the compressor map in the left as it is to a complete engine system is quite limited in terms of results, however, if the map could be scaled its usefulness would be dramatically increased. GasTurb allows the map to be scaled up or down in pressure ratio, efficiency, flow, or any combination of the three. An example of a compressor map scaling from reference [45] will be presented, using the data from Figure 4.10.

Assume that the design point is identified as 100 percent speed and 25 percent surge margin, resulting in an unscaled pressure ratio of 2.0, corrected airflow of 500 lbm/s, and adiabatic efficiency of 0.87. Further assume that the desired values of pressure ratio, flow, and efficiency at that point are 1.80, 475 lbm/s, and 87.5 percent respectively. The ratio of the desired value to the unscaled value of each parameter determines the scale factor applied to the map (one scale factor for each parameter).

(a) Example of an unscaled compressor map   (b) Scaled version of the map in the left.
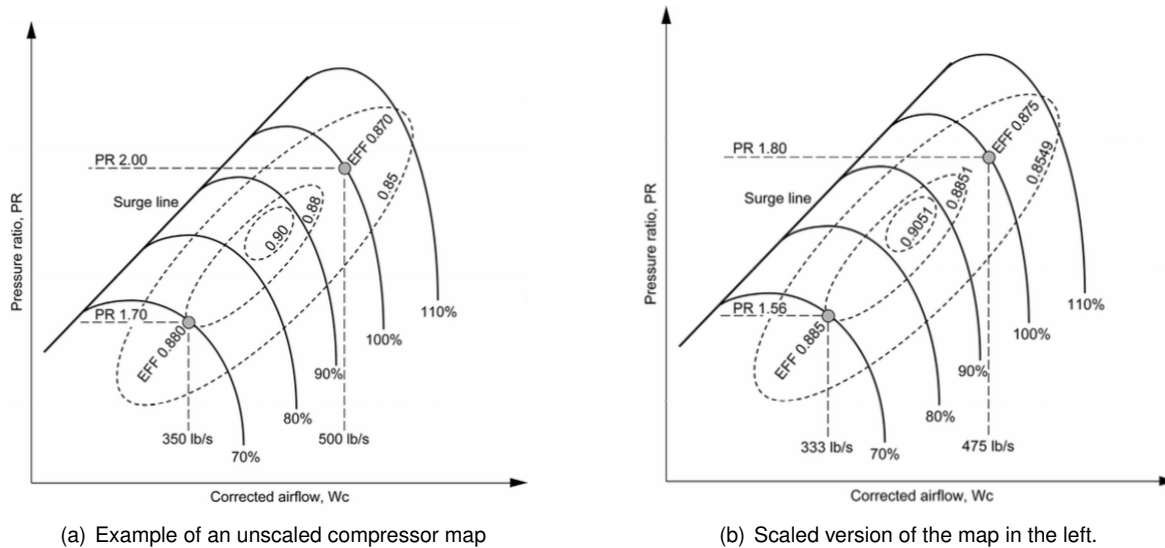
Figure 4.10: Scaling of compressor map [45].

According to reference [45], the scale factors are calculated for the design point and defined in Table 4.4.

Parameter	Scale Factor
Flow	$FlowScaleFactor = \frac{W_{CORR\|desired}}{W_{CORR\|unscaled}}$
Efficiency	$EfficiencyScaleFactor = \frac{\eta_{desired}}{\eta_{unscaled}}$
Pressure Ratio	$PRScaleFactor = \frac{PR_{desired}-1}{PR_{unscaled}-1}$

Table 4.4: Efficiency and flow scale factors.

Due to the shape of the speed characteristics in compressor maps (the curve at its top), two problems may arise:

1. for a given corrected speed and pressure ratio, it is possible to have two solutions of corrected flows (number 1 in figure 4.11);

2. for corrected flow and speed values near the vertical part of the speed characteristic, the value of the pressure ratio is indeterminate, (number 2 in figure 4.11).

Thus, in order to determine uniquely the corrected flow, speed and pressure ratio in a compressor map, it is required a second independent parameter (the first is the corrected speed), that parameter is called the R-line or, as Kurzke refers to it, β-line [11, 45].

For a β-line factor equal to 1.0, the β-line will coincide with the surge line. The remaining β-lines, for factors between 0.0 and 1.0, are roughly parallel to the surge line with decreasing β-line value corresponding to higher surge margin, as shown in Figure 4.12. As stated in Chapter 1, these lines have no physical meaning; they are simply lines (see figure 4.12) used so that for any value of β-line and corrected speed will uniquely define the compressor operating point. So, given β-line value and corrected speed, the compressor pressure ratio, corrected flow and adiabatic efficiency are known, and further,
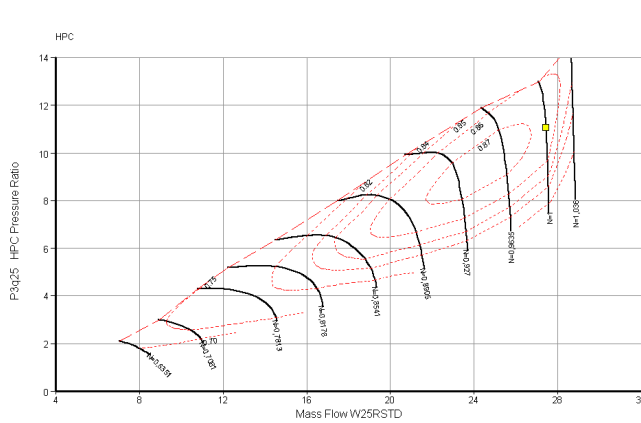
(a) Indetermination of flow/pressure ratio values in a compressor map.
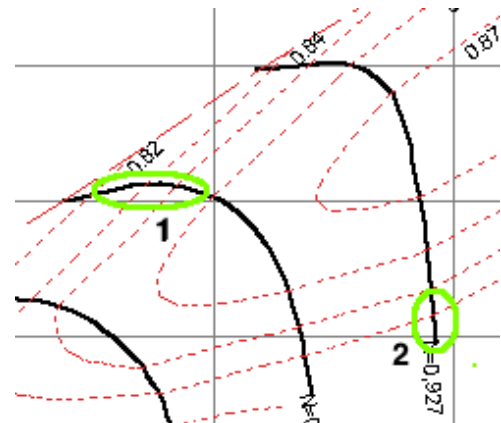
(b) Close up of the figure in the left.

Figure 4.11: Indetermination in a compressor map.

the derivatives of these parameters can be calculated with respect to β-line and corrected speed which is critical for computational convergence [45].
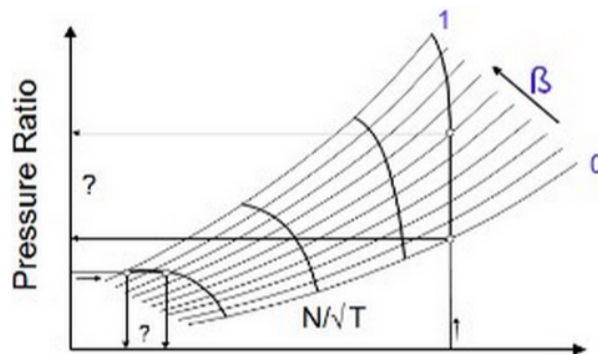
Figure 4.12: Generic compressor map with β-lines [11].

No β-lines are required for turbine maps since in these the problems referred for the compressor maps do not occur, in turbine maps pressure ratio and speed uniquely determine corrected flow and efficiency. As a last remark on this topic, the software will accept any value given for these factors by the user (may emit a warning but does not stop the calculations); thus, the user must possess critical spirit and review all the inputs of the calculations.

Additional data used in off-design matching   The data measured in the Correlation Test Report is composed of temperatures and pressures of multiple thermodynamic stations across the engine, thrust, fuel flow and spool speeds. Additionally, total air mass flow is presented not as a measurement, but calculated as a function of inlet area, total and static pressures and total temperature [37]. This data will be used to study the agreement between the model and the measured data from the CFMI Report, however, information about efficiencies, pressure ratios and air flows at component level (only total air flow is presented) would be much more useful during the matching process.

In order to get the off-design performance of the model matching the measured data, the component maps must be modified in order to modify the performance of the components.

40
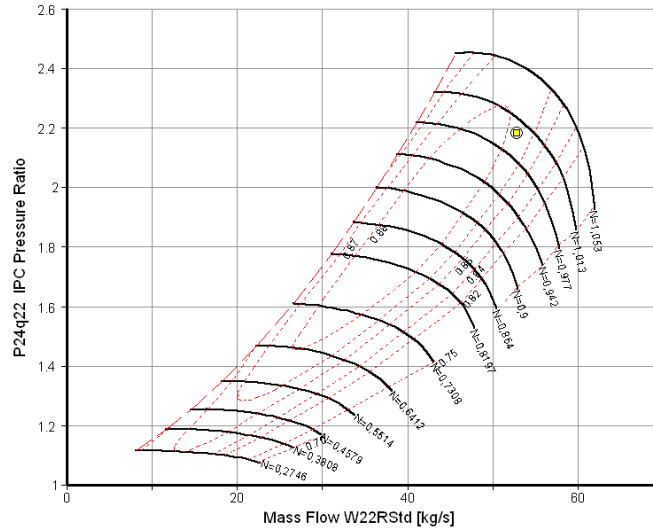
Figure 4.13: Booster map.

Figure 4.13 represents the Booster map, or Intermediate Pressure Compressor (IPC) map, its x-axis represents the core corrected flow (W_{22RStd}) and it has in the y-axis the Booster pressure ratio, $PR_{booster} = P25/P22$. Although none of these quantities is measured directly in the Correlation Test Report, they can be calculated from the data measured. The calculation of the pressure ratio is quite simple, it is calculated using the Booster outlet pressure, P25, corrected to Standard Day and dividing it by the core inlet pressure, P22, which is constant for all the engine operation, when corrected to Standard Day. P22 value is taken from Ridaura's model from reference [7], his work on the CFM56-3 was quite helpful for the present study since his model was accurate. Its data could therefore be used with confidence. The core corrected flow can be calculated as well as the by-pass ratio,

$$BPR = \frac{W2}{W22} = \frac{W2_{corr}}{W22_{corr}} \ . \tag{4.8}$$

The corrected core flow can only be calculated using Equation (4.8) due to the fact that the temperature and pressure at engine and core inlets are almost the same, so the Standard Day correction applied to the two is the same.

After having these values calculated, it is possible to print the operating line of the Booster in its map, using a comparative data file or TST file. For the model using the standard GasTurb maps results Figure 4.14.

It is possible to check in Figure 4.14 that the model data (yellow points) do not match the Correlation Test Report data (purple points), while using the unscaled standard maps.

Doing the same procedure for the HPC is not as direct, the HPC map has in its axis, as any compressor map, its pressure ratio $PR_{HPC} = P3/P25$ versus corrected mass flow W_{25RStd}. The problem is that the corrected mass flow is not within the measured data in the Correlation Test Report but is needed to place the operating line of the HPC in its map. In order to get an estimation of the corrected flow in the HPC, Ridaura's model will be used again, to study the correlation between the overall pressure ratio P3/P2 and the corrected flow and create a function of the type:
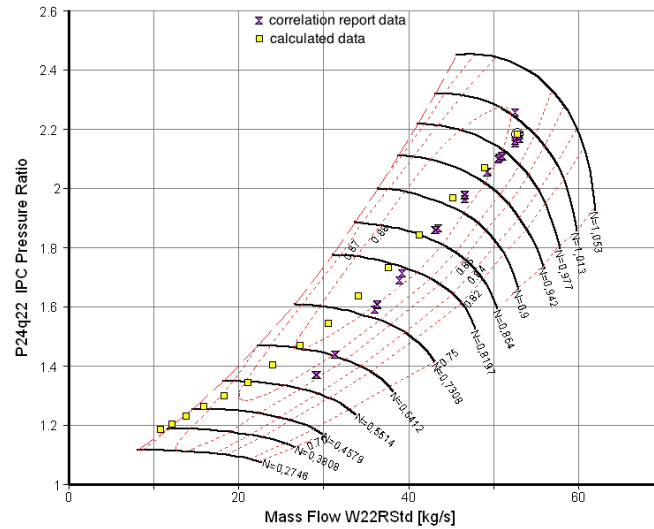
Figure 4.14: Booster map with operating line printed.

$$W25_{RStd} = f\left(\frac{P3}{P2}\right).\qquad(4.9)$$

Since the overall pressure ratio is measured, we have now an estimate of the HPC corrected flow and is now possible to print the HPC operating line in its map.

The introduction of this new data, referred as hybrid data by Kurzke, to the model will make the matching process easier since now it is possible to visually check the convergence of the model to the measured data.

Estimation of Components Maps   As stated before, the modelling of the off-design operation of the engine starts with the GasTurb standard maps. These maps are plots of total pressure ratio versus corrected mass flow for the lines of constant corrected speed. Contours of constant adiabatic efficiency are also visualized in the same plot. Figure 4.9 illustrates a general compressor map used in the model of a turbofan engine [42].

The first action performed on the model was to roughly position the cycle reference points of the different components, this was suggested by Wemming [43]. This procedure is composed of three parts:

- reduce the HP spool speed by a small step of 1 to 2%;

- check the position of the cycle reference points in terms of map coordinates, map speed coordinate and beta coordinate;

- remove the spool speed limitation and position the cycle reference points of the different components in the map coordinates read before.

Once the model reaches a good level of agreement, the cycle reference points are near their final positions.The next step is to change the operation of the components across their operating range, changing their efficiency and corrected speed.

Every compressor map (Fan, Booster or HPC) yields the following relations - referred to as correlations by Kurzke [19, 37] - along any given operating line:

- Corrected mass flow - efficiency;

- Corrected mass flow - corrected speed.

The procedure to modify these correlations is described in references [19, 42] and with the additional information from reference [37] presented before, the method became more systematic, since the new data calculated from the existing test data enabled to print the operating lines of the components to check convergence after every correction was made.

The following step is to re-locate the reference points in the maps in order to tune the model to the desired output. This changes the peak efficiency of the scaled map. As a consequence, moving the reference point to a region with poor efficiency will yield an efficiency increase towards part load. Should the reference point be located in the high-efficiency region of the map, the effect will be opposite. This brings small-changes to the corrected mass flow - corrected speed correlation. The two procedures must be done until the model can simulate the Correlation Test Report data with great precision.

Until now, only compressor maps were modified in the modelling and that is because changing turbine maps has a weaker effect on model performance for turbofan engines compared to the changes for the compressor maps described above [42]. No special procedures have been therefore developed for this components, since the software does not allow to modify these correlations in turbines. The only measure performed was to re-locate the cycle reference points in both LPT and HPT in order to optimize the simulation of the LPT exit temperature T5. The simulation of the temperature T5 is important since it is directly connected to EGT as shown in Equation (4.6).

4.4 Verification and Validation

Now that the model is developed, the first thing to do is to compare its accuracy simulating the measured data. According to reference [37], there are three important criteria:

- The SFC versus Engine Corrected Air Flow curve, which is a measure of thermal efficiency;

- Accuracy of the exhaust gas temperature, EGT;

- Accuracy of the LPT exit temperature, T5, which is usually the parameter with worst simulation results.

The SFC curve calculated by GasTurb agrees well with the measured data for corrected engine flows above 240kg/s, which corresponds to thrust values above 57kN. Bellow that value, the results are not precise due to the action of the HPT clearance control system, which causes the step in the SFC curve, as represented in Figure 4.15.

There are three types of thermodynamic models, according to their precision:
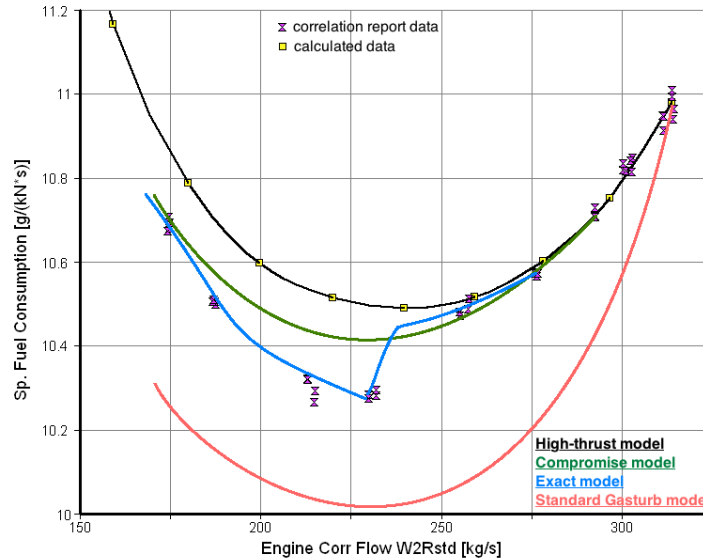
Figure 4.15: SFC curve for different types of models.

- Compromise model, a model that does not consider the HPT clearance control system and tries to be precise at low and high spool rotations; takes in consideration Variable bleed valves (VBV) and Variable stator vanes (VSV) schedules;

- High-thrust model, an accurate model for higher thrust settings, indicated for performance studies;

- Exact model, takes in consideration both the HPT clearance control system and the VBV's and VSV's schedules.

For this thesis, the objective was to develop a High-thrust model since this kind of model is precise for higher thrust settings, where the performance of the engine is critical. During a typical flight, the engine is always at thrust settings above 80%, which is within the zone where the developed model is more accurate.

Being a high-thrust model, the model developed agrees with the correlation data for thrust levels between 80% and 100% of the take-off thrust. Once the agreement of the SFC curve is confirmed for high-thrust ratings, the next thing to do is to check the model simulation of the EGT, as shown in Figure 4.16.

Figure 4.16 shows exactly what was expected: high accuracy for values of corrected engine flow above 240kg/s and a deviation bellow that point, of about 10K.

The last parameter to be checked is the LPT exit temperature, T5, which was the most inaccurate one (see Figure 4.17). This temperature is measured by two probes, T54E and T54J in CFMI nomenclature. The simulation of T5 lacks precision due to the fact that the circumferential temperature distribution in that thermodynamic station changes with W2RStd and, since the value of a single probe was used (T54J), these differences are normal to happen. Such study was conducted by Kurzke [37]. Thus, these small deviations may be ignored.

A full check of the model would require printing many more figures checking the simulation of other parameters such as spool speeds, fuel flow, pressure ratios, among others. All other correlations were
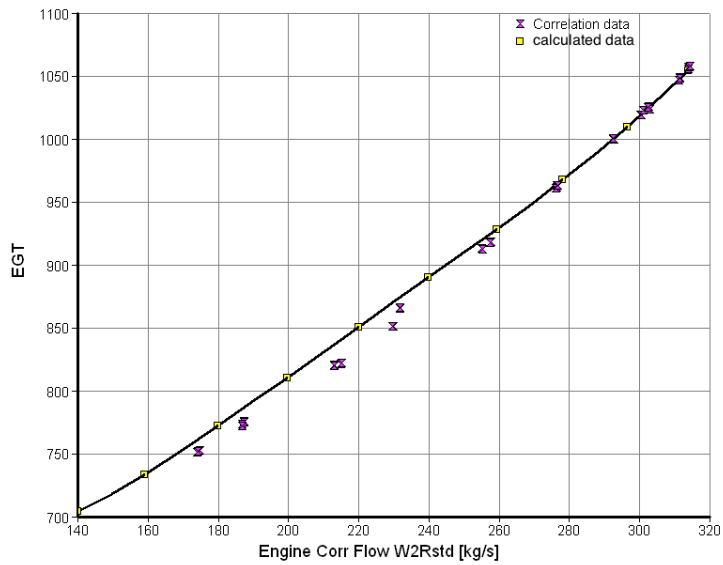
Figure 4.16: Comparison between measured and calculated EGT.
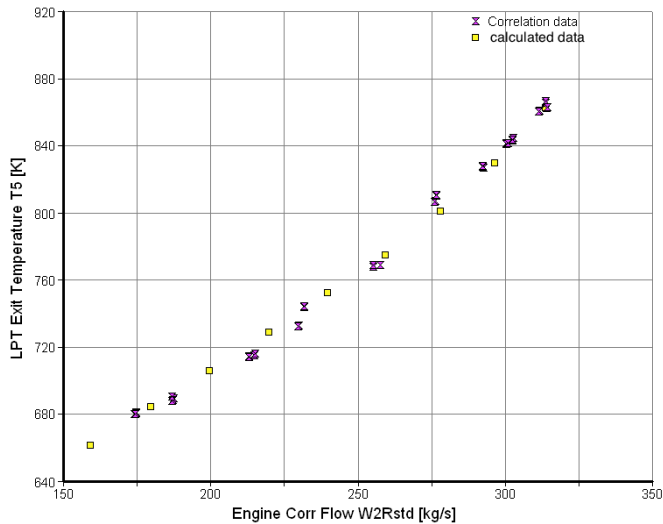
(a) Comparison between T5 measured and calculated

(b) Turbine Rear Frame.

Figure 4.17: T5 results and TRF [37].

simulated with great quality. Figure 4.18 represents the comparison between measured and calculated HPC exit pressure (static), Ps3.

The results of the modelling are very satisfactory, the engine model behaves well in high-thrust settings, as pretended. Apart from the LPT exit temperature, T5, all the other correlations match the measured variables with good precision, considering only the engine corrected flow range from 240.0 kg/s to 313.8 kg/s.

A refined model could be obtained with the consideration of three parameters: the Variable Stator Vanes and Variable Bleed Valves schedules and the HPT tip clearance control system.

Variable Stator Vanes The Variable Stator System is composed by the Inlet Guide Vanes (IGV's) located at the HPC inlet, and the Variable Stator Vanes, which form the stators for the first three stages

45
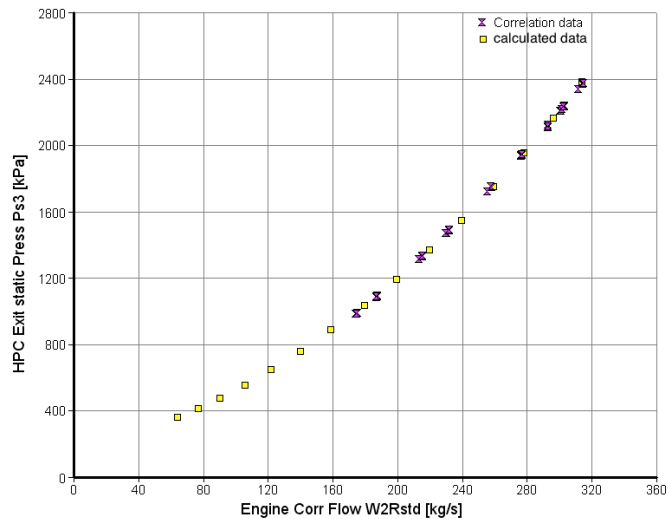
Figure 4.18: Comparison between measured and calculated HPC exit static pressure Ps3.

of the HPC [22]. Their function is to optimize the HPC performance for each combination of high pressure spool speed (N2) and compressor inlet temperature (T25). The VSV system changes the angle of the HP compressor IGVs and No. 1, 2 and 3 stator stages according to a defined schedule. The IGV's rotate separately from the VSV's. Figure 4.19 represents the VSV's schedule.
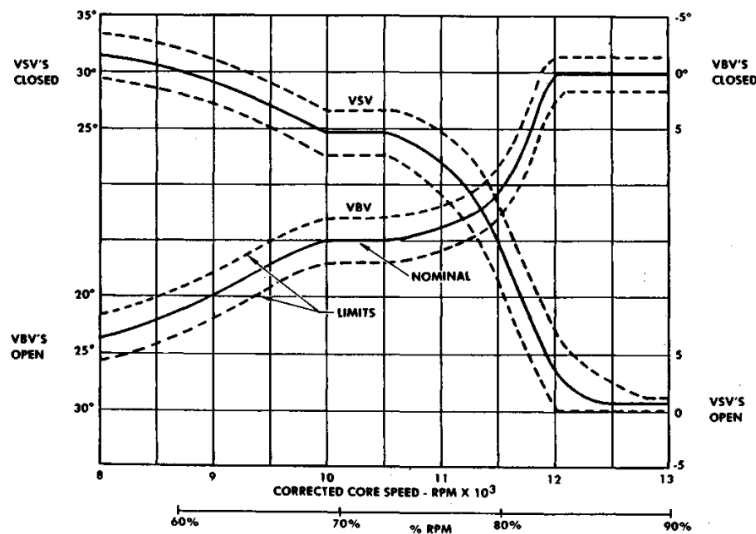
Figure 4.19: VSV's and VBV's schedules [22].

The correlation engine was tested for relative corrected core speeds from 86% to 100%, for this range of speeds the VSV's are almost opened (0 degrees of deflection). Thus, the effects of the VSV's can be ignored, as stated by Ridaura [7].

Variable Bleed Valves   The Variable Bleed Valves (VBVs) are located between the Booster exit and the HPC inlet. Their function is to regulate the primary flow entering the HPC, to optimize its efficiency, prevent it from surging and to regulate the fuel flow employed during the combustion process. The VBV's act primarily at low rotation speeds, where the surge margin of the HPC is lower. The operation of the

VBV's modify the mass flow entering the HPC which consequently changes its operating line. However, those changes are only visible for spool speeds bellow the ones where the developed high-thrust model has greater precision. Figure 4.19 shows the VBV's schedule. The VBV's schedule is opposite to the VSV's one; For higher rotations, the VBV's are closed. For the spool speed range where the engine was tested (86% to 100% of the take-off rating) the VBV's are closed, i.e. their schedule would not change anything and therefore was not implemented.

HPT tip clearance control, HPTCC The operation of the CFM56-3 engine can be separated in three modes according to the source of the HPT clearance control air [46]. The three modes, as well as their operation ranges and effects on HPT performance, are presented in Table 4.5.

Mode	Range (Corrected N2)	Range (W2RStd)	Air Source	$\Delta\eta_{HPT}$
I	[12000; 13200]rpm	[180; 230]kg/s	HPC 5th stage	1,5%
II	[13200; 13760]rpm	[230; 270]kg/s	HPC 5th & 9th stages	0.2%
III	[13760; 14300]rpm	[270; 314]kg/s	HPC 9th stage	0%

Table 4.5: HPT tip clearance control schedule.

The values presented in Table 4.5 for the variation of the HPT efficiency $\Delta\eta_{HPT}$ were calculated in GasTurb by implementing a mission profile with the model. Mission is a GasTurb tool where the user is able to look in detail to many different off-design conditions of a gas turbine. It is possible to combine up to 49 different operating conditions in a list of mission points. Such a list of points is also called a Design Table [11]. It is also possible to modify the components' efficiency or capacity using modifiers or modify ambient conditions such as ambient temperature or humidity.

It was conducted a study varying $\Delta\eta_{HPT}$ in modes I and II (in mode III the model is accurate, $\Delta\eta_{HPT} = 0$) of which resulted the tabulated values in Table 4.5. The objective was to study the effect on HPT efficiency caused by the clearance control air.

The efficiency of the HPT is the one that affects the most the overall efficiency of the engine. Thus, tip clearance must be maintained to the minimum in order to optimize the efficiency of this component. For spool speeds near the design point, the HPT disk and blades experience expansion due to the high temperature of the air (thermal expansion) and due to the centrifugal forces. In such conditions, the HPC bleed coming from its 9th stage is needed to heat the HPT shroud to make it expand, preventing the blades from touching the shroud. At lower regimes, both the centrifugal forces and the thermal expansion gets smaller so the HPT disk and blades shrink, increasing the tip clearance. The objective of using air from the HPC 5th stage is to cool the shroud to make it shrink equally, maintaining the tip clearance constant.

The implementation of the VSV's and VBV's schedules and the tip clearance control system in the model would improve it greatly, becoming an exact model. However, it was not possible to make a schedule for the $\Delta\eta_{HPT}$ to simulate the HPT tip clearance control system because it is not among the standard schedules offered by the software.

In the following chapter, the developed model will be used to explore two capabilities of GasTurb:

- Model Based Test Analysis (MBTA) or Analysis by Synthesis (AnSyn): when doing analysis by synthesis, the model of the engine is matched to test data of an engine coming to TAP M&E test cell, revealing its condition;

- Sensitivity tests, which will reveal the internal correlations of the engine, showing the effects of changing one parameter on the others.

Chapter 5

Application of the Model

The model developed in Chapter 4 is now a tool to study the performance of CFM56-3 engines coming to TAP M&E facilities. Its accuracy simulating the Correlation Test Report data permits to use it as a baseline for studying the degradations of the engines tested. The correlation engine can be used as a benchmark due to the amount of information available about its performance and because CFMI assured it as a stable engine with minimum levels of degradation. Thus, it is assumed that the engine tested by CFMI has optimal component efficiencies.

As stated in Section 3.4, an engine experiences degradations on different components. All those degradations will affect the performance of the engine. The effect of such degradation can be found looking at Test Bed results. According to the isentropic efficiency formulation (see Table 3.2), a decrease in compressor efficiency may be caused by an increase of the difference between outlet and inlet temperatures. The GasTurb model will be useful to check the effects of the degradations on the overall performance of the engine without needing to solve by hand the entire thermodynamic cycle.

The software offers a variety of tools to study engine performance degradations, such as Modifiers, Model Based Test Analysis and Sensitivity tests. The present chapter will introduce the reader to all of them, starting by the Model Based Test Analysis and finishing with the Sensitivity Tests. The Modifiers tool will not be used by itself, but as a supplementary tool in the Model Based Test Analysis, an example of a Modifier tool application can be found in reference [7], where Ridaura studied the effect of a 3% degradation of the HPC efficiency in the overall performance of the engine.

The objective for this thesis is to study the HPC blades replacement in the CFM56-3 engine and, to do so, it is imperative to be able to isolate the HPC performance from the rest of the components.

The solution to study the HPC isolated is to use data from an engine before and after an HPC intervention. This way, since only the HPC have been modified, the rest of the engine can be assumed to perform in the same way as before the intervention. Thus, testing the same engine before and after maintaining the HPC allows to isolate that component, however, it is rare to have the same engine tested in those conditions because it implies much larger costs to the customer. This type of testing, called back-to-back testing, happened only once for the CFM56-3 engine in TAP M&E facilities.

The tested engine, from now on referred as Back-to-Back engine, was tested after a core perfor-

mance restoration (test A), in which its EGT Margin for Hot day conditions was bellow the contracted value. Later, that same engine had the blades from the first three stages of the HPC replaced and was tested again (test B), reaching the contracted performance.

As referred in Section 3.4, compressor blades are exposed to many factors such as dust and high temperatures. The harsh conditions experienced by the compressor blades will have degrading effects on their performance. Blunting of their leading edges, erosion of the tips, pitting of the surface or the creation of deposits of solid matter are some examples of the degradations experienced by the blades of a compressor. There are maintenance actions to counteract these effects, such as:

- Restoration of blade chord length and height, using build-up welding, by creating extensions on the blade, which will later be reworked to restore the original geometry (see Figure 5.1);

- Replacement of an old blade with a new one, a more expensive procedure, that is used when restoration of chord length and height is not possible.
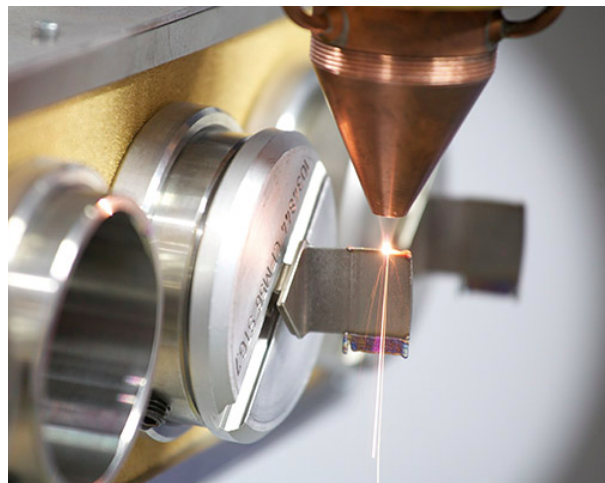
Figure 5.1: HPC blade chord length restoration [47].

The possibility of restoring the blade original geometry depends on the HPC stage. According to the CFM56-3 manual [22], in the first and second stages only the length of the blade can be restored, decreasing the tip clearance; for stages three to nine both length and chord length can be restored to the original geometry.

The objective of the implementation of the results of tests A and B is to study the HPC efficiency before and after the maintenance actions. The results will be later used in Chapter 6 to develop the performance map.

5.1 Model Based Test Analysis

5.1.1 Implementation Method

Model Based Test Analysis (MBTA) is the GasTurb tool that compares real engines with a benchmark, the model developed in Chapter 4. It incorporates the advantages from both analysis and synthesis pro-

grammes. Analysis programmes calculate component performance parameters using directly measured parameters and the laws of conservation of mass and energy. On the other hand, synthesis programs use predictions of component performance and find by iteration operating points in the maps that satisfy the laws of conservation of mass and energy, as stated by Brooks in reference [48].

In order to perform a MBTA, GasTurb requires a set of measured data, that depends on the type of engine being tested. The MBTA input window for a Turbofan engine is presented in Table 5.1.

Scan Identification No.		1	1
Meas. Rel.Humidity @ T2&P2 [%]		72,4821	1
Meas. Mass Flow W2	kg/s	306,275	1
Meas. LP Spool Speed [RPM]		4818,47	1
Meas. HP Spool Speed [RPM]		13978,7	1
Meas. Inlet Temperature T2	K	287,814	1
Meas. Inlet Pressure P2	kPa	101,773	1
Meas. Fan Exit Temp. T13	K	337,198	1
Meas. Fan Exit Press. P13	kPa	167,93	1
Meas. Fan Exit Temp. T21	K	288,658	1
Meas. Fan Exit Press. P21	kPa	101,404	1
M. Booster Exit Temp. T24	K	372,015	1
M. Booster Exit Press. P24	kPa	220,509	1
Meas. Compr.Exit Temp. T3	K	764,073	1
Meas. Comp. Exit Press. P3	kPa	2344,84	1
Meas. Fuel Flow WF	kg/s	1,09179	1
Meas. HPT Exit Press. P44	kPa	564,97	1
Meas. LPT Inlet Temp. T45	K	1127,9	1
Meas. Turb. Exit Press. P5	kPa	147,394	1
Meas. Turb. Exit Temp. T5	K	857,922	1
Meas. Amb. Pressure Pamb	kPa	102,34	1
Meas. Gross Thrust	kN	94,5336	1
Meas. Bleed Mass Flow	kg/s	0	1
Meas. Power Offtake	kW	50,1867	1
Meas. Fuel Heating Value	MJ/kg	43,0054	1
Measurement X1		1082,16	1
Measurement X2		0	1
Measurement X3		0	1
Measurement X4		0	1
Measurement X5		0	1

Table 5.1: MBTA Input window for turbofan engine.

The data to be introduced will be taken from *.log* files compiled in the TAP M&E test cell (see Figure 2.4). From the *.log* files, the data from three different operating points will be used, two at Maximum Continuous and one at Take Off. This data is then written to GasTurb Measured Data Files, or *.mea* files, in order to be automatically uploaded to the input window from Table 5.1. The input data consists of a set of temperatures, pressures, air mass and fuel flow rates, net thrust and spool speeds. Additionally, the software allows some extra measured data to be incorporated in the calculations. Those extra parameters are identified in Table 5.1 as *Measurement X1 to X5*.

A comparison between the data required by GasTurb and the data measured in TAP M&E test cell reveals that some of the required parameters are not among the measured ones or are incoherent, e.g. P5, which is measured in the LPT outlet, presents values near ambient pressure, which does not make sense, the LPT discharge air is still compressed (around 150kPa). Table 5.2 presents the missing parameters, as well as their location on the engine and their values at design point.

The data presented in Table 5.2 is needed and since it was not measured when tests A and B were performed, these parameters must be taken from the model, as explained by Kurzke [11]. This action will

Parameter	CFMI nomenclature	Units	Location	Value at design point
T13	T17	K	Fan outlet	338.15
P13	PT17	kPa	Fan outlet	167.69
T24	T25	K	Booster exit	369.92
P24	PT25	kPa	Booster exit	221.11
P44	PT45	kPa	HPT exit	569.63
T45	T45	K	HPT exit	1140.99
P5	PT5	kPa	LPT exit	148.14
T5	T5	K	LPT exit	862.66

Table 5.2: Parameters not measured at TAP M&E test cell.

introduce limitations to the model. The tested engine will have to use components from the correlation engine, i.e. since the listed parameters are not measured, the only way to act is to use values from the model, which will be considered as a benchmark engine, whose performance is representative of the performance of the engine tested.

Model Based Test Analysis tool offers the user the option to perform iterations to find missing values, however, this action has a toll on the simulation. To do so, the user has to fix a component performance relative to the performance of that same component in the correlation engine, meaning that the engine tested in the test cell will have to use data from the correlation model to substitute for the meassing variables that were not measured in the test bed.The iteration targets are either efficiency or flow factors. A value of one of this factors means that the tested engine component will have the same efficiency or corrected flow as the corresponding component of the correlation engine. Thus, a value above or bellow one correspond to better or worse performance of the tested engine components, respectively. The choice of the iteration variables and corresponding targets have to be reasonable otherwise the calculations will not converge to a solution.

With all the iterations and the corresponding targets computed (see Table 5.2), the software did not converge to a solution. Further analyses revealed that the origin of such a problem was the use of flow or efficiency factors of any of the turbines as iteration targets. GasTurb adapts the benchmark engine to the measured data by one of the following methods:

- HPT capacity method, the software tries to equal the HPT corrected flows of the model and the tested engines;

- LPT capacity method, the same method as the first but using LPT corrected flows;

- T45 heat balance method, in this method GasTurb tries to equal the model and the measured T45 values (HPT exit temperature);

- T5 heat balance method, GasTurb tries to equal the model and the measured T5 temperatures (LPT exit temperature).

Any of the above methods use a parameter from a turbine as the figure of merit of the cycle calculation, i.e. convergence is reached when the difference between the measured and model values of

that parameter (residual) is smaller than a certain value. Using a flow or efficiency factor from a turbine as a target will fix the operation of that component to a certain operating point which most likely will be different from the point that guarantees the convergence criterion of the used method.

The T45 heat balance method was used since it was the one that gave the best results. The solution was to use data from the model turbines without iterating it. However, the Correlation Test Report data could not be used directly unless the spool speeds and ambient conditions during the tests of the back-to-back and correlation engines were the same. To get the data from the correlation engine under the same conditions as the back-to-back engine was tested, the GasTurb Limiters tool was used.

During a test run, the engines are tested for different operating conditions, such as Idle, Maximum Continuous or Take Off. The test cell technicians fix a low pressure spool speed (N1R) as target, this parameter is the only one to be fixed and is the one that defines the operating regime of the engine. An engine is considered to be at Take Off for N1R values near the maximum value for which it is certified to be operated. Additionally, an engine is considered to be at Maximum Cruise if the N1R is close to 80% of the Take Off rating [49].

The GasTurb Limiter tool, presented in Figure 5.2, allows the user to constrain one or more parameters to a maximum, minimum or a range of values.

Figure 5.2: GasTurb limiter tool.

Using the N1R limiter, it is possible to set the model engine low pressure spool speed to the same values as the ones used testing the back-to-back engine and get the data from the engine for that operating point. The only thing missing is to make the correlation engine perform at the same ambient conditions. To do that, the following equations are used:

$$T_{corrected|test} = T_{corrected|model} * \frac{\Theta_{model}}{\Theta_{test}} \,, \tag{5.1a}$$

$$P_{corrected|test} = P_{corrected|model} * \frac{\delta_{model}}{\delta_{test}} \,, \tag{5.1b}$$

where Θ_{model} and Θ_{test} are the temperature ratios using the temperatures measured during the CTR engine run and the test engine run, respectively. The δ_{model} and δ_{test} are the pressure ratios using the pressures measured during the CTR engine run and the test engine run, respectively.

Using the ambient temperatures and pressures from the correlation and back-to-back tests, the temperatures taken from the model were uncorrected for the correlation ambient temperature and pressure and then corrected using the temperature and pressure measured in tests A and B.

Information from multiple operating points may be introduced using *.mea* files. A *.mea* file with the results of a test run with three sets of measurements taken is presented in Figure 5.3.

```
| ScanId    humid!     W2!         XN_LP_A!  XN_HP_A!  T2!       P2!       T13!      P13!
T21!       P21!       T24!        P24!      T3!       P3!       WF!       P44!      T45!
P5!        T5!        Pamb!       FG!       ZWBLD!    PWX!      FHV!      X1Mea     X2Mea
X3Mea      X4Mea      X5Mea
Tolerances
 1          1          1           1         1         1         1         1         1
 1          1          1           1         1         1         1         1         1
 1          1          1           1         1         1         1         1         1
 1          1          1
Measured Data
 1          72.89      306.615     4807.1    13997     288.15    101.325   336.777   167.101
288.159    101.335    368.267     220.294   766.999   2338.5    1.0959    564.434   1131.764
147.388    856.032    101.647      93.67    0         0         42.769    0   0           0          0
 0                // scan 1
 2          73.34      318.689     4937.4    14175     288.15    101.325   338.907   171.249
288.159    101.335    371.664     226.629   781.019   2472.986  1.1918    594.299   1160.663
152.3544   876.078    101.663     100.556   0         0         42.769    0   0           0          0
 0                // scan 2
 3          73.61      306.855     4813.8    14036     288.15    101.325   337.058   167.309
288.159    101.335    368.603     220.577   768.548   2347.098  1.100     565.879   1133.752
147.627    857.439    101.645      94.0799  0         0         42.769    0   0           0          0
 0                // scan 3
```

Figure 5.3: *.mea* file with measurements from three operating points.

Engine A was running at N1R equal to 4807.1 rpm, when tested at the first Maximum continuous operating point. Limiting the Corrected Low Pressure spool speed to 99.43% that speed is limited to 4807.4 rpm, as presented in Figure 5.4.

```
    Iteration converged after 13 loops.
    Engine Operation Limited by NL/sqrt(T2)

Spool Speeds:                LP Spool  IP Spool  HP Spool
Absolute [RPM]               4807,4    4807,4    14279,5
Relative                     0,9943    0,9943    0,9969
                               LPC       IPC       HPC
Surge Margin [%]             44,173    53,594    22,258
Handling Bleed WB,hd/W22               0,0000
```

Figure 5.4: Model operation with N1R limited.

5.1.2 Engine Performance Comparison

Once the data from the model, running at the corrected speed, is corrected to Standard day and introduced to the MBTA input window, the results presented in Figure 5.5 were obtained, for engine A (before chord length restoration).

Additionally, the deviation in EGT can be studied to measure the accuracy of the method used. The calculated value in MBTA for M/C#2 was 1084.64 K and the measured value in Test bed was 1086.61 K, the corresponding relative error is 0.109%. From Figure 5.5, it is possible to see that the engine tested did not perform as the benchmark engine did, otherwise the efficiency and flow factors would be equal to one. To make a complete study of the HPC, independent from the model, information about station 25

Fan Flow Factor		0,996659	
Fan Outer Efficiency Factor		1	
Fan Inner Efficiency Factor		1,01472	
Booster Flow Factor		1	
Booster Efficiency Factor		1	
HPC Flow Factor		1,06667	
HPC Efficiency Factor		0,976717	
HP Turbine Flow Factor		1,05496	
HP Turbine Efficiency Factor		1,03501	
LP Turbine Flow Factor		1,01216	
LP Turbine Efficiency Factor		0,97775	
Core Nozzle Area Factor		1,01698	
Bypass Nozzle Area Factor		0,978485	
Gross Thrust Factor		0,964041	
T45 measured - T45 calculated	K	0,00841076	
T5 measured - T5 calculated	K	-6,85389	

Figure 5.5: MBTA results for engine A at M/C#1.

would be needed, as stated by Ridaura [7]. Both the T25 and PT25 sensor had invalid measurements in both tests.

The solution to this problem is to fix the Booster performance, by using the model data in the MBTA input window for these two parameters. The iteration of T25 and PT25 to fix the Booster flow and efficiency factor worked well and it was possible to force these factors to one. The proposed solution has a cost in terms of results. Fixing the performance of the Booster for every test doesn't allow to see the impact of modifications in the Booster performance on the overall performance of the engine.

For test B, testing the same operating point, the procedure is repeated. The Booster exit temperature and pressure are iterated to fix the Booster performance in all tests. Since the HPC exit values (station 3) are measured in all tests, it is possible to study variations in the HPC performance. However, it is not possible to know if the calculated values of the HPC efficiency and capacity in the two tests are equal to the real value.

This procedure was made three times (one for each operating point) for both engines A and B. Table 5.3 presents the results for all simulations made.

Engine A						
Operating point	N1R (rpm)	HPC Eff. factor	HPC Flow factor	$EGT_{mea}(K)$	$EGT_{calc}(K)$	Error (%)
M/C # 1	4807.1	0.9767	1.0667	1084.94	1086,32	0.1272
T/O #1	4937.4	0.9777	1.0785	1113.72	1080.12	3.0169
M/C # 2	4813.8	0.9749	1.0606	1086.61	1084.64	0.1850
Engine B						
Operating point	N1R (rpm)	HPC Eff. factor	HPC Flow factor	$EGT_{mea}(K)$	$EGT_{calc}(K)$	Error (%)
M/C # 1	4816.5	0.9898	1.0901	1076.67	1068.28	0.7792
T/O #1	4948.7	0.9898	1.1080	1103.17	1083.35	1.7966
M/C # 2	4804.1	0.9847	1.0898	1071.00	1080.59	0.8954

Table 5.3: Results of the test runs simulations.

Additionally, comparing the variation in HPC efficiency and capacity between corresponding operating points, will reveal if the simulation of the HPC operation was correctly performed. Figure 5.6 presents the variation of the HPC efficiency and capacity after the HPC maintenance actions.

From Figure 5.6, it is possible to conclude that the raise in efficiency and capacity in the HPC was
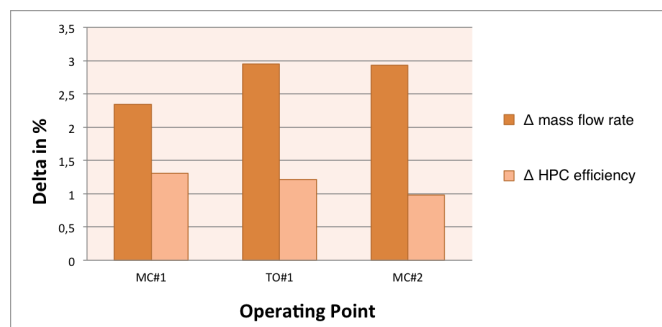
Figure 5.6: Variation of HPC efficiency and capacity.

similar for the different operating points that were simulated in the MBTA. The increase in these factors from engine A to B was expected since engine A had damaged blades (reduced chord length) which later were replaced by new ones. The choice of the operating point will be done after inspecting the results of the EGT simulation. The quality of the simulation of each operating point can be ascertained by comparing the measured and calculated EGT values.

Further analysis of Table 5.3 reveal that, in terms of EGT, the results are close for the two Maximum continuous points simulated in the MBTA but the results for the take off point are farther from the measured value in TAP M&E test cell.

The take off (T/O # 1) point is immediately excluded for having the largest discrepancies in the EGT values. The reason for this deviation may be related to the modelling of the engine. The correlation engine was tested for N1R values from 3000rpm to 4835rpm, the latter value corresponding to 100% of the engine loading. However, when TAP M&E tests an engine at T/O rating, it is usual to raise N1R to 105%, which falls out of the domain where the engine performance was modelled.

Both the maximum continuous points produced good EGT estimations but the best results belong to the first point, M/C # 1, which will be used as a baseline for developing the performance map in Chapter 6. The next section will introduce the reader to another GasTurb tool, called Sensitivity tests or studies. This tool is one of the more useful from this software, to understand the relations between different parameters in the engine. This tool will be used to estimate the needed increase in HPC efficiency to reach the contracted EGT HD margin.

5.2 Sensitivity Tests

5.2.1 Engine Sensitivity to Components Performance

Sensitivity studies is the GasTurb tool to study the effects of small changes of some of the engine parameters on the others. It can be very useful to study how important one or the other input quantity is for a certain cycle, e.g. check what degrades more the EGT on an engine: a 1% efficiency degradation in HPC or the same degradation in the HPT. A sensitivity study can solve that and many other problems [11]. Table 5.4 represents the results of a sensitivity test, where the effects of 1% variations in the efficiencies of the LPC, Booster, HPC, HPT and LPT on T45, T5, Net Thrust and SFC. The estimations

of the variations of T45 and T5 will allow to study the variations on EGT, using Equation (4.6). On Section 5.2 all the used EGT values are corrected for Standard Day using the factor Θ defined in Chapter 4. Although TAP M&E checks the operability of an engine using the EGT margin for Hot day conditions, this margin is always bigger than for Standard Day conditions, as stated by Ridaura [7].

Degradation	$\Delta T45_{1\%}$ (K)	$\Delta T5_{1\%}$ (K)	$\Delta EGT_{1\%}$ (K)	$\Delta NetThrust_{1\%}$ (KN)	$\Delta SFC_{1\%}$ (g/(h KN))
$\Delta LPCefficiency$	-4.09	-3.02	-3.762	-0.22	-0.73
$\Delta IPCefficiency$	-3.23	-2.57	-3.010	-0.06	-0.28
$\Delta HPCefficiency$	-8.17	-6.81	-7.683	-0.02	-0.69
$\Delta HPTefficiency$	-12.61	-10.58	-11.874	-0.02	-0.84
$\Delta LPTefficiency$	-5.88	-7.85	-6.153	-0.33	-1.04

Table 5.4: Sensitivity study example.

Further study of Table 5.4 reveals how relevant are deviations from the design point value of a certain component efficiency. All the efficiencies listed were increased by 1%, one at a time. This study was conducted in the correlation engine model. From Table 5.4 some important information can be extracted:

- Changing a component efficiency will bring modifications to the whole engine. T45 and T5 are measured respectively before and after the HPT and yet they are influenced by changes in the Fan efficiency;

- The high pressure components, HPC and HPT, are the one that influence T45 and T5 the most. Thus, they will also influence EGT the most;

- A 1% efficiency loss in the HPT leads to a large loss in EGT margin of almost 12 degrees Celsius;

- Net thrust remains practically unchanged when an efficiency is changed. This parameter is influenced by changes in flow, specially in the Fan (1% increase in Fan capacity lead to an increase of 2.06kN);

- Changing the components efficiency brings changes to the Fuel Flow, observable by the changes in SFC, which is directly connected to Fuel Flow and Net thrust (which remained almost unchanged).

5.2.2 Replication of MBTA Results using Engine Sensitivities

The calculation of the EGT variations in the back-to-back engine was performed using Tables 5.3 and 5.4. Only the differences in HPC efficiency were accounted for this study, the effects on EGT of the variations of HPC capacity were not used because they had a small effect on the results.

From Table 5.3, it is possible to see that for the first operating point the HPC efficiency increased 1.31% from engine A to B. Together with the information from the sensitivity tests, presented in Table 5.4, the following equations that will be used for calculating the modified T45 and T5 values arise:

$$T_{final} = \Delta T + T_{initial}, \tag{5.2a}$$

$$\Delta T = \Delta \eta * \Delta T_{1\%} \, , \tag{5.2b}$$

where $\Delta \eta$ is the difference between the HPC efficiency factor from engine A to B, 1.31%. Equations (5.2) are used twice, one time for T45 and the other for T5. The resultant temperatures are then introduced in Equation (4.6) and the drop in EGT can now be estimated and compared to the value obtained in test cell. Table 5.5 presents the results of the EGT drop for the two maximum continuous points, M/C#1 and M/C#2.

Operating Point	EGT_A (K)	EGT_B (K)	ΔEGT_{calc} (K)	ΔEGT_{meas} (K)	Deviation (%)
M/C #1	1086.611	1076.875	-9.737	-9.944	2.08
M/C #2	1084.944	1077.212	-7.732	-13.944	44.55

Table 5.5: EGT variation from engine A to B.

Table 5.5 reveals a great discrepancy between the results for the two operating points used. The reason why the last point fails in the calculations is presented in Table 5.3 where is possible to see that the raise in HPC efficiency in M/C#1 and T/O#1 operating points is almost the same and equal to 1.31%, however, for M/C#2 the value obtained was only 0.98%. The first maximum continuous point revealed to be the one with better results in terms of both EGT and HPC efficiency.

The results obtained in this chapter will now be applied to a specific problem in the HPCs to develop a tool to study the HPC blade replacement.

Chapter 6

Performance Studies

The results from the past chapters will now be used to develop a tool to help TAP M&E improve its maintenance and overhaul actions on the HPC of CFM56-3 engines.

6.1 Motivation for the Application

TAP M&E is interested in understanding the internal relations of the CFM56-3 engine. The HPC of the CFM56-3 is presented in Figure 6.1.
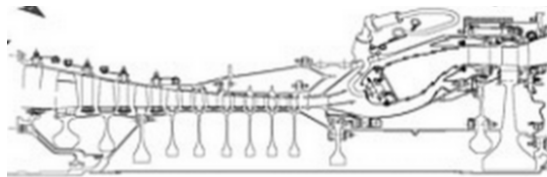
Figure 6.1: CFM56-3 high pressure compressor [22].

The HPC is composed by three mini-modules [22]. These three divisions are:

- HPC rotor, composed by nine stages of different geometry;

- Front stator case, this component covers the whole compressor, both the rotor and the rear stator case, however, only the first five stages of the compressor are directly involved by this case;

- Rear stator case, mounted inside the Front stator case, involves the last four HPC stages.

A more complete description of the CFM56-3 HPC can be found in references [17, 22].

According to the Engine Manual [22], the overhaul of the HPC includes actions such as checking the seals diameters to minimize air leakage in the engine, measurement of concentricity between the stator cases and correction of the stator cases and the rotor stages diameters, using high speed grinding in the rotor and machining in the stator cases.

As stated in Chapter 3, the ingestion of sand and dust leads to erosion in the HPC blades, modifying their shape and consequently reducing the efficiency of the compressor.

The blades are eroded in two different ways. They are eroded in their leading edge, reducing their chord length and in the tip, decreasing their height and, consequently, increasing tip clearance.

The engine manual offers solutions to these problems, in different manners according to the stage of the blades:

- Blade height restoration, this action is possible to perform on blades from any stage;

- Blade chord length restoration, this procedure is only possible for blades from stages three to nine.

Figure 6.1 reveals that different HPC stages have different geometries, different blade shapes and size, and different spool diameters. This leads to a problem: modifications in different stages must have different impacts on the overall compressor performance. It is of primary importance for TAP M&E to understand which stages have more influence on the overall performance of the compressor. Using the data from the back-to-back engine, in which the blades from the first three stages were replaced, the influence in overall performance of each of these stages will be studied individually.

6.2 Effects of Stage Efficiency Modifications on Overall Compressor Efficiency

6.2.1 Methodology

In order to understand how to maintain the HPC in an efficient way, knowing the relation between stage and overall efficiencies is mandatory. This study will be conducted using a simplified three-stage version of the CFM56-3 HPC. Studying only the first three stages of the compressor will simplify the calculations. This simplification is acceptable since only the first three stages of the HPC were modified, while all the others remained unchanged.

The methodology used for calculating the stage efficiencies is presented in references [26, 50].

The calculation of stage efficiency begin with the calculation of the lift and profile drag coefficients, C_L and C_{DP}, respectively. From the diagram of forces acting on the cascade, presented in Figure 6.2, the static pressure rise across the stage is given by

$$\Delta p = p_2 - p_1 = (p_{02} - 0,5\rho V_2^2) - (p_{01} - 0,5\rho V_1^2). \tag{6.1}$$

Since the variations of air density are small, it is possible to assume that the flow is incompressible [26]. Equation (6.1) then becomes

$$\Delta p = 0,5\rho V_a^2(\tan^2\alpha_1 - \tan^2\alpha_2) - \overline{\omega}. \tag{6.2}$$

where $\overline{\omega}$ are the static pressure losses and V_a is the axial velocity, which is assumed constant and α_1 and α_2 are the angles between the axial direction and a tangent to the mean centerline at the leading and trailing edges of the blades, respectively.
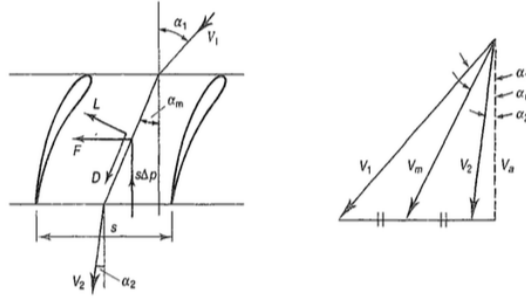
Figure 6.2: Forces and velocities acting on a cascade [26].

The force per unit length acting along the cascade is given by

$$F = S\rho V_a^2(\tan \alpha_1 - \tan \alpha_2),$$ (6.3)

where S is the spacing between consecutive blades.

The lift and drag coefficients will be based on a vector mean velocity V_m presented in Figure 6.2, the mean velocity and angle are given respectively by

$$V_m = V_a \sec \alpha_m,$$ (6.4a)

$$\tan \alpha_m = 0.5(\tan \alpha_1 + \tan \alpha_2).$$ (6.4b)

Drag and lift forces are defined along and perpendicular to the direction defined by the mean velocity. Resolving along that direction gives

$$D = 0.5\rho c V_m^2 C_{DP} = F \sin \alpha_m - S\Delta p \cos \alpha_m,$$ (6.5)

where c is the blade chord length and S is the spacing between the blades. Combining Equation (6.5) with Equations (6.2) and (6.3) leads to

$$C_{DP} = \left(\frac{S}{c}\right)\left(\frac{\overline{\omega}}{0.5\rho V_1^2}\right)\left(\frac{\cos^3 \alpha_m}{\cos^2 \alpha_1}\right).$$ (6.6)

Repeating for the perpendicular direction results in

$$L = 0.5\rho c V_m^2 C_L = F \cos \alpha_m + S\Delta p \sin \alpha_m,$$ (6.7a)

$$C_L = 2\left(\frac{S}{c}\right)(\tan \alpha_1 - \tan \alpha_2)\cos \alpha_m - C_{DP}\tan \alpha_m.$$ (6.7b)

The second term of Equation (6.7b) may be neglected, a theoretical value for C_L may be calculated, in which the effect of profile drag in lift creation is ignored.

When studying a complete blade row of a compressor stage, two additional contributions to the drag coefficient must be taken into account. These new contributions to the drag coefficient are the

contribution due to the walls of the compressor annulus and the losses due to trailing edge vortices and tip clearance. According to reference [26] these losses are given by empirical formulas, for typical axial compressor designs:

$$C_{DS} = 0.018 C_L^2 \,, \tag{6.8a}$$

$$C_{DA} = 0.020 \left(\frac{S}{h} \right) \,, \tag{6.8b}$$

where C_L is the lift coefficient given by Equation (6.7b) and h is the blade height. An improvement to Equation (6.8a) is presented by Vavra [50]. A new equation which takes into account the tip clearance effects arises:

$$C_{DS} = \left(0.25 \frac{\delta}{S \cos \alpha_2} + 0.055 \right) C_L^2 \left(\frac{c}{h} \right) \,. \tag{6.9}$$

The overall drag coefficient in the stage can now be defined as the sum of the others presented before, $C_D = C_{DP} + C_{DS} + C_{DA}$, where C_{DP} is read from Figure 6.3.
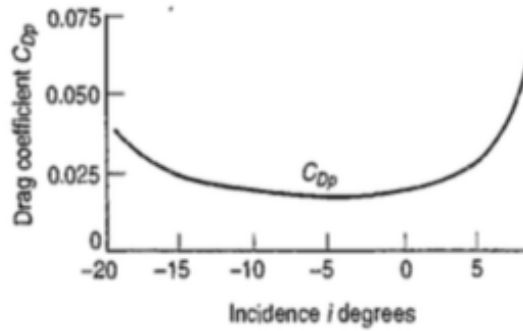
Figure 6.3: Profile drag coefficient versus incidence angle i [50].

The value for the profile drag coefficient defined before for a two-dimensional cascade, apply equally for the annular case if C_D is substituted for C_{DP}. Thus, for the annular cascade

$$C_D = \left(\frac{S}{c} \right) \left(\frac{\overline{\omega}}{0.5 \rho V_1^2} \right) \left(\frac{\cos^3 \alpha_m}{\cos^2 \alpha_1} \right) \,. \tag{6.10}$$

Once the drag coefficients are estimated, the loss coefficient, $\overline{\omega}/.5\rho V_1^2$, can be calculated.

The efficiency of the blade row, η_b, is defined as the ratio between the actual pressure rise in the blade row and the theoretical value and can be found from

$$\eta_b = \frac{\Delta p_{th} - \overline{\omega}}{\Delta p_{th}} = 1 - \frac{\overline{\omega}/0.5\rho V_1^2}{\Delta p_{th}/0.5\rho V_1^2} \,, \tag{6.11}$$

where Δp_{th} is the theoretical pressure rise in the blade row. In terms of the inlet dynamic head and cascade air inlet and outlet angles, is given by

$$\Delta p_{th} = 0.5 \rho V_1^2 \left(1 - \frac{\cos^2 \alpha_1}{\cos^2 \alpha_2} \right) \,. \tag{6.12}$$

For the present study it is assumed that the reaction is 50% at the mean diameter of the stage, which

is given by $\phi_m = \phi_{disk} + h$. According to reference [30], the degree of reaction, R, is given by

$$R = \frac{\Delta enthalpy in rotor}{\Delta entalpy in stage} ,$$ (6.13)

where the enthalpy drop in the stage is equal to the sum of the enthalpy drops in the rotor and stator. A degree of 50% means that the pressure rise is equally shared by the stator and the rotor. A degree of reaction of 50% leads to symmetrical velocity triangles, since $\alpha_2 = \beta_2$, the exit angle of the stator is the same as the entry angle of the rotor, as presented in Figure 6.4. This is confirmed by measurements made in the actual engine, for thrust settings near the design point, where the geometry of the engine is fixed and, therefore, the stators of the first stages (IGV's and VSV's) are fixed and aligned ($\alpha_2 = \beta_2$) with the rotor stages. Note that the angle β used in rotor stages corresponds to α in cascade terminology.
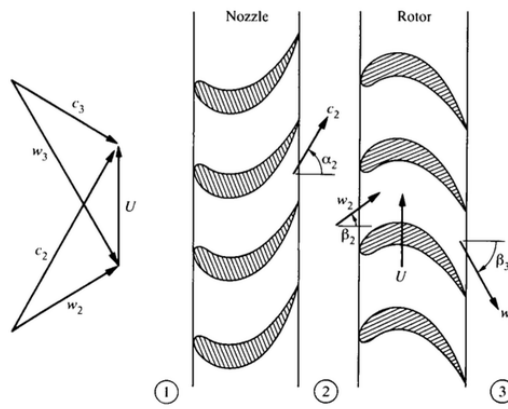
Figure 6.4: Degree of reaction of 50% [30].

Using a 50% degree of reaction it is possible to assume that the efficiency of the stage will be equal to the efficiencies of the rotor and stator stages, $\eta_{Stg} = \eta_{rotor}$. This result was demonstrated by Cohen *et al* in reference [26].

The compressor efficiency is connected to the compressor stages efficiencies. The calculation of the overall isentropic efficiency will be made using the first equation presented in Table 3.2. To calculate this parameter, it is required to estimate the overall pressure ratio and the inlet and outlet temperatures of the compressor. The nine stage HPC from the correlation engine increased the air temperature from 369.92K to 770.80K, which leads to a stage temperature rise (ΔT_{Stg}) of 44.5K. As presented in reference [26], the pressure ratio in each stage is calculated from

$$R_S = \left[1 + \frac{\eta_{Stg} \Delta T_{0Stg}}{T_1} \right]^{\gamma/(\gamma-1)} ,$$ (6.14)

where T_1 is the inlet temperature of each stage of the HPC, η_{Stg} is the stage efficiency and ΔT_{0Stg} is the stage stagnation temperature raise. The GasTurb values of the temperatures T25 and T3 correspond to static temperatures, however, Equation (6.14) uses stagnation temperatures instead of static. The solution is to assume that the stages are periodic, which leads to $C_3 = C_1$, the inlet and outlet velocities in each stage are equal. Making use of Equations (3.7) and (3.9) it is possible to reach the conclusion that,

63

using the $C_3 = C_1$ condition, the difference between the static temperatures or stagnation temperatures will be the same. Thus, T_{0Stg} can be replaced for T_{Stg} in Equation (6.14) and the static pressure ratio may be calculated.

6.2.2 Geometrical Blade Rows Measurements

The calculation of the stage efficiencies require some geometric data from the blade rows. Such measurements were performed in a 3D Coordinate Measuring Machine, CMM [51], presented in Figure 6.5.

(a) Coordinate Measuring Machine.

(b) HPC rotor in the CMM.

Figure 6.5: 3D Measurement equipment [51].

The measured parameters were the blade height (h), the blade spacing (S), the leading edge angle and the trailing edge angle. The measurements made on the first three rotor stages are presented in Table 6.1. Each measurement was performed three times, the values presented in Table 6.1 are the average of the measured values.

Stage	α_1 (degrees)	α_2 (degrees)	h (in)	S (in)
1	66.185	51.626	3.360	1.439
2	72.407	44.900	2.574	1.032
3	71.289	45.014	2.000	0.908

Table 6.1: Measurements performed on the 3D CMM.

Additionally, the blade chord length of the blades from the first three stages of the HPC was measured. Table 6.2 presents the averages of the measured values for both engine A and B.

Engine A			
Stage	Number of blades	Total Chord (in)	Average Chord (in)
1	38	86.473	2.276
2	53	61.990	1.632
3	60	49.332	1.298
Engine B			
Stage	Number of blades	Total Chord (in)	Average Chord (in)
1	38	90.499	2.382
2	53	65.900	1.705
3	60	51.366	1.332

Table 6.2: Measurements performed on the CFM56-3 HPC blades.

6.2.3 Results

The HPC of the back-to-back engine studied had the blades from its first three stages replaced for new ones. Thus, the remaining stages kept unchanged and will not be studied. In order to simplify the calculations and to reduce the amount of measurements to be taken, a compressor constituted by the first three stages of the actual HPC will be used. For a full analysis of the HPC, all the inlet and outlet angles of all the nine stages would be required as well as the average blade height and spacing for these stages. Since a full analysis is not possible to be achieved due to the fact that the Booster exit temperature (T25) was not measured in both tests A and B, the objective is not to estimate the actual compressor efficiency but to study which stages are more sensitive to deterioration and which stages influence the HPC overall efficiency the most.

The calculations were performed twice, first for the engine with the deteriorated blades (engine A) and the other for the engine with the new blades (engine B). The average chord length of the blades of each stage was the only parameter to change between the two simulations.

After implementing the methodology described in Section 6.2.1, the results of the simulations are presented in Table 6.3.

Engine A						
Stage	S/c	C_L	C_D	$\overline{\omega}/.5\rho V_1^2$	$\Delta p_{th}/.5\rho V_1^2$	η_{Stg}
1	0.632	0.540	0.0383	0.084	0.519	0.8384
2	0.633	1.284	0.0847	0.128	0.818	0.8437
3	0.699	1.243	0.0862	0.134	0.794	0.8308
Engine B						
Stage	S/c	C_L	C_D	$\overline{\omega}/.5\rho V_1^2$	$\Delta p_{th}/.5\rho V_1^2$	η_{Stg}
1	0.604	0.516	0.0378	0.0867	0.519	0.8332
2	0.605	1.194	0.0821	0.130	0.818	0.8415
3	0.682	1.212	0.0846	0.135	0.794	0.8294

Table 6.3: Stage performance calculations.

It is now possible to estimate the overall efficiency of the compressor making use of the equation indicated for compressors presented in Table 3.2.

Engine	η_{Stg1}	η_{Stg2}	η_{Stg3}	η_{OVR}
A	0.8384	0.8437	0.8308	0.8238
B	0.8332	0.8415	0.8294	0.8206

Table 6.4: Simulation of the chord length restoration effects on stage efficiency.

Further analysis of Table 6.4 reveal that the efficiency of the HPC decreased when using the new blades, note that in this analysis only the variation of the blade chord length was studied. The decrease of the HPC efficiency is not supported by the simulation performed in Chapter 5, in which the efficiency of the HPC increased 1.31% from test A to B. Thus, the assumption that the increase of the blades chord length would lead to an improvement in the HPC performance may not be correct.

Analysing Equations (6.10) and (6.11) it is possible to see that, maintaining the angles α_1 and α_m between the two tests, an increase in chord length leads to an increase of the loss factor, $\overline{\omega}$. Thus, since Δp_{th} is constant, the efficiency of the stage must decrease (C_D changes are minimal compared to the changes in chord length).

Figure 3.6, presented in Section 3.4 reveals the reason why this simulation fails to replicate the results obtained in the MBTA. As the number of flight cycles increase, the erosion that the blades experience wear both their height and chord length. The objective of this study is to analyse the effect of an increase of blade chord length in the compressor efficiency. Thus, it was considered that the tip clearance is kept constant (only the influence of the chord length is being studied), modifications in the chord length of the blade are accompanied by a distortion of the blade airfoil, i.e. the inlet and outlet angles as well as the thickness of the blades change [33]. These changes will introduce modifications in the air flow such as variations of the incidence angle which, consequently, will change the profile drag coefficient of the blade row (see Figure 6.3). Thus, it is not possible to use Figure 6.3 to estimate the profile drag coefficient when studying worn blades and, therefore, it is not possible to study the deterioration of the HPC performance based only on modifications of chord length. More complex methods such as Computational Fluid Dynamics analyses would be useful to study the changes of the profile drag coefficient with more precision.

Even though the influence of the blade deterioration in the compressor efficiency could not be estimated, some important data can be extracted from the simulation of the engine with new blades. It is possible to study the influence of the different stages on the overall efficiency of the HPC, revealing which influences it the most. Changing by steps of -0.01 the efficiency of each stage, one at a time, leads to the results presented in Figure 6.6.

Figure 6.6 reveal that the first stage is the one who influences the overall efficiency the most, for a given variation in the stages efficiencies. Thus, from a thermodynamics point of view, the first stage is the best to act on, i.e., overhaul actions are more effective in this stage rather than any other. However, the introduction of economic aspects, such as the cost of blades, may change the answer since the blades from the first stage cost approximately twice the blades from the second and third stages [52].

	Delta Efficiency Stage				
	-0,01	-0,02	-0,03	-0,04	-0,05
Stage 1	-0,003926	-0,007846	-0,011766	-0,015696	-0,019616
Stage 2	-0,003536	-0,007076	-0,010606	-0,014146	-0,017676
Stage 3	-0,003226	-0,006446	-0,009676	-0,012896	-0,016116
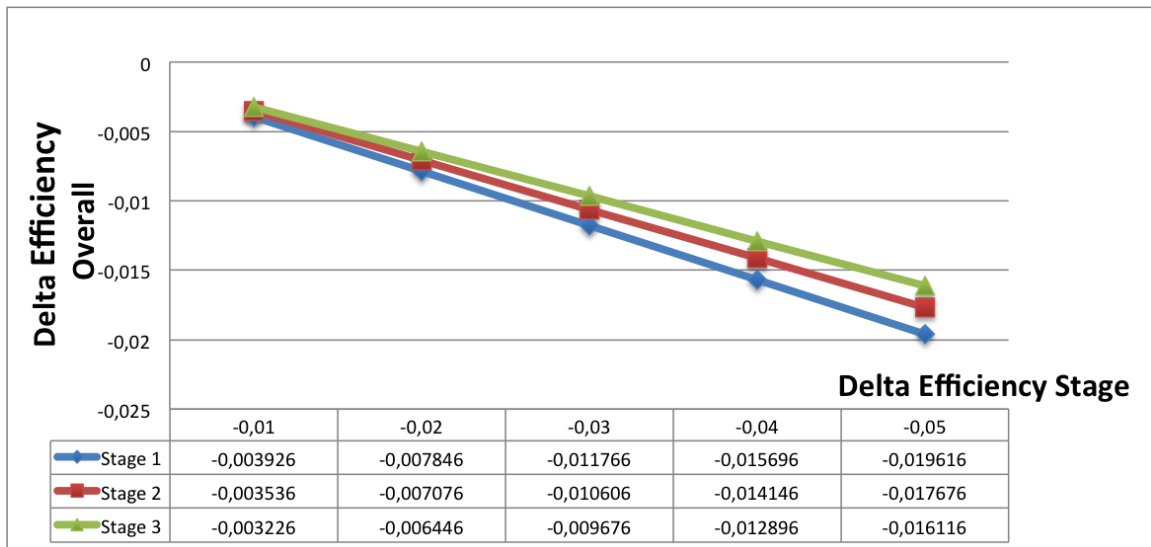
Figure 6.6: Stage efficiency influence on overall efficiency.

This fact may be related to their larger dimensions and more complex geometry, as presented in figure 6.7.

The introduction of economics in this study was not be possible due to the fact that it was not possible to relate the variations in efficiency of each stage with the number of blades exchanged in them. The only statement possible to make is that the replacement of the blades from the first three stages of the HPC for new ones lead to an increase of the HPC efficiency of 1.22%.

Figure 6.7: HPC blades from the first, second and third stages.

6.3 Effects of Tip Clearance Modifications on Overall Compressor Efficiency

As mentioned in Section 3.4, the increase in tip clearance is a common deterioration in both compressor and turbines [33]. This clearance allows the air to escape between the blade tip and the annulus wall just like in an aircraft wing tip, creating tip vortexes. The existence of such phenomena is proven by photographs of experimental flow patterns and by measurements, as mentioned by Vavra [50]. Figure 6.8 presents the tip vortexes created by the flow of air through the clearance, flowing in the direction of decreasing pressures.
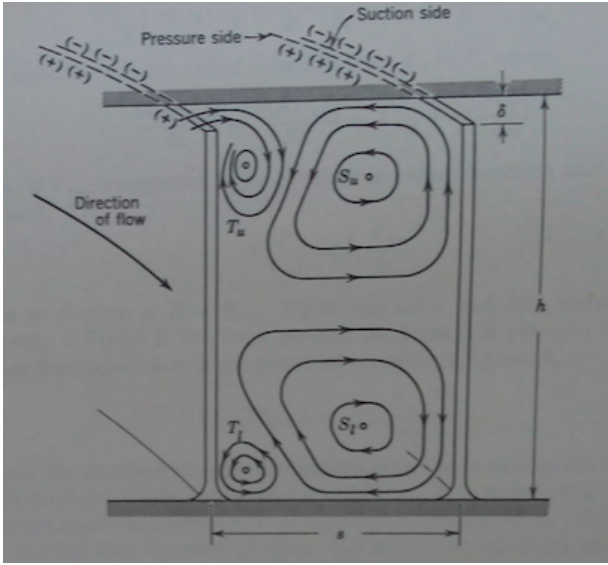
Figure 6.8: Vortex pattern in a cascade [50].

6.3.1 Methodology

TAP M&E is interested in understanding how the performance of the CFM56-3's HPC changes, and in what way these changes affect the engine performance. Tip clearance influences the overall efficiency of the compressor by increasing the end losses which, consequently, increases the loss factor of the different stages.

The tool that will now be developed will map the performance degradation of the HPC for several combinations of tip clearances in the first three stages. It will be assumed that the shape of the blade remains constant, i.e. only the height of the blade will be reduced. According to Vavra [50], usual tip clearance in a compressor stage range from 1% to 2% of the average blade height of that same stage. This study will be conducted for combinations of tip clearances equal to 0.5%, 1%, 1.5% and 2%. It will be assumed that the engine with the old blades has tip clearance equal to 2% of the blades height in each stage, with 33% of the old blades exchanged for new ones it will have 1.5% of tip clearance, with 67% of the blades renewed will have tip clearance equal to 1% and for the engine with all the blades from the three stages exchanged the tip clearance is assumed to be 0.5% of the blades height in each stage.

Note that the values of tip clearance are averages, i.e. the blades will have not all the same exact height. Thus, the efficiency drop will be estimated for a total of 64 combinations of tip clearances. This will give some important information about how much the HPC efficiency can be increased by decreasing the tip clearances in these three stages of the compressor.

An increase of the tip clearance affects two of the stage parameters:

1. The annulus drag coefficient will increase, from Equation (6.8b), the increase in tip clearance, corresponding to a blade height reduction, increases the value of C_{DA};

2. The secondary drag coefficient, which accounts for secondary and tip losses, will also increase due to two effects, the increase in δ and the decrease of h.

It is also possible to perform this performance mapping procedure assuming that the blades keep their geometry and that it is the annulus diameter that changes. This assumption lead to smaller efficiency drops since the only parameter to change is the tip clearance δ (h would remain constant).

6.3.2 Results

The results for a tip clearance reduction of 1%, for both assumptions, are presented in table 6.5.

Blade height increase							
Stage	δ_{Stg}/h_{Stg}	δ_{Stg} (in)	C_{DS}	$\Delta\eta_{OVR}$	% Blades exchanged	Cost ($)	$\Delta\eta_{OVR}/Cost$
1	0.01	0.034	0.012	0.425	67	43325	0.010
2	0.01	0.025	0.060	0.760	67	30905	0.025
3	0.01	0.020	0.061	0.669	67	27040	0.025
Annulus diameter decrease							
Stage	δ_{Stg}/h_{Stg}	δ_{Stg} (in)	C_{DS}	$\Delta\eta_{OVR}$	% Blades exchanged	Cost ($)	$\Delta\eta_{OVR}/Cost$
1	0.01	0.033	0.012	0.382	67	n/a	n/a
2	0.01	0.025	0.061	0.710	67	n/a	n/a
3	0.01	0.020	0.062	0.615	67	n/a	n/a

Table 6.5: Simulation of the tip clearance reduction effects on stage efficiency.

When assuming that the reduction of the tip clearance is caused by a reduction of the annulus diameter it is not possible to estimate the cost of this repair, since it varies much from case to case. The only price present in reference [52] is for a new HPC front case, which is much higher than the cost of repairing a used one and, therefore, will not be used.

The results presented in Table 6.5 reveal a surprising result. The overall performance of the compressor is more sensitive to changes in tip clearance in the second and third stages rather than changes in the first stage. Even though a 1% tip clearance reduction in the first leads to a tip clearance of 0.034in in the first stage and only 0.025in and 0.020in, for the second and third stages respectively, the smaller gaps in the second and third stages implicate greater losses in the overall efficiency of the compressor. The second and third stages affect the overall efficiency of the compressor the most due to their greater

Secondary drag coefficient, C_{DS}. From Table 6.5 it is possible to see that this coefficient is five times bigger for the second and third stages than for the first stage. Secondary drag coefficient, as Equation (6.9) reveals, depends of the square of the lift coefficient, C_L, which in the second and third stages is two times larger than in the first stage. The cause for such increase in the lift coefficient is revealed by inspection of Table 6.1 and Equations (6.4b) and (6.7b), where it is possible to see that the difference between inlet and outlet angles ($\alpha_1 - \alpha_2$), as well as the average angle (α_m), are greater for the second and third stages of the compressor. The increased air deflection then leads to the increase in the lift coefficient (see Equation (6.7b)).

The final output of this performance study is a map of performance increase vs repair cost, for different combinations of tip clearances in the first three stages of the HPC. For estimating the cost of the repairs, it is assumed that the starting engine has 2% tip clearance in all the three stages and the engine with the new blades has this value reduced to 0.5% of the blades height.

The results are presented in two tables, one for the blades exchange assumption and the other for the annulus diameter decrease assumption. The complete tables are presented in Appendix B. Due to their large dimensions, only an excerpt of each table will be presented now in Table 6.6.

(a) HPC Efficiency for different tip clearances combinations, assuming changes in blades height.

combination	% blades exchanged	Stage Pressure ratio			Overall Efficiency	Delta efficiency	Delta eff %	Cost	Delta eff/cost
		1	2	3					
1	100-100-100	1,3939	1,3508	1,3083	0,8104	0,0220	2,7844	153 213	0,0182
2	100-100-67	1,3939	1,3508	1,3049	0,8078	0,0193	2,4492	139 693	0,0175
3	100-100-33	1,3939	1,3508	1,3015	0,8051	0,0167	2,1138	126 173	0,0168
4	100-100-0	1,3939	1,3508	1,2982	0,8025	0,0140	1,7781	112 653	0,0158
5	100-67-100	1,3939	1,3468	1,3083	0,8074	0,0190	2,4034	137 319	0,0175
6	100-67-67	1,3939	1,3468	1,3049	0,8048	0,0163	2,0685	123 799	0,0167
7	100-67-33	1,3939	1,3468	1,3015	0,8021	0,0137	1,7334	110 279	0,0157
8	100-67-0	1,3939	1,3468	1,2982	0,7995	0,0110	1,3979	96 759	0,0144
9	100-33-100	1,3939	1,3428	1,3083	0,8044	0,0159	2,0221	121 425	0,0167
10	100-33-67	1,3939	1,3428	1,3049	0,8018	0,0133	1,6875	107 905	0,0156
33	33-100-100	1,3894	1,3508	1,3083	0,8071	0,0186	2,3580	108 155	0,0218
34	33-100-67	1,3894	1,3508	1,3049	0,8044	0,0160	2,0231	94 635	0,0214
35	33-100-33	1,3894	1,3508	1,3015	0,8018	0,0133	1,6880	81 115	0,0208
36	33-100-0	1,3894	1,3508	1,2982	0,7991	0,0107	1,3526	67 595	0,0200
37	33-67-100	1,3894	1,3468	1,3083	0,8041	0,0156	1,9774	92 261	0,0214

(b) HPC Efficiency for different tip clearances combinations, assuming changes in annulus diameter.

combination	% blades exchanged	Stage Pressure ratio			Overall Efficiency	Delta efficiency	Delta eff %
		1	2	3			
1	100-100-100	1,3939	1,3508	1,3083	0,8104	0,0202	2,5613
2	100-100-67	1,3939	1,3508	1,3052	0,8080	0,0178	2,2524
3	100-100-33	1,3939	1,3508	1,3021	0,8055	0,0154	1,9436
4	100-100-0	1,3939	1,3508	1,2989	0,8031	0,0129	1,6348
5	100-67-100	1,3939	1,3471	1,3083	0,8076	0,0174	2,2068
6	100-67-67	1,3939	1,3471	1,3052	0,8052	0,0150	1,8982
7	100-67-33	1,3939	1,3471	1,3021	0,8027	0,0126	1,5896
8	100-67-0	1,3939	1,3471	1,2989	0,8003	0,0101	1,2810
9	100-33-100	1,3939	1,3434	1,3083	0,8048	0,0146	1,8523
10	100-33-67	1,3939	1,3434	1,3052	0,8024	0,0122	1,5440
33	33-100-100	1,3898	1,3508	1,3083	0,8074	0,0172	2,1772
34	33-100-67	1,3898	1,3508	1,3052	0,8049	0,0148	1,8686
35	33-100-33	1,3898	1,3508	1,3021	0,8025	0,0123	1,5601
36	33-100-0	1,3898	1,3508	1,2989	0,8001	0,0099	1,2515
37	33-67-100	1,3898	1,3471	1,3083	0,8046	0,0144	1,8230

Table 6.6: HPC performance study results.

Test case

Consider now a general CFM56-3 engine tested in TAP M&E facilities. The test data was then introduced in the GasTurb MBTA and the engine HPC revealed a 2% HPC efficiency degradation. In order

to re-establish the contracted performance, engine maintenance actions on the HPC are required. Measurements performed on the first three stages of the HPC and in the HPC front case resulted in tip clearances of 2% in the three stages. From Table 6.6(a) it is possible to see that there are four combinations that result in an improvement of 2% in the HPC efficiency:

- Combination 3, changing all the blades from the first two stages and 33% from the third, leading to 2.11% efficiency improvement and costs of 126173$;

- Combination 6, changing all the blades from the first stage and 67% from the second and third stages, leading to 2.07% efficiency improvement and costs of 123799$;

- Combination 9, changing all the blades from the first and third stages and 33% from the second, leading to 2.02% efficiency improvement and costs of 121425$;

- Combination 34, changing 33% of the blades of the first stage, all the blades from the second stage and 67% from the third, leading to 2.02% efficiency improvement and costs of 94635$;

- Combination 49, changing all the blades from the second and third stages and not acting on the first stage, leading to 2.14% efficiency improvement and costs of 87359$.

The best option is the one with the best $\Delta\eta/cost$, which in this case is combination 49.

This tool will be useful for TAP M&E to understand how much can increase the EGT Margin of an engine by reducing the tip clearances in the first three stages in the HPC.

However, this tool does not solve all the TAP M&E problems from HPC degradations. It is possible that an engine HPC has reduced tip clearances but still perform bellow the expected. This happened with the back-to-back engine, in which the tip clearances were reduced and the efficiency of the HPC was still 2.4% bellow the efficiency of the HPC from the correlation engine (see Figure 5.5). Such degradation was caused by the reduction of the blades chord length and consequent distortion of the blades airfoil, as studied in Section 6.2.

Chapter 7

Conclusions

The present chapter will present the reader with the major achievements of this thesis, the obstacles found during the development of this dissertation and will finish with a list of recommendations and suggestions for future work in this area of expertise.

Gas turbine manufacturers only publish some information and test data for the commercial gas turbines, which only give little information about that specific machine. Most of the important information, such as components maps, remain hidden from the general public and even from MRO facilities. The main objective for this thesis was to provide TAP M&E additional information about the internal relations on a specific engine, the widely used CFM56-3 engine.

The modelling software chosen was GasTurb, which provides the user the possibility to model his own engine, using his own data. For this thesis, the chosen engine was the engine used by CFMI for composing the Correlation Test Report. This engine was chosen for being a stable engine and for having a greater level of instrumentation than the engines tested by TAP M&E in its test bed.

In order to model an engine, model data has to be fitted to match the available test bed data. The first thing to do is to model the engine design point, the operating point that will define the engine geometry. The use of a different point from the one used by Ridaura [7] lead to a better estimation of the engine by-pass ratio, which consequently lead to better estimations of the core and by-pass flows and components efficiencies. Once the geometry of the engine was defined, the next thing to do was to model the engine for off-design conditions, for different ambient conditions or different thrust settings. The engine model was developed and adjusted for high-thrust ratings, where the performance of an engine is critical. The developed model is able to simulate the correlation engine with great precision for thrust ratings over 80% of the design point rating.

GasTurb tool Model Based Test Analysis was used to study the performance improvement in an engine which had the blades from the first three stages of its high pressure compressor exchanged for new ones. The implementation of the test bed data lead to the conclusion that the engine had its HPC efficiency improved by 1.31%. The precision of the model was tested during this analysis comparing the calculated values of the EGT with the measured values during the two test runs. The deviations between tested and measured values were of the order of 1%. The Model Based Test Analysis was limited due

to the fact that some of the parameters needed for a complete analysis were not measured during both the tests. The solution to this problem was to take that data from the model and correct it to the ambient conditions during the test runs.

Using GasTurb tool called Sensitivity, two studies were performed. The first had the objective of studying which component had more influence on the EGT Margin degradation. The second study was performed to validate the results from the MBTA. The EGT of the engine A (before the blades replacement) was degraded using the results from the Sensitivity tests. The engine was tested for two Maximum Continuous points and one Take Off point. The results for the first Maximum Continuous operating point were the more satisfactory, resulting in a deviation of 2.08% between the EGT drop (from engine A to B) calculated in the MBTA and in the Sensitivity tests.

TAP M&E is interested in understanding the effects of two HPC blades degradations on the overall efficiency of the engine, the reduction in chord length and the increase in tip clearance. An analysis was performed to study which HPC stage degradations affect the overall compressor efficiency the most. The results show that the first stage of the HPC is the one with more influence on the overall efficiency of this component. Studying the influence of chord length on overall efficiency was a challenge since only one back-to-back test is available for CFM56-3 engines. The study of the effect of blade chord length reduction on the overall compressor efficiency was not possible to perform due to the fact that a reduction of the first parameter alone does not lead to the efficiency degradation observed in the back-to-back engine, this reduction in the chord length must be accompanied with the distortion of the airfoil, which increases the drag coefficient of the blades row, reducing the overall efficiency of the compressor. This increase could not be estimated with confidence and, therefore, this implementation was abandoned.

The effect of tip clearance in the different stages of the HPC was studied for 64 combination of tip clearances between 0.5% and 2% of the blades height. This study resulted in the conclusion that, due to the higher deflection imposed to the air in these stages, the second and third stages influence the overall compressor efficiency the most, for a given tip clearance value.

This thesis provided TAP M&E with some very useful tools that will help estimating the performance of the engines coming to the shop and to reveal which component of an engine is responsible for the degradation of the engine performance. This will help TAP Maintenance & Engineering save both financial and human resources.

7.1   Achievements

The major achievements of this thesis may now be enumerated:

1. Tuning of the CFM56-3 model to high-thrust ratings;

2. Implementation of test bed data in Model Based Test Analysis;

3. Study of the internal relations of the CFM56-3 engine using Sensitivity tool;

4. Study of the influence of stage efficiency degradations on overall efficiency for the first three stages of the HPC;

5. Creation of a map of HPC efficiency degradation due to tip clearance in the first three stages of the HPC.

7.2   Future Work

The model developed can be further improved in order to perform as the correlation engine for the entire range of operating points. Such improvement is possible with the implementation of the HPT clearance control schedule, which was not possible in this thesis.

In order to perform a full Model Based Test Analysis, GasTurb requires a set of test bed data. If some of the required data is not measured in the test cell, it is necessary to use model data to perform the analysis. This limits the results, the engine tested is using components of the model engine, i.e. the engine analysis is not independent from the model. This problem can be solved with the instrumentation of the engines coming to the shop. This will greatly increase both the accuracy and the confidence on the results.

At last, deeper analyses of eroded blades may be useful to estimate the variation of the incidence angle of the air to the blade since with that information it would be possible to understand the increase of the profile drag of the blade rows, which would allow to map the variations of the high pressure compressor efficiency for different combinations of blade chord length reduction.

With these recommendations, the estimation of the engine performance would be done with much more accuracy and the process would become faster and easier since the data borrowed from the model would not be needed.

Bibliography

[1] TAP Maintenance & Engineering. `https://www.tap-mro.com/Pages/About%20TAP%20ME/AboutUs.aspx`, . [Accessed April 2015].

[2] MTU Aero Engines. `http://www.mtu.de/maintenance/`. [Accessed April 2015].

[3] Lufthansa Technik. `http://www.lufthansa-technik.com/web/lht/home`, . [Accessed April 2015].

[4] S. S. S. Goh. Sustainment of commercial aircraft gas turbine engines an organizational and cognitive engineering approach. Master's thesis, MIT, Cambridge MA, 2003.

[5] TAP Portugal. `http://www.tapportugal.com/Info/pt/sobre-tap`, . [Accessed April 2015].

[6] TAP quality report, company confidential. Technical report, TAP, 2014.

[7] J. A. R. Ridaura. Correlation analysis between hpc blade chord and compressor efficiency for the CFM56-3. Master's thesis, Instituto Superior Técnico, October 2014.

[8] Power for the Airline. `http://www.aviation-news.co.uk/archive/powerfortheairline.html`. [Accessed April 2015].

[9] M. P. Boyce. *Gas turbine Engineering Handbook*. Gulf Professional Publishing, 2nd edition, 2002.

[10] Lufthansa Technik Project - Engine Performance Analysis. `http://www.lufthansa-technik.com/engine-performance-analysis`, . [Accessed April 2015].

[11] J. Kurzke. *Gasturb 11: Design and Off-Design Performance of Gas Turbines*. 2011.

[12] P. Compenat, F. Trimouille, and approved by R. Mouginot. Correlation Report of TAP Air Portugal for CFM56-3 engine. Technical report, CFM, 1991.

[13] European Federation of National Maintenance Societies. `http://www.efnms.org/What-EFNMS-stands-for/m1312/What-EFNMS-stands-for.html`. [Accessed May 2015].

[14] TAP quality report, company confidential. Technical report, TAP, 2015.

[15] P. P. Walsh and P. Fletcher. *Gas turbine performance*. John Wiley & Sons, Inc, 2004.

[16] R. Royce. *The Jet Engine*. Rolls Royce plc, fifth edition, 1986.

[17] P. M. A. Ribeiro. Análise da Performance da Família de Motores de Avião CFM56-3. Master's thesis, Instituto Superior Engenharia Lisboa, 2012.

[18] A. M. A. R. Henriques. Análise da influência dos procedimentos de manutenção do motor CFM56-3 no seu desempenho no banco de ensaios. TAP Portugal, 2011.

[19] J. Kurzke. How to create a performance model of a gas turbine from a limited amount of information. ASME Turbo Expo 2005: Power for Land, Sea and Air. *American Society of Mechanical Engineers*, 2005.

[20] F. M. White. *Fluid Mechanics*. McGraw Hill, 7th edition, 2011.

[21] CFM. CFM56-3 Engine Shop Manual - Engine Test - Test 003 - Engine Acceptance Test, Task 72-00-00-760-003-0, 2011.

[22] CFM. *CFM56-3 Basic Engine, B737-300. Formação Profissional TAP. Revision 3*. 1992.

[23] D. Unger and H. Herzog. Comparative study on energy R&D performance: Gas turbine case study. Technical report, Massachusetts Institute of Technology, Energy Laboratory, August 1998.

[24] T. Nada. Performance characterization of different configurations of gas turbine engines. *Propulsion and Power Research*, 3(3), September 2014. doi:10.1016/j.jppr.2014.07.005.

[25] R. Storm, M. Skor, L. D. Koch, T. Benson, and C. Galica. *Pushing the envelope: A NASA Guide to Engines*. National Aeronautics and Space Administration, 2007.

[26] H. Cohen, G. Rogers, and H. Saravanamuttoo. *Gas Turbine Theory*. Longman Group Limited, fourth edition, 1996.

[27] R. Royce. RR Trent XWB infographic, February 2015.

[28] P. M. Sforza. *Theory of Aerospace Propulsion*. Butterworth-Heinemann, first edition, 2011.

[29] S. L. Dixon. *Fluid Mechanics and Thermodynamics of Turbomachinery*. Elsevier Butterworth–Heinemann, 4th edition, 1998.

[30] P. G. Hill and C. R. Peterson. *Mechanics and Thermodynamics of Propulsion*. Addison-Wesley publishing company, second edition, 1992.

[31] K.A.B.Pathirathna. Gas turbine thermodynamic and performance analysis methods using available catalog data. Master's thesis, Faculty of engineering and sustainable development - University of Gavle, 2013.

[32] J. Moran and H. Shapiro. *Fundamentals of engineering thermodynamics*, chapter 10, pages 500 – 600. 5th edition, 2006.

[33] M. S. Grewal. *GAS TURBINE ENGINE PERFORMANCE DETERIORATION MODELLING AND ANALYSIS*. PhD thesis, Cranfield Institute of Technology, School of Mechanical Engineering, February 1988.

[34] J. Leite. *CFM56-3 - Basic Engine. Lisboa TAP Maintenance & Engineering*. 1992.

[35] *CFM56-3 maintenance analysis & budget*, pages 18–28. Number 45. Aircraft Commerce, April/May 2006.

[36] J. Kurzke. Gas turbine design and performance. Seminar in Aachen, Germany, 2014.

[37] J. Kurzke. CFM56-3 in TAP. Private communication.

[38] Gas Turbine Simulation Program. `http://www.gspteam.com/about-gsp`. [Accessed May 2015].

[39] R. Sung. A comparative study of the gas turbine simulation program (gsp) 11 and gasturb 11 on their respective simulations for a single-spool turbojet. Master's thesis, Tennessee University, 2013.

[40] MATLAB software, property of MathWorks. `http://www.mathworks.com/products/matlab/`. [Accessed May 2015].

[41] S. M. Camporeale, B. Fortunato, and M. Mastrovito. A modular code for real time dynamic simulation of gas turbines in simulink. *ASME - Journal of engineering for Gas Turbines and Power*, 128 (3):506–517, March 2002. doi:10.1115/1.2132383.

[42] S. A. Shakariants. Generic methods for aero-engines exhaust emission prediction. Master's thesis, Moscow State Aviation Institute, 2008.

[43] H. Wemming. Validation and integration of a rubber engine model into an MDO environment. Master's thesis, Linkoping University, 2010.

[44] J. Kurzke. The importance of component maps for gas turbine performance simulations. 12th International Symposium on Transport Phenomena and Dynamics of Rotating Machinery (ISROMAC-12), Honolulu, HI, 2008.

[45] S. M. Jones. *An Introduction to Thermodynamic Performance Analysis of Aircraft Gas Turbine Engine Cycles Using the Numerical Propulsion System Simulation Code*, pages 37–40. NASA, Glenn Research Center, Cleveland, Ohio, March 2007.

[46] CFM. *CFM56-3 Systems training manual.* 1990.

[47] Lufthansa Technik Project - Blade Width Restoration. `http://www.lufthansa-technik.com/chord-width-restoration`, . [Accessed August 2015].

[48] F. Brooks. *Gas Turbine Performance Characteristics. GE Power Systems*. GE, 2010.

[49] T. C. Corke. *Design of Aircraft*. Prentice Hall, New Jersey, 2003.

[50] M. H. Vavra. *Aero-thermodynamics and Flow in Turbomachines*. John Wiley & Sons, 1st edition, 1960.

[51] Mitutoyo Coordinate Measuring Machines Catalogue. `http://www.mitutoyo.com/wp-content/uploads/2015/04/L-Section-US-1003.pdf`, 2015. [Accessed September 2015].

[52] *CFM56-3 Engine - Spare Parts Price Catalogue*. CFM International, S.A., 2015.

Appendix A

Model Validation

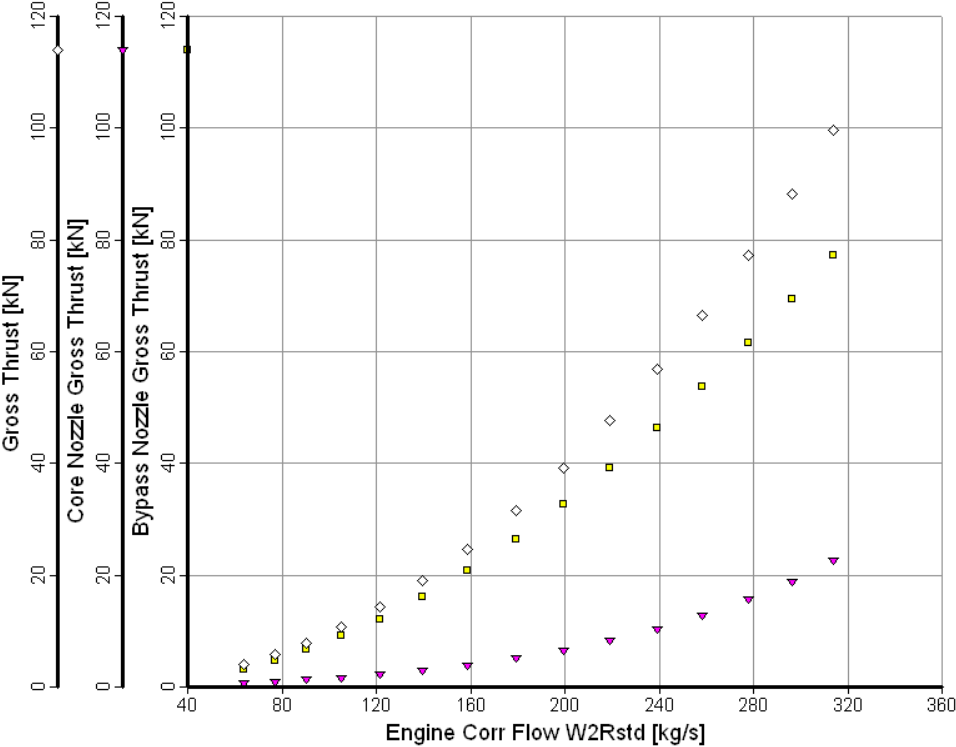Figure A.1: Evidence that 80% of the total thrust is produced by the by-pass flow (Fan).
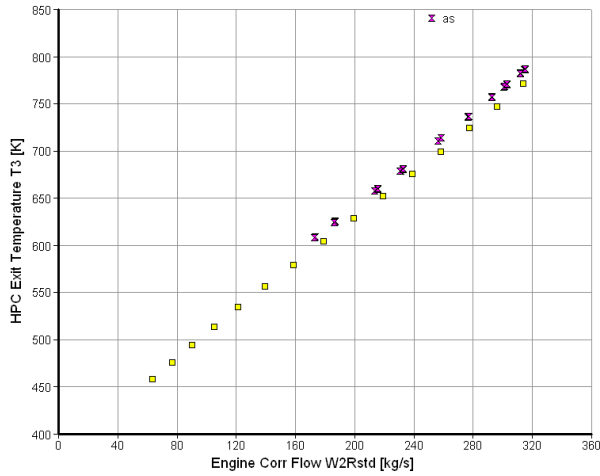
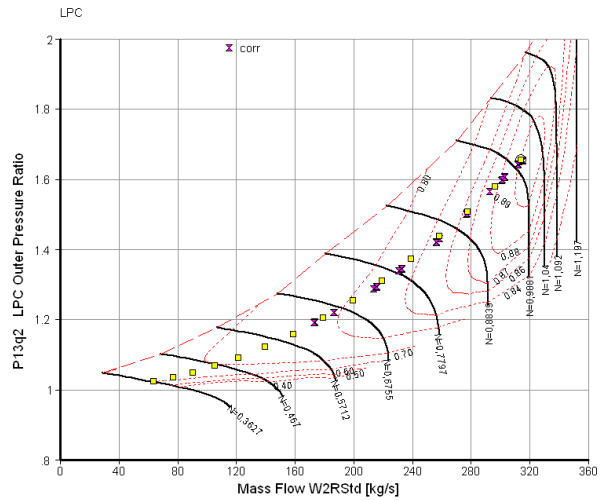Figure A.2: Deviation between T3 and T4127 measurements.

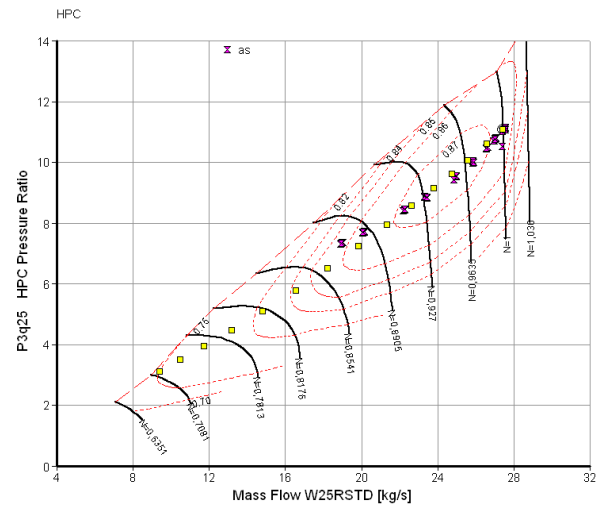Figure A.3: Measured and calculated operating lines in LPC Map.

Figure A.4: Measured and calculated operating lines in HPC Map.

Appendix B

Performance Study - Complete Maps

B.1 Modification of the Blades Height

B.2 Modification of the Annulus Diameter

combination	% blades exchanged	Stage Rs			Overall Efficiency	Delta efficiency	Delta eff %	Cost	Delta eff/cost
		1	2	3					
1	100-100-100	1,3939	1,3508	1,3083	0,8104	0,0220	2,7844	153 213	0,0182
2	100-100-67	1,3939	1,3508	1,3049	0,8078	0,0193	2,4492	139 693	0,0175
3	100-100-33	1,3939	1,3508	1,3015	0,8051	0,0167	2,1138	126 173	0,0168
4	100-100-0	1,3939	1,3508	1,2982	0,8025	0,0140	1,7781	112 653	0,0158
5	100-67-100	1,3939	1,3468	1,3083	0,8074	0,0190	2,4034	137 319	0,0175
6	100-67-67	1,3939	1,3468	1,3049	0,8048	0,0163	2,0685	123 799	0,0167
7	100-67-33	1,3939	1,3468	1,3015	0,8021	0,0137	1,7334	110 279	0,0157
8	100-67-0	1,3939	1,3468	1,2982	0,7995	0,0110	1,3979	96 759	0,0144
9	100-33-100	1,3939	1,3428	1,3083	0,8044	0,0159	2,0221	121 425	0,0167
10	100-33-67	1,3939	1,3428	1,3049	0,8018	0,0133	1,6875	107 905	0,0156
11	100-33-33	1,3939	1,3428	1,3015	0,7991	0,0107	1,3527	94 385	0,0143
12	100-33-0	1,3939	1,3428	1,2982	0,7965	0,0080	1,0175	80 865	0,0126
13	100-0-100	1,3939	1,3389	1,3083	0,8014	0,0129	1,6406	106 414	0,0154
14	100-0-67	1,3939	1,3389	1,3049	0,7988	0,0103	1,3063	92 894	0,0141
15	100-0-33	1,3939	1,3389	1,3015	0,7961	0,0077	0,9717	79 374	0,0122
16	100-0-0	1,3939	1,3389	1,2982	0,7935	0,0050	0,6369	65 854	0,0097
17	67-100-100	1,3916	1,3508	1,3083	0,8087	0,0203	2,5713	130 684	0,0197
18	67-100-67	1,3916	1,3508	1,3049	0,8061	0,0176	2,2363	117 164	0,0191
19	67-100-33	1,3916	1,3508	1,3015	0,8035	0,0150	1,9010	103 644	0,0183
20	67-100-0	1,3916	1,3508	1,2982	0,8008	0,0123	1,5655	90 124	0,0174
21	67-67-100	1,3916	1,3468	1,3083	0,8057	0,0173	2,1905	114 790	0,0191
22	67-67-67	1,3916	1,3468	1,3049	0,8031	0,0146	1,8557	101 270	0,0183
23	67-67-33	1,3916	1,3468	1,3015	0,8005	0,0120	1,5208	87 750	0,0173
24	67-67-0	1,3916	1,3468	1,2982	0,7978	0,0093	1,1855	74 230	0,0160
25	67-33-100	1,3916	1,3428	1,3083	0,8027	0,0143	1,8094	98 896	0,0183
26	67-33-67	1,3916	1,3428	1,3049	0,8001	0,0116	1,4750	85 376	0,0173
27	67-33-33	1,3916	1,3428	1,3015	0,7975	0,0090	1,1402	71 856	0,0159
28	67-33-0	1,3916	1,3428	1,2982	0,7948	0,0063	0,8053	58 336	0,0138
29	67-0-100	1,3916	1,3389	1,3083	0,7997	0,0113	1,4281	83 885	0,0170
30	67-0-67	1,3916	1,3389	1,3049	0,7971	0,0086	1,0939	70 365	0,0155
31	67-0-33	1,3916	1,3389	1,3015	0,7945	0,0060	0,7595	56 845	0,0134
32	67-0-0	1,3916	1,3389	1,2982	0,7918	0,0033	0,4248	43 325	0,0098

Figure B.1: Performance map A.

combination	% blades exchanged	Stage Rs			Overall Efficiency	Delta efficiency	Delta eff %	Cost	Delta eff/cost
		1	2	3					
33	33-100-100	1,3894	1,3508	1,3083	0,8071	0,0186	2,3580	108 155	0,0218
34	33-100-67	1,3894	1,3508	1,3049	0,8044	0,0160	2,0231	94 635	0,0214
35	33-100-33	1,3894	1,3508	1,3015	0,8018	0,0133	1,6880	81 115	0,0208
36	33-100-0	1,3894	1,3508	1,2982	0,7991	0,0107	1,3526	67 595	0,0200
37	33-67-100	1,3894	1,3468	1,3083	0,8041	0,0156	1,9774	92 261	0,0214
38	33-67-67	1,3894	1,3468	1,3049	0,8014	0,0130	1,6428	78 741	0,0209
39	33-67-33	1,3894	1,3468	1,3015	0,7988	0,0103	1,3079	65 221	0,0201
40	33-67-0	1,3894	1,3468	1,2982	0,7961	0,0077	0,9728	51 701	0,0188
41	33-33-100	1,3894	1,3428	1,3083	0,8011	0,0126	1,5965	76 367	0,0209
42	33-33-67	1,3894	1,3428	1,3049	0,7984	0,0100	1,2622	62 847	0,0201
43	33-33-33	1,3894	1,3428	1,3015	0,7958	0,0073	0,9276	49 327	0,0188
44	33-33-0	1,3894	1,3428	1,2982	0,7931	0,0047	0,5928	35 807	0,0166
45	33-0-100	1,3894	1,3389	1,3083	0,7981	0,0096	1,2153	61 356	0,0198
46	33-0-67	1,3894	1,3389	1,3049	0,7954	0,0069	0,8813	47 836	0,0184
47	33-0-33	1,3894	1,3389	1,3015	0,7928	0,0043	0,5470	34 316	0,0159
48	33-0-0	1,3894	1,3389	1,2982	0,7901	0,0017	0,2125	20 796	0,0102
49	0-100-100	1,3871	1,3508	1,3083	0,8054	0,0169	2,1445	87 359	0,0245
50	0-100-67	1,3871	1,3508	1,3049	0,8027	0,0143	1,8098	73 839	0,0245
51	0-100-33	1,3871	1,3508	1,3015	0,8001	0,0116	1,4748	60 319	0,0245
52	0-100-0	1,3871	1,3508	1,2982	0,7975	0,0090	1,1396	46 799	0,0244
53	0-67-100	1,3871	1,3468	1,3083	0,8024	0,0139	1,7640	71 465	0,0247
54	0-67-67	1,3871	1,3468	1,3049	0,7997	0,0113	1,4296	57 945	0,0247
55	0-67-33	1,3871	1,3468	1,3015	0,7971	0,0086	1,0949	44 425	0,0246
56	0-67-0	1,3871	1,3468	1,2982	0,7945	0,0060	0,7600	30 905	0,0246
57	0-33-100	1,3871	1,3428	1,3083	0,7994	0,0109	1,3833	55 571	0,0249
58	0-33-67	1,3871	1,3428	1,3049	0,7967	0,0083	1,0492	42 051	0,0250
59	0-33-33	1,3871	1,3428	1,3015	0,7941	0,0056	0,7148	28 531	0,0251
60	67-33-0	1,3871	1,3428	1,2982	0,7915	0,0030	0,3801	15 011	0,0253
61	0-0-100	1,3871	1,3389	1,3083	0,7964	0,0079	1,0023	40 560	0,0247
62	0-0-67	1,3871	1,3389	1,3049	0,7937	0,0053	0,6685	27 040	0,0247
63	0-0-33	1,3871	1,3389	1,3015	0,7911	0,0026	0,3344	13 520	0,0247
64	0-0-0	1,3871	1,3389	1,2982	0,7885	0,0000	0,0000	0	n/a

Figure B.2: Performance map B.

combination	% blades exchanged	Stage Rs			Overall Efficiency	Delta efficiency	Delta eff %
		1	2	3			
1	100-100-100	1,3939	1,3508	1,3083	0,8104	0,0202	2,5613
2	100-100-67	1,3939	1,3508	1,3052	0,8080	0,0178	2,2524
3	100-100-33	1,3939	1,3508	1,3021	0,8055	0,0154	1,9436
4	100-100-0	1,3939	1,3508	1,2989	0,8031	0,0129	1,6348
5	100-67-100	1,3939	1,3471	1,3083	0,8076	0,0174	2,2068
6	100-67-67	1,3939	1,3471	1,3052	0,8052	0,0150	1,8982
7	100-67-33	1,3939	1,3471	1,3021	0,8027	0,0126	1,5896
8	100-67-0	1,3939	1,3471	1,2989	0,8003	0,0101	1,2810
9	100-33-100	1,3939	1,3434	1,3083	0,8048	0,0146	1,8523
10	100-33-67	1,3939	1,3434	1,3052	0,8024	0,0122	1,5440
11	100-33-33	1,3939	1,3434	1,3021	0,7999	0,0098	1,2356
12	100-33-0	1,3939	1,3434	1,2989	0,7975	0,0073	0,9273
13	100-0-100	1,3939	1,3397	1,3083	0,8020	0,0118	1,4979
14	100-0-67	1,3939	1,3397	1,3052	0,7996	0,0094	1,1898
15	100-0-33	1,3939	1,3397	1,3021	0,7971	0,0070	0,8817
16	100-0-0	1,3939	1,3397	1,2989	0,7947	0,0045	0,5735
17	67-100-100	1,3919	1,3508	1,3083	0,8089	0,0187	2,3692
18	67-100-67	1,3919	1,3508	1,3052	0,8065	0,0163	2,0605
19	67-100-33	1,3919	1,3508	1,3021	0,8040	0,0138	1,7518
20	67-100-0	1,3919	1,3508	1,2989	0,8016	0,0114	1,4431
21	67-67-100	1,3919	1,3471	1,3083	0,8061	0,0159	2,0149
22	67-67-67	1,3919	1,3471	1,3052	0,8037	0,0135	1,7065
23	67-67-33	1,3919	1,3471	1,3021	0,8012	0,0110	1,3980
24	67-67-0	1,3919	1,3471	1,2989	0,7988	0,0086	1,0895
25	67-33-100	1,3919	1,3434	1,3083	0,8033	0,0131	1,6606
26	67-33-67	1,3919	1,3434	1,3052	0,8009	0,0107	1,3524
27	67-33-33	1,3919	1,3434	1,3021	0,7984	0,0083	1,0442
28	67-33-0	1,3919	1,3434	1,2989	0,7960	0,0058	0,7360
29	67-0-100	1,3919	1,3397	1,3083	0,8005	0,0103	1,3063
30	67-0-67	1,3919	1,3397	1,3052	0,7981	0,0079	0,9983
31	67-0-33	1,3919	1,3397	1,3021	0,7956	0,0055	0,6903
32	67-0-0	1,3919	1,3397	1,2989	0,7932	0,0030	0,3824

Figure B.3: Performance map C.

combination	% blades exchanged	Stage Rs			Overall Efficiency	Delta efficiency	Delta eff %
		1	2	3			
33	33-100-100	1,3898	1,3508	1,3083	0,8074	0,0172	2,1772
34	33-100-67	1,3898	1,3508	1,3052	0,8049	0,0148	1,8686
35	33-100-33	1,3898	1,3508	1,3021	0,8025	0,0123	1,5601
36	33-100-0	1,3898	1,3508	1,2989	0,8001	0,0099	1,2515
37	33-67-100	1,3898	1,3471	1,3083	0,8046	0,0144	1,8230
38	33-67-67	1,3898	1,3471	1,3052	0,8022	0,0120	1,5147
39	33-67-33	1,3898	1,3471	1,3021	0,7997	0,0095	1,2064
40	33-67-0	1,3898	1,3471	1,2989	0,7973	0,0071	0,8981
41	33-33-100	1,3898	1,3434	1,3083	0,8018	0,0116	1,4689
42	33-33-67	1,3898	1,3434	1,3052	0,7994	0,0092	1,1608
43	33-33-33	1,3898	1,3434	1,3021	0,7969	0,0067	0,8527
44	33-33-0	1,3898	1,3434	1,2989	0,7945	0,0043	0,5446
45	33-0-100	1,3898	1,3397	1,3083	0,7990	0,0088	1,1147
46	33-0-67	1,3898	1,3397	1,3052	0,7966	0,0064	0,8069
47	33-0-33	1,3898	1,3397	1,3021	0,7941	0,0039	0,4990
48	33-0-0	1,3898	1,3397	1,2989	0,7917	0,0015	0,1912
49	0-100-100	1,3877	1,3508	1,3083	0,8059	0,0157	1,9852
50	0-100-67	1,3877	1,3508	1,3052	0,8034	0,0132	1,6767
51	0-100-33	1,3877	1,3508	1,3021	0,8010	0,0108	1,3683
52	0-100-0	1,3877	1,3508	1,2989	0,7986	0,0084	1,0599
53	0-67-100	1,3877	1,3471	1,3083	0,8031	0,0129	1,6312
54	0-67-67	1,3877	1,3471	1,3052	0,8006	0,0105	1,3230
55	0-67-33	1,3877	1,3471	1,3021	0,7982	0,0080	1,0148
56	0-67-0	1,3877	1,3471	1,2989	0,7958	0,0056	0,7066
57	0-33-100	1,3877	1,3434	1,3083	0,8003	0,0101	1,2771
58	0-33-67	1,3877	1,3434	1,3052	0,7978	0,0077	0,9692
59	0-33-33	1,3877	1,3434	1,3021	0,7954	0,0052	0,6612
60	67-33-0	1,3877	1,3434	1,2989	0,7930	0,0028	0,3533
61	0-0-100	1,3877	1,3397	1,3083	0,7975	0,0073	0,9231
62	0-0-67	1,3877	1,3397	1,3052	0,7950	0,0049	0,6154
63	0-0-33	1,3877	1,3397	1,3021	0,7926	0,0024	0,3077
64	0-0-0	1,3877	1,3397	1,2989	0,7902	0,0000	0,0000

Figure B.4: Performance map D.